NISTIR 4857

Application of Inelastic Damage Analysis to Double-Deck Highway Structures

John L. Gross

Sashi K. Kunnath

States Department of Commerce
ogy Administration
Institute of Standards and Technology
burg, Maryland 20899

Prepared for:
U. S. Geological Survey
Department of the Interior
Reston, Virginia 22092

NISTIR 4857

Application of Inelastic Damage Analysis to Double-Deck Highway Structures

John L. Gross
Building and Fire Research Laboratory, NIST

Sashi K. Kunnath
University of Central Florida

Contract No. USGS-9900-0247

August, 1992

U.S. Department of Commerce
Barbara Hackman Franklin, *Secretary*
Technology Administration
Robert M. White, *Under Secretary for Technology*
National Institute of Standards and Technology
John W. Lyons, *Director*

Prepared for:
U. S. Geological Survey
Dallas L. Peck, *Director*

Abstract

The Loma Prieta earthquake of October 17, 1989, caused extensive damage to many highway structures and particularly to double-deck structures. The most notable was the collapse of the Cypress Viaduct (Interstate 880). A study was undertaken by NIST to identify, using computer-based analysis methods, causes of structural failure of elevated highway structures resulting from the Loma Prieta earthquake and thereby reveal the potential for damage or collapse of similar structures nationwide. The IDARC analysis program, developed at the University of Buffalo, was used in the inelastic seismic analysis. Features of the program and enhancements incorporated to model the Cypress Viaduct structure are described. To accurately determine beam and column moment-curvature relationships, separate computer analyses were conducted. In addition, a smeared-crack approach finite element analysis was employed to determine the lateral load-deformation relationship of the pedestal regions. The model of the Cypress Viaduct was subjected to the Oakland Outer Harbor Wharf ground acceleration record in the plane of the bent. The analytical model was calibrated using static lateral load tests, ambient and forced vibration tests, and observed performance. Results of time-history analyses, which include a prediction of member damage, indicate that collapse was initiated by a shear failure of the pedestal regions as concluded by the Governor's Board of Inquiry. The analytical and modeling procedures reported herein may be used to facilitate comparison and selection of effective approaches to seismic strengthening.

Keywords: Computer analysis; computer modeling; damage; earthquake; finite element analysis; highway structures; inelastic analysis; reinforced concrete; seismic analysis; structural analysis.

Acknowledgements

Support for the research reported herein by the U. S. Geological Survey is gratefully acknowledged.

In addition, the writers would like to thank Mr. James Gates and Mr. Raymond Zelinski of the California Department of Transportation for providing drawings of the Cypress Viaduct.

Dr. Andrei Reinhorn and Mr. Roy Lobo, along with Dr. Sashi Kunnath, developed the IDARC computer program at the University of Buffalo. Mr. Sami El-Borgi of Cornell University developed the computer program to determine flexural member moment-curvature relationships and Mr. Robert Ewing of Ewing & Associates provided the FEM/I computer program for the pedestal analysis. Their contributions are greatly appreciated.

Finally, the writers appreciate the toughtful comments of the reviewers, Dr. Richard Marshall, Ms. Geraldine Cheok and Ms. Sheila Duwadi.

Contents

List of Figures

List of Tables

1.0 Introduction

The Loma Prieta earthquake of October 15, 1989, caused extensive damage to highway structures, particularly double-deck structures. The highway structures that failed were designed and constructed in the 1950's and early 1960's. During this period such structures were designed primarily for gravity loads; lateral load resistance was checked for loads on the order of 5 percent of the gravity load. In addition, no ductility requirements were imposed by the codes. Bridge structures designed according to such simplistic approaches are highly susceptible to severe damage and possibly to total collapse under moderate ground shaking.

The objective of this study was to identify, using computer-based analysis methods, causes of structural failure of elevated bridge structures resulting from the Loma Prieta earthquake and thereby reveal the potential for damage or collapse of similar structures nationwide. A computer program for the inelastic damage analysis of reinforced concrete structures was used to analyze the Cypress Viaduct which collapsed in the earthquake. A model of the Cypress Viaduct was developed on the basis of computed beam and column moment-curvature relationships and lateral load-deformation relationships of the pedestal regions as determined by a smeared-crack approach finite element analysis. The model of the Cypress Viaduct was subjected to the Oakland Outer Harbor Wharf ground acceleration record in the plane of the bent. Experimental data from both static and dynamic tests of a portion of the Cypress Viaduct that remained standing, demonstrated the effectiveness of both the inelastic damage computer analysis capability as well as the modeling techniques employed. Results of subsequent time-history analyses compared favorably with observed performance. Thus, the analytical and modeling procedures reported herein may be used to facilitate comparison and selection of effective approaches to seismic strengthening.

1.1 Inelastic Analysis of Reinforced Concrete Structures

Reinforced concrete structures will, under strong ground motions associated with major earthquakes, deform inelastically and dissipate energy. A reliable prediction of the inelastic response of such structures is essential. Scale-model testing of structures using seismic simulators (shake tables) and full-scale quasi-static testing of components offer a means of assessing seismic performance. These methods, however, are very time-consuming and expensive and preclude the investigation of all parameters that contribute to the structural response. Experiments are generally necessary to calibrate analytical models, which then can be used to simulate a variety of existing structural configurations. Well-calibrated analytical

models can be used in parametric studies to investigate both the performance of existing structures as well as the relative merits of retrofit strategies.

Development of reliable analytical models for nonlinear response prediction of reinforced concrete requires careful consideration of both member load-deformation behavior and hysteretic behavior under repeated loads. The past two decades have seen a number of advances in modeling of reinforced concrete primarily based on component testing. Some of the modeling schemes proposed in the past include: concentrated or distributed-plasticity models to represent member deformations; and linear segmented or smooth hysteretic models using various degrading rules to describe the hysteretic behavior at member cross-sections. The earliest nonlinear computer program for reinforced concrete structures, DRAIN-2D, was released in 1973 [Kanaan and Powell, 1973]. Since it used a simple bi-linear hysteretic model with concentrated plasticity, a number of researchers at various institutions have extended DRAIN-2D to include more sophisticated models or have modified basic flexibility formulations such as SARCF-II [Rodriguez-Gomez, et al, 1990]. Most versions of available computer programs for nonlinear analysis of reinforced concrete structures have been successful in reproducing experimental test results following a certain degree of tuning and calibration. This suggests that users of nonlinear computer codes must be fairly knowledgeable about reinforced concrete behavior in order to put them to effective use.

A survey of recent developments in inelastic analysis of reinforced concrete structures indicated that IDARC [Park, et al., 1987], a program for seismic damage analysis of reinforced concrete structures, offered a suitable computational platform for the proposed analytical study. Features were added to the basic version of the program to permit the analysis of typical elevated highway structures. In addition, changes were made to the IDARC program as a result of applying it to the analysis of the Cypress Viaduct. An overview of the basic program features, enhancements and modifications is presented.

1.2 Analysis of the Cypress Viaduct

The Loma Prieta earthquake provided the engineering profession with data on the performance of structures against which analytical simulations can be compared. The Cypress Viaduct which collapsed in the earthquake, provides an excellent opportunity to evaluate and, if necessary, improve upon current analytical procedures that attempt to predict damage and limit states of reinforced concrete structures subjected to strong motion earthquakes.

1.3 Scope of Report

In the following report, the IDARC computer program is described, including basic program theory and capabilities, features added to permit the modeling of elevated highway structures, and changes made to the program as a result of analytical studies performed. Next, the Cypress Viaduct, which forms the basis for calibration of the IDARC program, is described. Procedures for determining member properties, especially in the regions known to have experienced failure, are explained. Static load test and vibration measurements provide validation of the material, member and geometric modeling. Finally, results from a full inelastic time-history analysis are provided and comparison is made with observed performance.

2.0 Inelastic Analysis of Reinforced Concrete

The IDARC computer program was selected as the most suitable program for the inelastic dynamic analysis of reinforced concrete elevated highway structures. While the IDARC program should be considered a research tool, it provided capabilities not found in other available programs. These capabilities are highlighted in the next section. It was, however, still necessary to incorporate additional features to the basic version of the IDARC program to permit the analysis of typical elevated highway structures. Also, changes were made to the IDARC program as a result of applying it to the analysis of the Cypress Viaduct. An overview of the basic program features, enhancements and modifications are presented in this section.

2.1 IDARC - An Overview

The basic structure of the IDARC computer program conforms to standard solution techniques involving the displacement method of matrix structural analysis. The main differences between conventional frame analysis programs and IDARC can be summarized as follows:

- A distributed flexibility model is used to construct the element stiffness matrices so that the effects of spread of plasticity are implicitly included. Closed form solutions of the flexibility coefficients are used where possible as are the terms in the inverted flexibility matrix to minimize computation time during stiffness matrix formulation.

- A versatile force-deformation hysteretic model is used to compute the instantaneous tangent stiffness at a member cross-section directly in terms of the flexural rigidity, *EI*. Additional degrees-of-freedom to separate plastic deformations and elastic deformations are, therefore, not needed. The hysteretic model is able to capture the following behavior characteristics common to reinforced concrete: (i) stiffness degradation due to inelastic action, (ii) strength decay due to repeated cycling (generally attributed to dissipated hysteretic energy), and (iii) pinching behavior due to opening and closing of cracks.

- A shear wall element is included which has the capability to model shear and flexure independently, thereby enabling shear-type failures to be detected. Equilibrium loss due to premature shear failure is accommodated.

- Measures of member damage are monitored through the use of an improved damage model which accounts for local ductility demands and dissipated energy at critical sections.

2.2 IDARC Basic Features

IDARC is a program for two-dimensional analysis of three-dimensional structures which can be modeled as parallel frames interconnected by transverse beams. A three-dimensional structural system composed of beams, columns, and shear-walls is synthesized into an assemblage of single-component inelastic elements with coupled shear and flexural deformations. Element stiffness matrices are constructed using a distributed flexibility scheme which implicitly accounts for the effects of spread of plasticity. The resulting dynamic equations of motion are solved using Newmark's unconditionally stable algorithm for constant average acceleration. Analysis results are ultimately expressed as damage indices which provide a qualitative interpretation of the structural response. A brief summary of the underlying theory and basic features of the IDARC program are given below.

2.2.1 Structure Modeling

A three-dimensional structural system composed of columns, shear-walls, beams, and inter-connecting slabs and transverse beams, is modeled using discrete components. A section of a typical building is shown in Fig. 2-1 where the structural configuration is idealized as a series of plane frames linked by transverse beams. Two typical frames in the loading direction are shown in this case. Since a rigid floor assumption is used, the individual lateral frame degrees-of-freedom are reduced to a single master degree-of-freedom. Also, identical frames can simply be lumped together. The following element types are used: (i) beam elements; (ii) column elements; (iii) shear wall elements; (iv) edge column elements; and (v) transverse beam elements.

Beam-column elements are modeled as continuous springs that combine flexure and shear. For shear walls, flexure and shear are modeled independently with flexure and shear springs

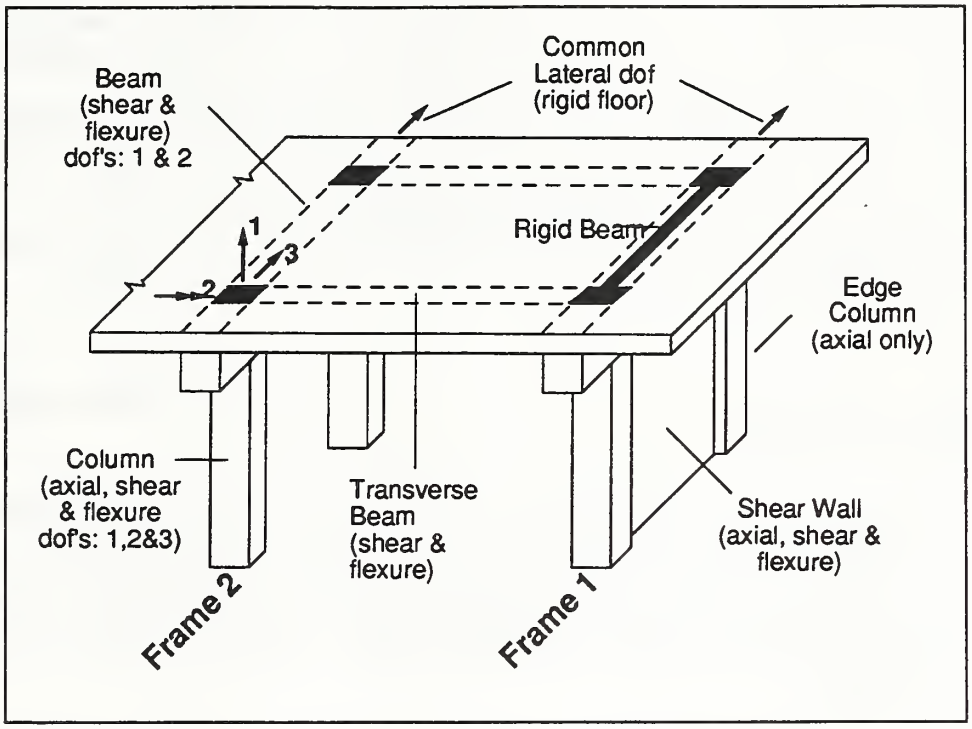

Figure 2-1 Component Modeling of Three-Dimensional Structural System

connected in series. The inelastic behavior of each spring is modeled independently, thereby making it possible to specify independent shear hysteresis. Edge columns of shear walls can be modeled separately using inelastic axial springs. Transverse elements are included primarily to provide flexural-torsional coupling with the main elements. They are assumed to have an effect on both the vertical and rotational deformation of the shear walls or main beams to which they are connected and are modeled using elastic linear and rotational springs. The combination of the above element types can be used to model a variety of three-dimensional structural configurations.

In general, the system of equations to be solved, at any stage of the analysis, assumes the following form:

$$[K]\{u\} = \{F\} \tag{2-1}$$

where $[K]$ is the global stiffness matrix, $\{u\}$ is the vector of unknown nodal displacements, and $\{F\}$ is the vector of applied equivalent forces on the system. Since the stiffness matrix is symmetric and banded, a compact scheme is used to store the resultant matrix in which

the main diagonal is offset to the first column and only the remaining half-band width is saved. Stiffness matrices are stored at the element level. These matrices are then assembled into the global stiffness matrix. The load vector corresponding to the right-hand side of Eq. (2-1) is established depending upon the type of analysis being performed; static, cyclic, or dynamic. Following the solution of the equilibrium equations, the inelastic moments at the ends of each element are computed from the member nodal displacements, and the stiffness matrices are updated in the event of a stiffness change.

2.2.2 Component Modeling

A typical element model is shown in Fig. 2-2. For beams, there are two degrees-of-freedom per node while; for columns and shear walls, an additional axial degree-of-freedom (not shown in the figure) is included at each node. The element formulation is based on an assumed flexibility distribution along the member length. Rigid panel zones are accounted for in the formulation.

Element Flexibility

The moment distribution for a flexural member in a frame subjected to lateral loads, such as those arising from seismic forces, is linear, as shown in Fig. 2-3. In the case of a beam, the presence of gravity loads will alter the distribution somewhat, but for practical purposes, the linear distribution is valid for lateral load moments which far exceed the gravity load moments. The moments produce tensile stresses and, when they exceed the tensile strength of the concrete, cracks form perpendicular to the member axis. The presence of a crack influences the moment of inertia of the section; therefore, the moment of inertia varies along the length of a cracked member. The member curvature, which is inversely proportional to the moment of inertia, also varies along the member length as shown in Fig. 2-3. In the IDARC flexibility formulation, a linear variation of curvature is assumed. This assumption is more realistic than the figure suggests, since the additional inelastic curvature due to yield penetration in the joint and possible diagonal tension cracking is not shown.

For the assumed flexibility distribution, the 2x2 flexibility matrix may be derived from virtual work principles. Flexibility coefficients are obtained from the following relationship:

$$f_{ij} = \int_0^L m_i(x)\, m_j(x)\, \frac{1}{EI(x)}\, dx \qquad (2\text{-}2)$$

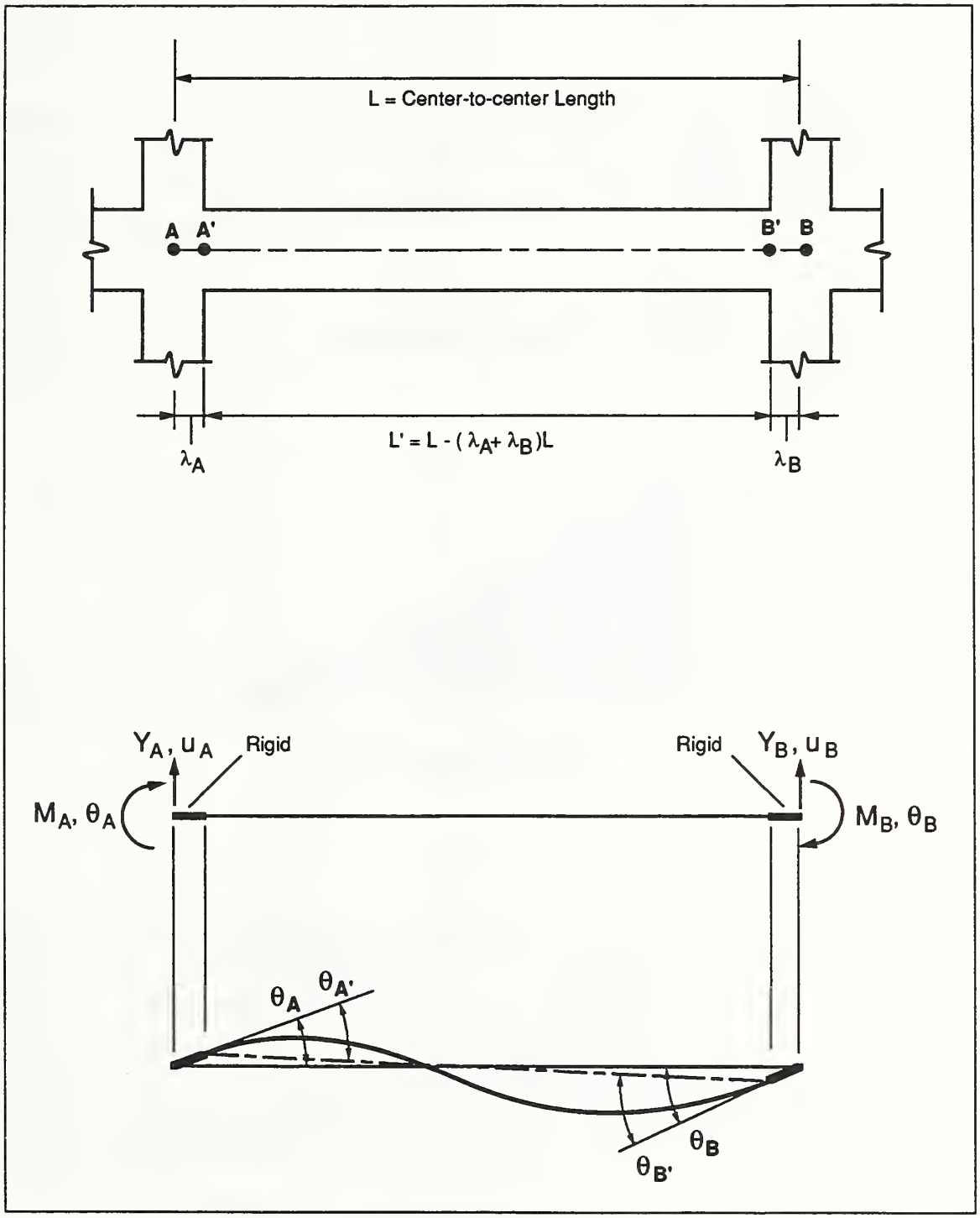

Figure 2-2 Flexural Element Model

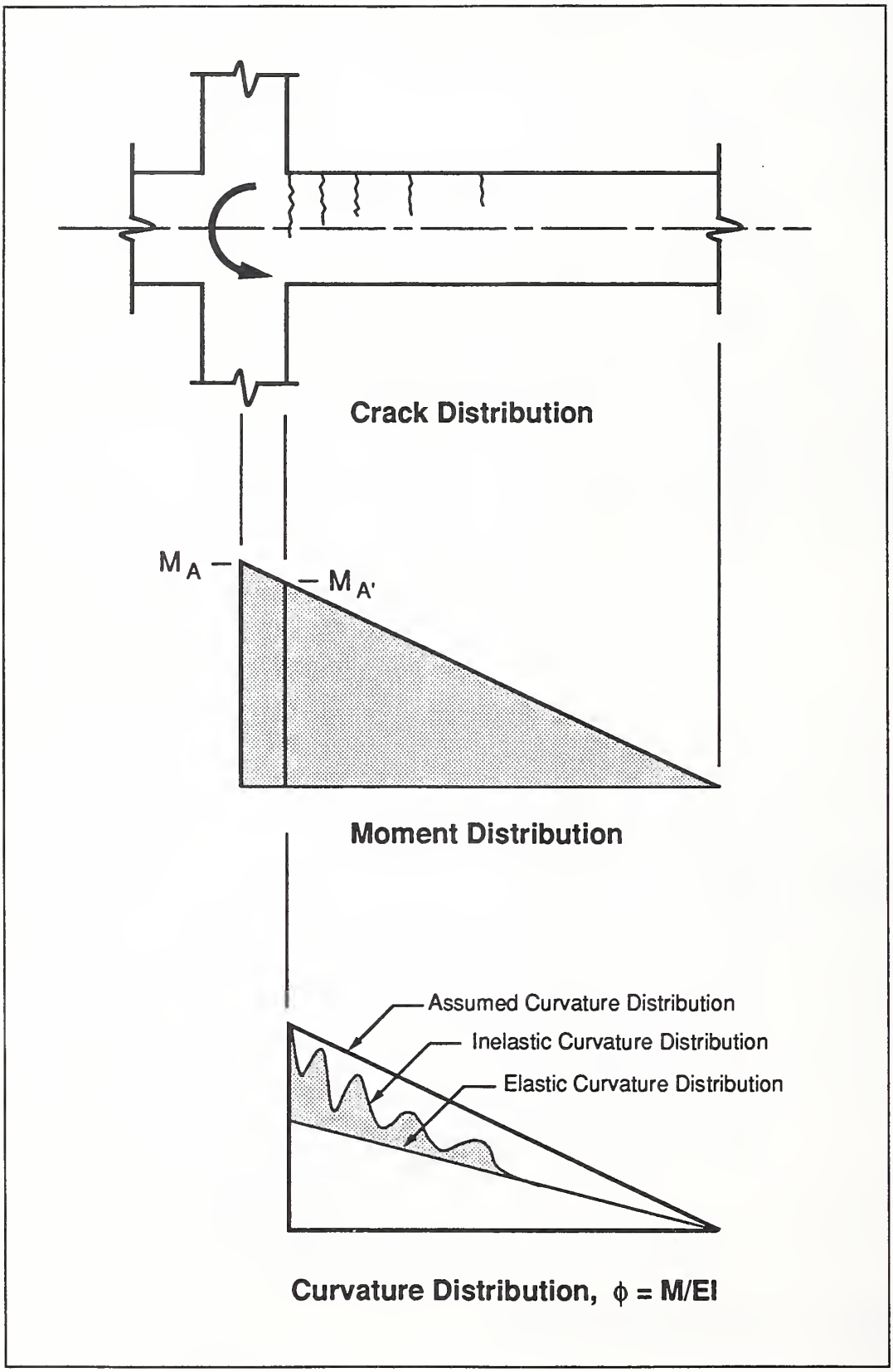

Figure 2-3 Moment and Curvature Distributions along a Flexural Member

where

$m_i(x)$ = moment distribution for unit moment at end i
$m_j(x)$ = moment distribution for unit moment at end j
$EI(x)$ = flexural rigidity

Integration of Eq. (2-2) is carried out in closed form for the assumed linear variation in curvature for members bent in double curvature with a contraflexure point within the member, and members in single curvature with no contraflexure point. The flexibility coefficients are given in Appendix A.

The flexural rigidity, EI, at the ends of the member is monitored throughout the analysis, and the incremental moment-rotation relationship is established from integration of the (M/EI) diagram. The flexibility matrix is expressed in the following incremental form:

$$\begin{Bmatrix} \Delta\theta_A' \\ \Delta\theta_B' \end{Bmatrix} = [f_s] \begin{Bmatrix} \Delta M_A' \\ \Delta M_B' \end{Bmatrix} \tag{2-3}$$

where $\Delta\theta_A'$, $\Delta\theta_B'$ are the incremental rotations corresponding to the moment increments $\Delta M_A', \Delta M_B'$, and

$$[f_s] = L' \begin{bmatrix} f_{11} & f_{12} \\ f_{21} & f_{22} \end{bmatrix} + \frac{1}{GA^*L} \begin{bmatrix} 1 & -1 \\ -1 & 1 \end{bmatrix} \tag{2-4}$$

in which L' is the clear length of the member, G is the shear modulus, A^* is the effective shear area, and f_{ij} are the flexibility coefficients. The combination of shear and flexure in series, as suggested in Eq. (2-4), is used only for the shear wall elements so that a shear failure of the component may be taken into account. Shear effects are implicitly included in the flexural rigidity term for columns and beams, and consequently, the second term in Eq. (2-4) is not needed. Details of this equivalent shear-flexure spring are reported in Kunnath et al [1990].

Rigid Panel Zones

The following transformation matrices are required to relate the moments and rotations across the rigid panel zones:

$$\begin{Bmatrix} \Delta M_A \\ \Delta M_B \end{Bmatrix} = [C] \begin{Bmatrix} \Delta M_A' \\ \Delta M_B' \end{Bmatrix} \tag{2-5}$$

and

$$\begin{Bmatrix} \Delta \theta_A' \\ \Delta \theta_B' \end{Bmatrix} = [C]^T \begin{Bmatrix} \Delta \theta_A \\ \Delta \theta_B \end{Bmatrix} \tag{2-6}$$

where

$$[C] = \frac{1}{1-\lambda_A-\lambda_B} \begin{bmatrix} 1-\lambda_B & \lambda_A \\ \lambda_B & 1-\lambda_A \end{bmatrix} \tag{2-7}$$

and λ_A and λ_B are the lengths of the rigid panel zones as shown in Fig. 2-2.

Element Stiffness Matrix

A sub-element stiffness, involving only the rotational degrees-of-freedom, can be obtained from Eqs. (2-3), (2-5) and (2-6) as follows:

$$\begin{Bmatrix} \Delta M_A \\ \Delta M_B \end{Bmatrix} = [k_s] \begin{Bmatrix} \Delta \theta_A \\ \Delta \theta_B \end{Bmatrix} \tag{2-8}$$

where

$$[k_s] = [C][f_s]^{-1}[C]^T \tag{2-9}$$

where $[f_s]^{-1}$ is the inverse of the flexibility matrix given by Eq. (2-4) and $[C]$ is the transformation matrix given by Eq. (2-7)

From force-equilibrium, the following relationship is obtained:

$$\begin{Bmatrix} \Delta Y_A \\ \Delta M_A \\ \Delta Y_B \\ \Delta M_B \end{Bmatrix} = [R_B] \begin{Bmatrix} \Delta M_A \\ \Delta M_B \end{Bmatrix} \tag{2-10}$$

where $[\Delta Y]$ and $[\Delta M]$ are the incremental form of the transverse force and moment, respectively, (shown in Fig. 2-2) and

$$[R_B] = \begin{bmatrix} -1/L & -1/L \\ 1 & 0 \\ 1/L & 1/L \\ 0 & 1 \end{bmatrix} \tag{2-11}$$

where L is the member length.

Substitution of Eq. (2-8) into Eq. (2-10) yields:

$$\begin{Bmatrix} \Delta Y_A \\ \Delta M_A \\ \Delta Y_B \\ \Delta M_B \end{Bmatrix} = [R_B][k_s] \begin{Bmatrix} \Delta \theta_A \\ \Delta \theta_B \end{Bmatrix} \tag{2-12}$$

From the geometry of the deformed shape of the element, it is possible to show that:

$$\begin{Bmatrix} \Delta\theta_A \\ \Delta\theta_B \end{Bmatrix} = [R_B]^T \begin{Bmatrix} \Delta u_{yA} \\ \Delta\theta_A \\ \Delta u_{yB} \\ \Delta\theta_B \end{Bmatrix} \tag{2-13}$$

Hence, combining Eqs. (2-12) and (2-13) one obtains

$$\begin{Bmatrix} \Delta Y_A \\ \Delta M_A \\ \Delta Y_B \\ \Delta M_B \end{Bmatrix} = [K_B] \begin{Bmatrix} \Delta u_{yA} \\ \Delta\theta_A \\ \Delta u_{yB} \\ \Delta\theta_B \end{Bmatrix} \tag{2-14}$$

where

$$[K_B] = [R_B][k_s][R_B]^T \tag{2-15}$$

is the beam element stiffness matrix.

2.2.3 Hysteretic Modeling

IDARC includes a versatile hysteretic model in which a non-symmetric tri-linear curve, in conjunction with three user-specified parameters, is used to produce the effects of stiffness degradation, strength deterioration and pinching. Stiffness degradation is achieved by reducing the unloading stiffness as a function of ductility. Strength deterioration is introduced as a function of dissipated hysteretic energy. Finally, pinching or slip behavior (caused by crack-closing) is incorporated by lowering the target point of the force-deformation curve upon crossing the force-axis. The hysteretic loop behavior illustrating each of the above effects is shown in Fig. 2-4. The three parameters can be combined in a variety of ways to produce a range of hysteretic behavior. Details of the implementation of the hysteretic model can be found in Park et al [1987].

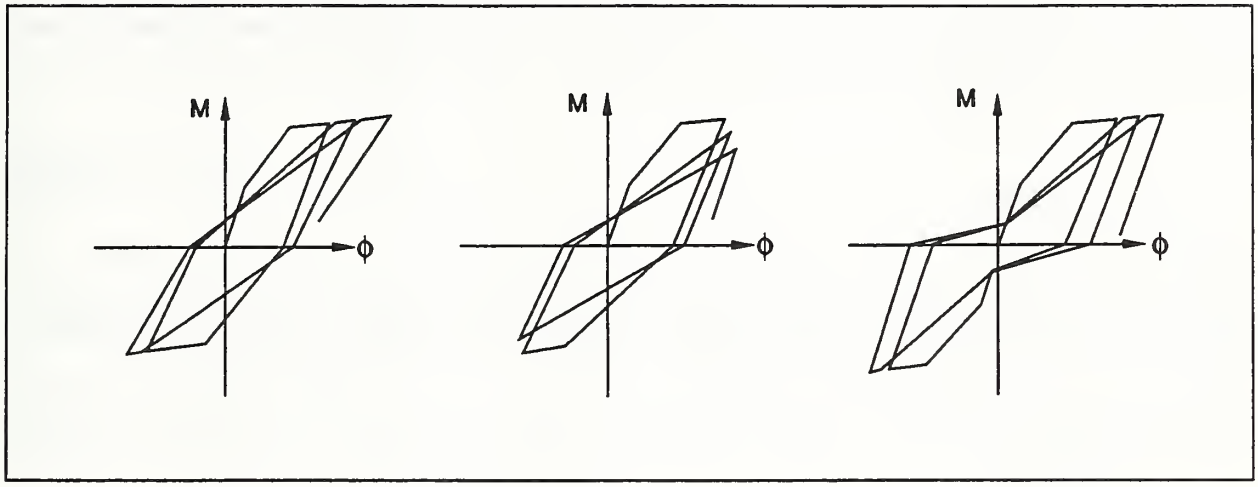

Figure 2-4 Modeling of Hysteretic Behavior

2.2.4 Damage Modeling

The damage model proposed by Park, Ang and Wen [1984] is incorporated in the IDARC program. The model requires member deformations to be specified in terms of equivalent lateral displacement. The component damage index, D_c, is computed as follows:

$$D_c = \frac{\delta_m}{\delta_u} + \beta \frac{E_T}{\delta_u P_y} \tag{2-16}$$

where P_y is the yield capacity of the section, δ_u is the ultimate deformation capacity of the component, β is an empirical strength degrading parameter [Park, 1984], δ_m is the maximum member deformation and E_T the total dissipated energy. The yield capacity, ultimate deformation, and strength degrading parameter are determined from section properties of the member prior to the dynamic analysis while the maximum member deformation and total dissipated energy are established from the analysis.

Three damage indices are computed as follows:

i) A damage index for each of the main building components, D_c (i.e., beams, columns and shear walls)

ii) A story level damage index, D_s

iii) A global damage index for the structure, D_g

The story level damage indices are computed from the damage index values of the components comprising that story level, as follows:

$$D_s = \sum_{i=1}^{n} \lambda_{ci} D_{ci} \tag{2-17}$$

where n is the number of componemts contributing to the story level damage index and

$$\lambda_{ci} = \frac{E_{ci}}{\sum E_{ci}} \tag{2-18}$$

where λ_i is a weighting factor, E_{ci} is the energy dissipated by a component and $\sum E_{ci}$ is the energy dissipated by all components in a story. The vertical components (columns, shear walls) are separated from the horizontal components (beams) in computing the story index. The same concept is also used to combine the damage indices of independent story levels to calculate the global structural damage index, D_g.

2.2.5 Analysis Capabilities

Several different analysis capabilities are available in IDARC including static analysis, fundamental mode calculation, and dynamic analysis. These are explained in more detail here.

Static Analysis

A static analysis capability is provided in IDARC to provide an estimate of the initial stress state in the structure prior to application of the seismic load. The presence of initial stresses, such as those arising from dead loads, may be crucial to the overall system response, especially if the pre-existing loads lead to cracking of components and a shift in the initial period estimate. Loads may be specified in any combination of the following:

- distributed vertical loads on beams
- concentrated vertical nodal loads or moments
- concentrated lateral loads at floor levels

The moments, shears and axial forces resulting from this analysis are carried forth to the dynamic or quasi-static cyclic analysis.

Fundamental Mode Calculation

The fundamental period of the structure is determined using the conventional Stodola method [Clough and Penzien, 1975]. This period is used primarily to assign a constant viscous damping factor during the response analysis. It is important to note that the assigned viscous damping is critical only for elastic response analysis, since the contributions of viscous damping in the inelastic range is negligible when compared to the energy that is dissipated through hysteretic action.

Dynamic Analysis

The incremental solution of the assembled system of equations involves the following dynamic equation of equilibrium:

$$[M]\{\Delta\ddot{u}\} + [C]\{\Delta\dot{u}\} + [K_G]\{\Delta u\} = -[M]\{\Delta\ddot{u}_g\} + \{F_{corr}\} \tag{2-19}$$

where

$[M]$ = lumped mass matrix
$[C]$ = viscous damping matrix
$\{K_G\}$ = instantaneous global stiffness matrix
$\{F_{corr}\}$ = corrective load vector due to unbalanced forces from previous step
$\{\Delta u\}$ = incremental relative displacement vector
$\{\Delta\dot{u}\}$ = incremental relative velocity vector, and
$\{\Delta\ddot{u}\}$ = incremental relative acceleration vector.

Solution of Eq. (2-19) is accomplished by a direct step-by-step integration procedure using Newmark's unconditionally stable algorithm assuming constant-average-acceleration [Bathe and Wilson, 1976]. A constant time step is used throughout the analysis. The effective load vector may consist of both the horizontal and vertical components of the seismic excitation. The program can scale a ground motion record to any specified peak acceleration.

2.3 IDARC Enhancements

The release version of IDARC [Park et al., 1987], despite its advantages over other existing computer programs, was not suitable for the analysis of typical elevated highway structures which are characterized by circular columns, tapered members, internal hinges, etc. In particular the Cypress Viaduct, which serves as the case study for this investigation, could not be modeled. Several development tasks were, therefore, undertaken to enhance the program and render it suitable for analysis of typical elevated highway structures subjected to simultaneous horizontal and vertical base excitations. The various tasks are summarized in the following sections.

2.3.1 Specification of Section Properties at Member Ends

The release version of IDARC assumed constant section properties throughout a member. Clearly, this is not the case for many elements, especially beams where positive and negative reinforcement varies along the member length. Also, the use of tapered members could not be accommodated because of this limitation. The IDARC program was changed to accommodate different section properties at the two ends of a member. Furthermore, this also enables the possibility to model members with continually changing cross-section by sub-dividing the member into sub-elements.

2.3.2 User-Defined Section Properties

IDARC develops cross-sectional moment-curvature characteristics for most elements, except shear walls (where a fiber model analysis is carried out), using empirical models based on available experimental data. It is foreseeable that the results obtained using such empirical expressions may be unsuitable for certain cross-sections and non-standard reinforcement details. It was, therefore, essential to incorporate into the program an alternative to allow users to specify directly moment-curvature or force-deformation envelopes for each member. These envelopes are characterized by both cracking and yield points and may be non-symmetric in tension and compression.

2.3.3 User-Defined Mass Distribution

Since the program is written primarily for lateral load analysis, the moment distribution in a member is assumed to be linear. However, for the case where dead loads produce transverse loading on a member, the moment distribution is not linear. To simulate the dead load moment distribution in beams, it is necessary to specify masses or loads at internal beam nodes. Thus, the existing option for specifying floor weights was modified to allow for a user-defined distribution of masses across a floor. This option permits the simulation of gravity load moments and shears in the inelastic range by prescribing a vertical excitation in the form of a ramp which gradually attains a peak ground acceleration of 1.0 g.

2.3.4 Quasi-static Cyclic Loading

The modeling of reinforced concrete in the inelastic range is a complex task, given the range of probable post-yield behavior phenomena. The use of hysteretic models simplifies the overall modeling problem but introduces a new set of unknowns, viz., the hysteretic parameters which control the hysteresis characteristics. Commonly, these parameters can be identified more accurately through laboratory tests of components and subassemblages. Hence, an option was added to IDARC to perform a quasi-static analysis under either load or displacement controlled increments, with the objective of providing a tool to simulate laboratory experiments and thereby ascertain the nature of the hysteretic control parameters.

2.3.5 Circular Column Element

A circular column element was added to the existing library of inelastic elements since a number of bridge piers have this configuration. The yield moment, ultimate moment and corresponding curvatures are obtained from standard methods to be found in the literature [Park and Paulay, 1975]. Fig. 2-5 shows a cross-section of a circular column with circular arrangement of longitudinal bars. If a linear strain distribution is assumed, it is possible to obtain the depth to the neutral axis from equilibrium of the concrete and steel forces in the presence of axial forces.

The force in the concrete is given by

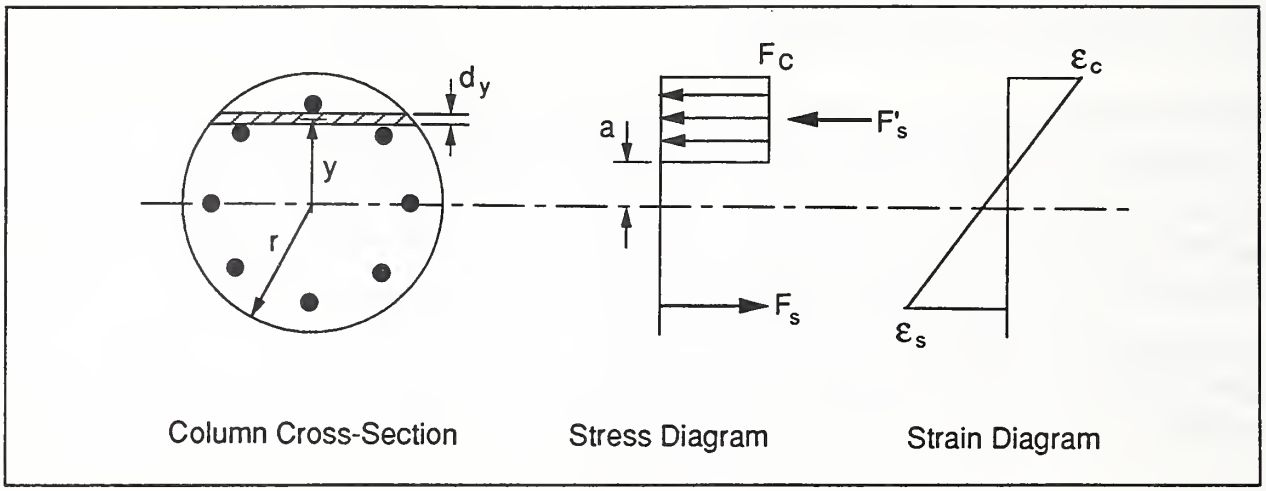

Figure 2-5 Circular Column with Circular Arrangement of Longitudinal Reinforcement

$$F_c = 0.85 f_c' \int_a^r 2\sqrt{r^2 - y^2}\, dy \tag{2-20}$$

where r, y and a are as shown in Fig. 2-5 and f_c' is the unconfined concrete compressive stress. The moment resisted by the concrete about the center line, M_c, is

$$M_c = 0.85 f_c' \int_a^r 2\sqrt{r^2 - y^2}\, y\, dy \tag{2-21}$$

or, upon evaluation of the integral,

$$M_c = 0.85 f_c' \left\{ \frac{2\left(\sqrt{r^2 - a^2}\right)^3}{3} \right\} \tag{2-22}$$

The force in the steel is determined by assuming a maximum extreme concrete strain of 0.3% and the stress in the bottom steel is obtained from the corresponding strain (limited to a maximum of f_y). The total moment resisted by the section is referred to as its yield capacity and is given by

$$M_y = 0.85 f_c' \left\{ \frac{2\left(\sqrt{r^2 - a^2}\right)^3}{3} \right\} + \sum_{i=1}^{n} y E_s \varepsilon_s A_{st} \tag{2-23}$$

where E_s is the modulus of elasticity of steel, ε_s is the strain in the reinforcing steel, A_{st} is the area of the reinforcing steel, and n is the number of reinforcing bars.

Effect of Hoop Spacing on Column Capacity

The effect of hoop spacing on the moment-curvature envelope is introduced in the following manner. It is assumed that the capacity of the column remains unchanged after the concrete cover has spalled. Hence,

$$0.85 f_c' A_g = f_{cc}' A_{cc} \tag{2-24}$$

where f_{cc}' is the confined compressive strength, A_g is the gross area of concrete, and A_{cc} is the area of core concrete.

An expression relating confined-to-unconfined strength of concrete is given by Park and Paulay [1975] as

$$f_{cc}' = f_c' + 2.05 \rho_s f_y \tag{2-25}$$

where f_y is the yield strength of the reinforcing steel and ρ_s is the volumetric ratio of confinement steel-to-concrete core and is computed as

$$\rho_s = \frac{A_h \pi d_c}{s A_{cc}} \tag{2-26}$$

where A_h is the cross-sectional area of hoop steel, d_c is the diameter of the concrete core, s is the hoop spacing, and A_{cc} is the area of the concrete core.

By substituting Eq. (2-25) into Eq. (2-24) and solving for f_c', one obtains the following expression for the modified concrete compressive stress, f_{cm}':

$$f'_{cm} = \frac{(f'_c + 2.05\,\rho_s f_y) A_{cc}}{0.85 A_g} \tag{2-27}$$

2.3.6 Tapered Element With Distributed Flexibility

A new distributed flexibility formulation was derived for tapered prismatic members. In the original IDARC program, the flexural rigidity, $1/EI$, was assumed to vary linearly for prismatic members with constant cross-sections. However, for tapered members, the moment of inertia is assumed to vary linearly along the member length, resulting in the flexural rigidity varying nonlinearly as shown in Fig. 2-6.

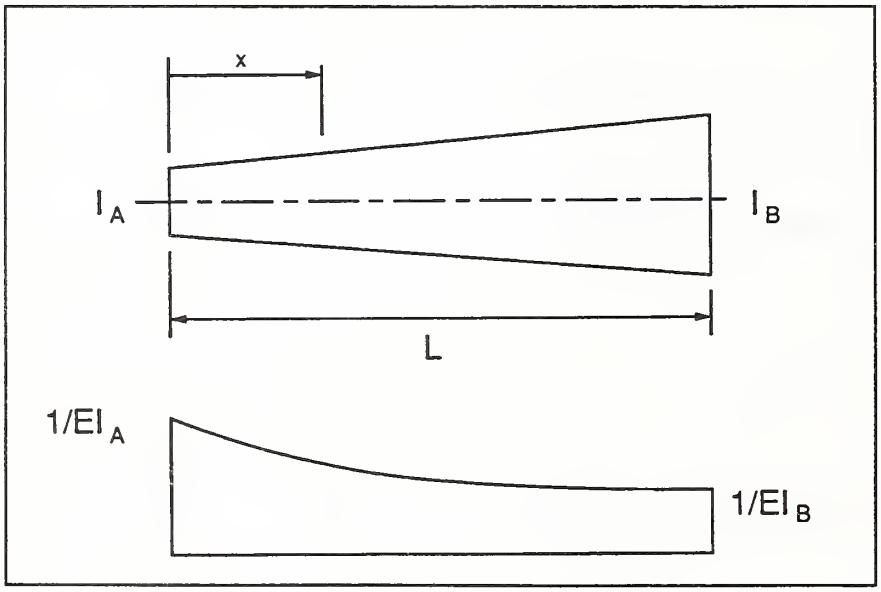

Figure 2-6 Tapered Flexural Element with Distributed Flexibility

It is therefore necessary to carry out a numerical integration along the member to evaluate the flexibility coefficients. The flexibility coefficients are obtained from the following integrals:

$$f_{11} = \int_0^L \frac{1}{EI_x}\left(1 - 2\frac{x}{L} + \frac{x^2}{L^2}\right) dx \tag{2-28}$$

$$f_{12} = -f_{21} = \int_0^L \frac{1}{EI_x}\left(-\frac{x}{L} + \frac{x^2}{L^2}\right)dx \tag{2-29}$$

$$f_{22} = \int_0^L \frac{1}{EI_x}\left(\frac{x^2}{L^2}\right)dx \tag{2-30}$$

where

$$\frac{1}{EI_x} = \frac{1}{EI_A} + \frac{x}{L}\left(\frac{1}{EI_B} - \frac{1}{EI_A}\right) \tag{2-31}$$

2.3.7 Rotational Spring Element

A new program module incorporating rotational springs was created with two options: (i) discrete inelastic spring at any node; and (ii) a perfect hinge.

Modeling of Discrete Inelastic Spring

A discrete spring connecting a member to a joint may be located at any node in the structure. The moment-rotation characteristics of the spring can be specified as a non-symmetric tri-linear envelope with degrading parameters. Alternatively, the spring stiffness may be specified either as a relatively small value or an infinitely large value to simulate a hinge or rigid connection, respectively. A maximum of three springs is allowed at any node, as shown in Fig. 2-7. The spring stiffness is incorporated into the overall structural stiffness matrix as follows:

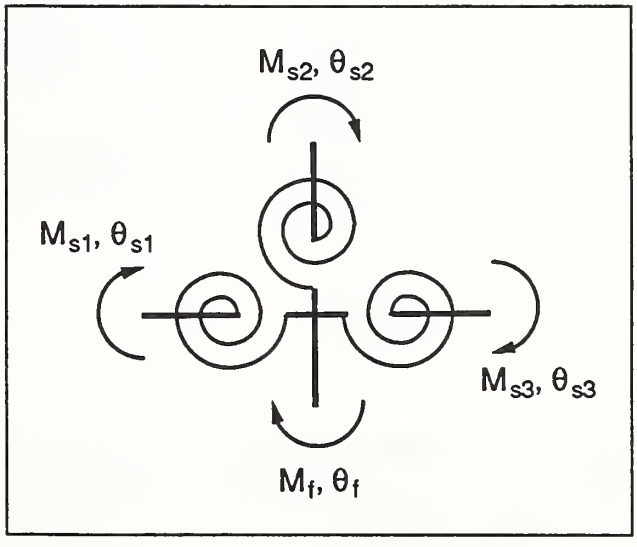

Figure 2-7 Inelastic Spring Element

$$\begin{Bmatrix} M_{si} \\ M_f \end{Bmatrix} = k_{\theta i} \begin{bmatrix} 1 & -1 \\ -1 & 1 \end{bmatrix} \begin{Bmatrix} \theta_{si} \\ \theta_f \end{Bmatrix} \tag{2-32}$$

where M_{si} and M_f refer to the spring moment and the fixed moment respectively, θ_{si} and θ_f are the corresponding rotations, and $k_{\theta i}$ is the instantaneous tangent stiffness of the spring element. Spring rotations are always expressed as a function of the independent joint rotation which must remain fixed.

Modeling of Perfect Hinge

A perfect member hinge is modelled by setting the hinge moment to zero and condensing out the corresponding degree-of-freedom. Using the notation in Fig. 2-8, one obtains the following relationship between the moments at the center of the joint and the face of the member:

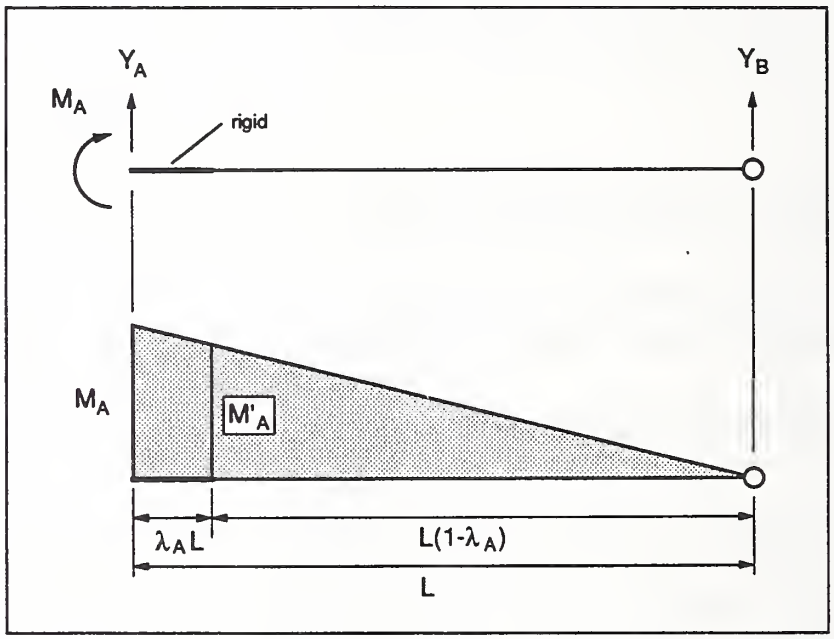

Figure 2-8 Modeling Member Releases

$$M_A = \left[\frac{1}{1-\lambda_A}\right] M'_A \tag{2-33}$$

The element stiffness equation relating moment and rotation is

$$\{M_A\} = k_s \{\theta_A\} \tag{2-34}$$

and

$$k_s = k_{11} - \frac{(k_{12})^2}{k_{22}} \tag{2-35}$$

where k_{ij} are the coefficients of the inverted flexibility matrix. Finally, from equilibrium of forces, the 3x3 element stiffness matrix is constructed as follows:

$$\begin{Bmatrix} Y_A \\ M_A \\ Y_B \end{Bmatrix} = \{R_B\}\left[\frac{1}{1-\lambda_A}\right]\{R_B\}^T \begin{Bmatrix} \theta_A \\ \theta_A \\ \theta_B \end{Bmatrix} \tag{2-36}$$

and

$$\{R_B\} = \left\{-\frac{1}{L} \quad 1 \quad \frac{1}{L}\right\}^T \tag{2-37}$$

2.4 Modeling Improvements Based on Case Study

The enhancements outlined in this section pertain to specific tasks that were undertaken as a result of problems encountered in the analysis of the Cypress structure. Specifically the following issues were addressed: (i) calibration and estimation of damage indices, (ii) study of numerical drift in observed response, and (iii) criteria for handling unequilibrated forces due to stiffness changes.

2.4.1 Modifications to Damage Model

The damage model in the original release version of IDARC is that developed by Park, Ang and Wen [1985] wherein structural component damage, D_c, is expressed as a linear combination of ductility (deformation) damage and that contributed by hysteretic energy dissipation due to repeated cyclic loading. Direct application of the model to structural systems requires determination of an overall member deformation. Since inelastic behavior is confined within plastic zones near the ends of a member, the relationship between overall member deformation, local plastic rotations and the damage index is difficult to correlate.

Moreover, the presence of internal member hinges (as is the case in the Cypress structure) renders the model unusable. Therefore, a modified version of the component damage model was developed, based on moment and curvature, as follows:

$$D_c = \frac{\phi_m - \phi_r}{\phi_u - \phi_r} + \frac{\beta}{M_y \phi_u} A_T \tag{2-38}$$

where

ϕ_m = maximum curvature attained during load history
ϕ_u = ultimate curvature capacity of section
ϕ_r = recoverable curvature at unloading
β = strength degrading parameter
M_y = yield moment of section
A_T = total area contained in $M-\phi$ loops

The quantity A_T does not correspond to the original energy term in Park's model. However, it does represent an implicit measure of energy, and when normalized as indicated above, was found to correlate fairly well with the original strength-degrading parameter, β.

A similar relationship for shear deformation was also incorporated. This damage index can be used directly to determine damage at each member cross-section. In the present study, the maximum of the two end-section damage indices was used to represent the component damage index. As in the original IDARC program, two additional indices are also reported: a story level damage index; and an global structural damage index. However, the weighting factor used in the revised IDARC code is different from that used in the original program. For vertical elements, viz., columns and walls, the weighting factor is directly proportional to the axial stress level in the element, whereas for beams, an equal weighting factor is given to all elements. The global damage index is computed by combining story level indices and using a new weighting factor for each level. In this program version, the lowest story level was given the maximum weight, decreasing proportionally to the top story level as a function of cumulative story weights.

2.4.2 Modeling of Distributed Flexibility

The initial set of displacement response histories from the seismic analysis of the Cypress Viaduct structure subjected to the Outer Harbor Wharf record indicated a significant

amount of permanent drift. To ascertain that this was not entirely numerical in nature, a detailed study of the distributed flexibility approach in IDARC was undertaken.

Continuously Varying Flexibility Model

The original model in the IDARC program will be termed the continuously varying flexibility model. As shown in Fig. 2-9, this model results in a flexibility that is influenced greatly by the location of the contraflexure point. It has been suggested by Otani [1974] that such a model may sometimes lead to numerical instability. An ideal situation would be one wherein the average location of the contraflexure point for each member is established based on some preliminary analyses using a varying contraflexure point. This data could then be re-input into the computer program for subsequent analysis. Obviously, such an approach is not suitable for a general user of the IDARC code. It was decided, therefore, to investigate a model with a fixed point of contraflexure.

Fixed Contraflexure Point

In the fixed contraflexure points model, the flexural rigidity, *EI*, was assumed to remain elastic at the mid-point of the member. Since the stiffness was allowed to vary only at the ends of a member, it was reasoned that this approach should result in a more stable form of the flexibility matrix. The distinction is shown in Fig. 2-9. A comparison of the upper level lateral displacement time-history of the Cypress Viaduct structure subjected to the Outer Harbor Wharf ground acceleration (see Section 3) using a fixed and varying contraflexure point is shown in Fig. 2-10.

A number of other alternatives were also investigated. These involved a partial variation of the contraflexure point based on an average location as determined from previous analyses. It was found that most of these variations oscillated around the solution obtained for the case of the fixed contraflexure point, indicating that the use of a fixed contraflexure point is both convenient and appropriate.

2.4.3 Equilibrium Loss in Shear Springs

Since the various distributed flexibility models produced nearly identical results, another aspect of system instability was investigated. This has to do with the loss of equilibrium between applied and restoring forces at the end of a time step following a change of state in one or more members. Presently, all unbalanced forces are added at the start of the next

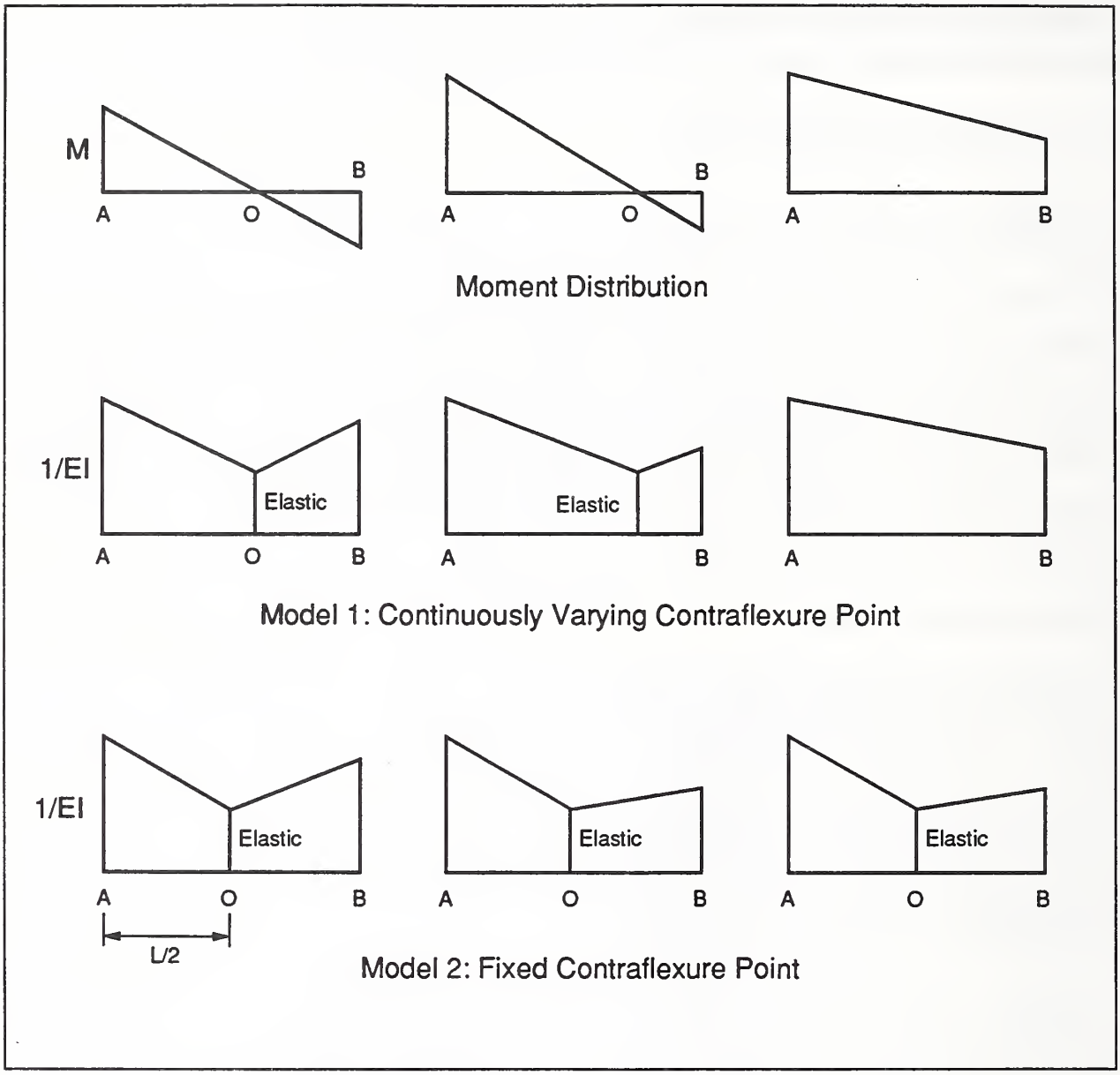

Figure 2-9 Modeling Distributed Flexibility

step (and removed subsequently to prevent accumulation of erroneous external forces). Such a unbalanced force correction was applied only to the moments, since they represented the primary yielding mechanism. However, in the present study of the Cypress Viaduct, a significant source of inelastic behavior comes from the pedestal regions, modeled in this study as shear wall elements. The correction of unbalanced moments caused by shear failure is not straight-forward. A procedure was devised to include this correction, as follows (see Fig. 2-11).

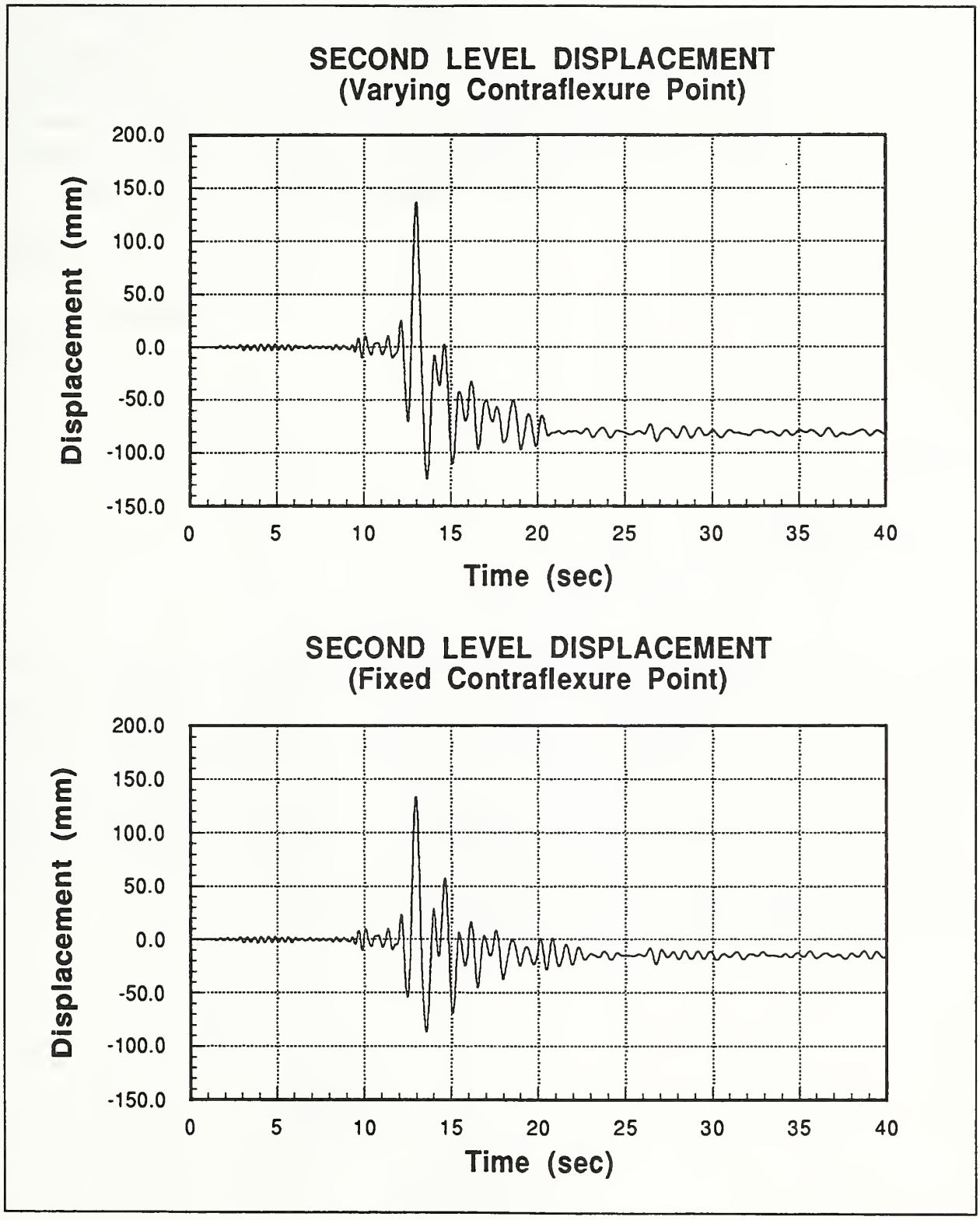

Figure 2-10 Comparison of Response for Fixed and Varying Contraflexure Point

Assume that, at time t_i the moments at ends A and B are M_A and M_B, respectively. At time step t_{i+1}, let the incremental moments at the ends be ΔM_A and ΔM_B. This gives rise to an incremental shear, $\Delta V = V_{i+1} - V_i$, given by $(\Delta M_A - \Delta M_B)/L$ using the sign convention shown. If this incremental shear causes a change of state in the shear spring, the hysteretic model returns an unbalanced force, ΔV_e, as illustrated in Fig. 2-11. Corrective moments are then applied resulting in corrected incremental moments, ΔM_A^* and ΔM_B^*, as follows:

$$\Delta M_A^* = \Delta M_A - C_f \Delta V_e \tag{2-39}$$

$$\Delta M_B^* = \Delta M_B - (1 - C_f) \Delta V_e \tag{2-40}$$

where

$$C_f = \frac{M_A}{(M_A - M_B)} L \tag{2-41}$$

The use of corrective forces as described above was implemented in the model with a fixed contraflexure point. The comparative response is shown in Fig. 2-12. It can be seen that this approach has the tendency to modify the input history, resulting in a slightly different response. Based on this and other case studies using a number of different records, it was found that the use of corrective forces as suggested in this section is not warranted for this study. However, since this technique is implemented in other programs such as DRAIN-2D [Kanaan and Powell, 1973] and SAKE [Otani, 1974], and has been found to improve responses in certain cases, it has been retained as a user option.

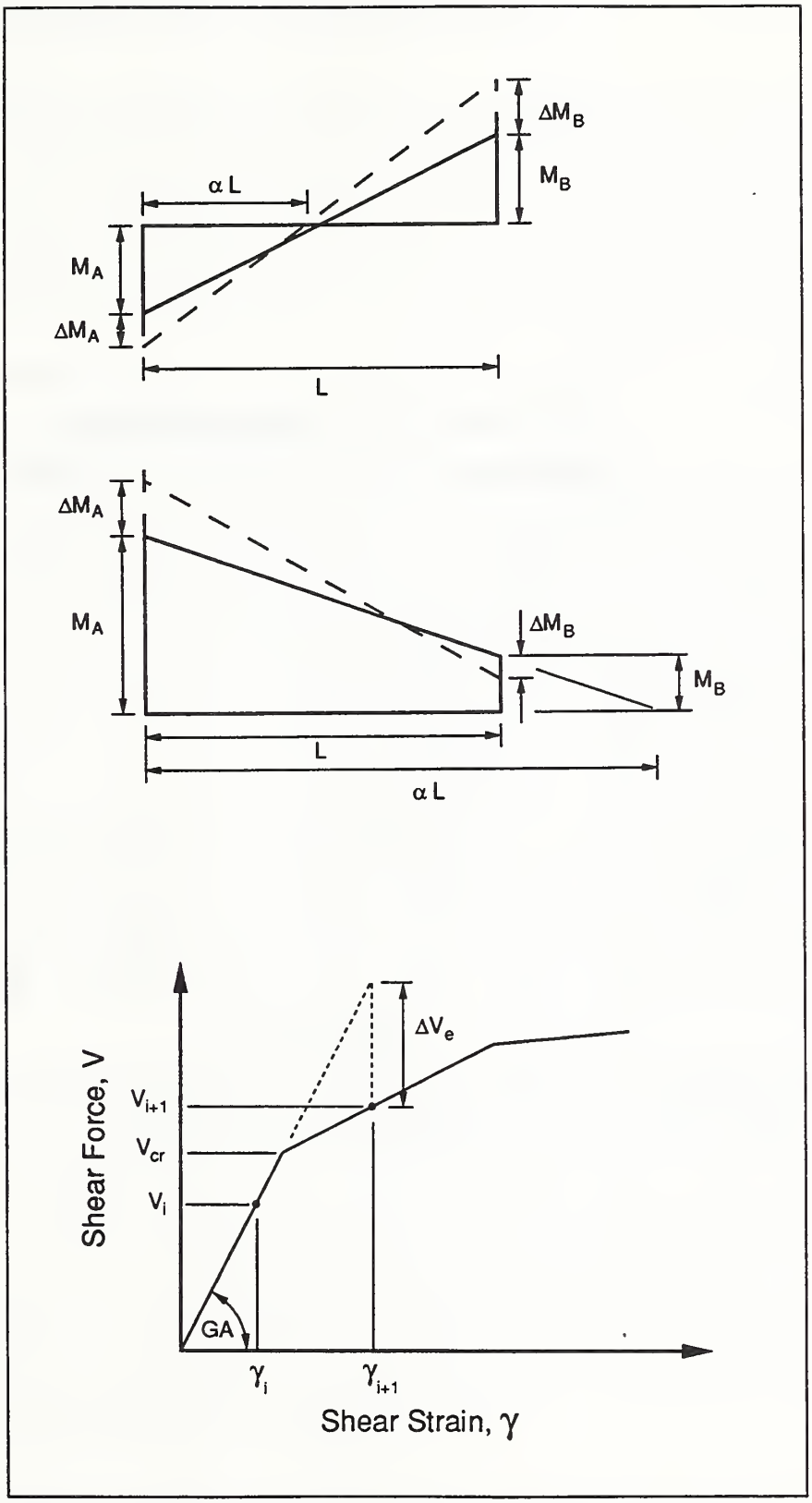

Figure 2-11 Procedure for Compensating for Equilibrium Loss in Shear Springs

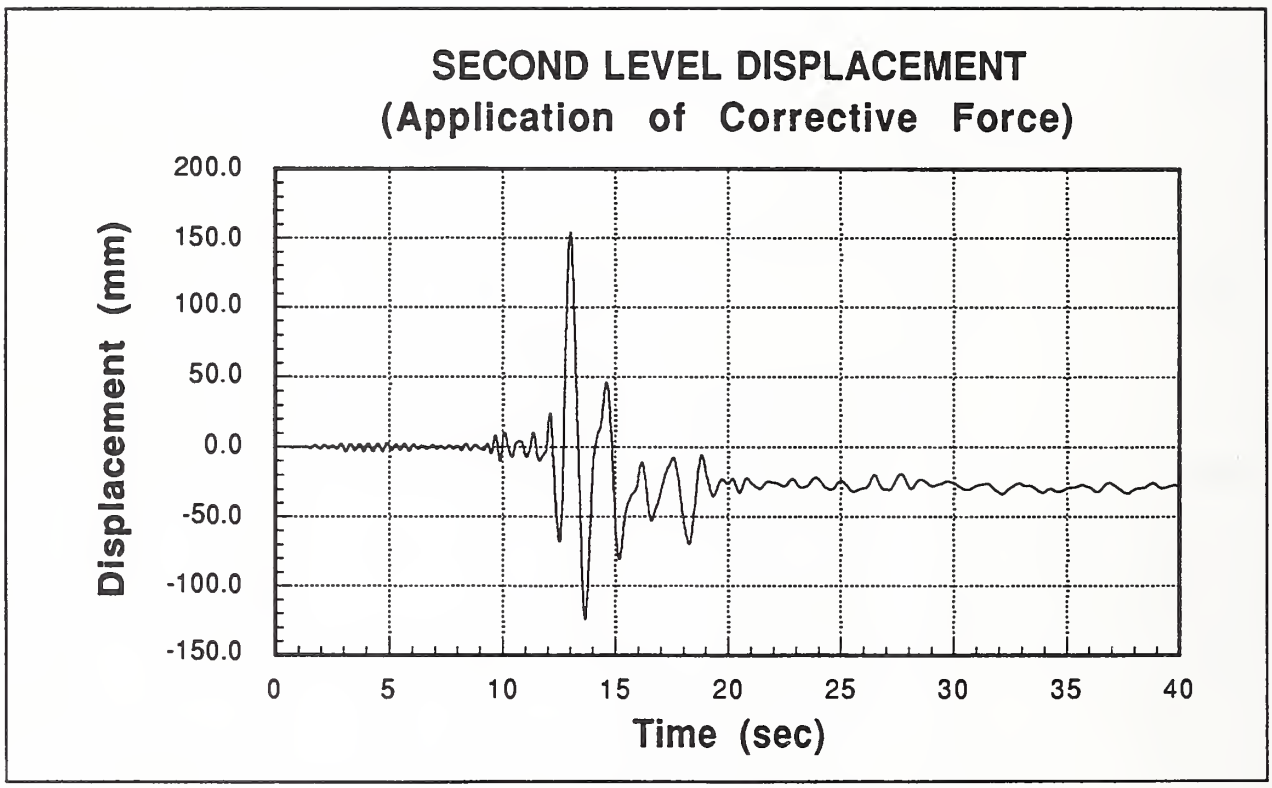

Figure 2-12 Response for Model with Applied Corrective Force

3.0 Case Study: The Cypress Viaduct

The 1989 Loma Prieta earthquake has provided the engineering profession with data on the performance of structures against which analytical simulations can be compared. The Cypress Structure which collapsed in the earthquake, and for which there exists experimental data from both static and dynamic tests, provides an excellent opportunity to evaluate the effectiveness of both the inelastic damage computer analysis as well as modeling techniques. In this section, the application of IDARC to the analysis of the Cypress Viaduct is described.

3.1 Description of the Cypress Viaduct

The Cypress Viaduct, a two-mile elevated section of the Nimitz Freeway, was part of a major interstate highway (I 880) linking Oakland with the San Francisco-Oakland Bay Bridge (see Fig. 3-1). It was located approximately 100 km (62 mi) from the epicenter of the earthquake. The Cypress Viaduct followed Cypress Street and was bounded by 7th Street on the south and 34th Street on the north (see Fig. 3-2). The double deck viaduct carried four lanes of northbound traffic on the lower level and four lanes of southbound traffic on the upper level.

The upper and lower level box girder roadway decks were supported by 83 reinforced concrete bents. There were 11 different bent configurations as shown in Fig. 3-3. Of the 83 total bents, 53 (or 64%) were Type B1 bents, and of the 48 bents that collapsed, 29 (or 60%) were Type B1 bents. In this study, only the Type B1 bent is considered.

Type B1 bents consisted essentially of two portal frames, one on top of the other. Typical dimensions for the Type B1 bent are shown in Fig. 3-4. The lower portal frame consisted of two rectangular columns measuring 1.22 m (48 in) wide by 1.83 m (72 in) deep, and a transverse beam measuring 1.22 m (48 in) wide by 2.44 m (96 in) deep. Above the lower level transverse beam were short column sections, 0.69 m (27 in) high, referred to here as pedestals. The upper portal frame was supported on top of the pedestals and connected by means of a shear key, which provided essentially no moment resistance. The columns of the upper portal frame were tapered, ranging from 0.91 m (36 in) deep at the bottom to 1.22 m (48 in) at the top and were 1.22 m (48 in) wide . The upper level transverse beam had the same dimensions as the lower beam.

The center-to-center spacing between bents ranged from 21.6 to 27.4 m (71 to 90 ft) with a typical spacing of 24.4 m (80 ft). The height of the roadways varied along the length of the viaduct with typical heights above the foundation of 7.62 m (25 ft) for the lower deck

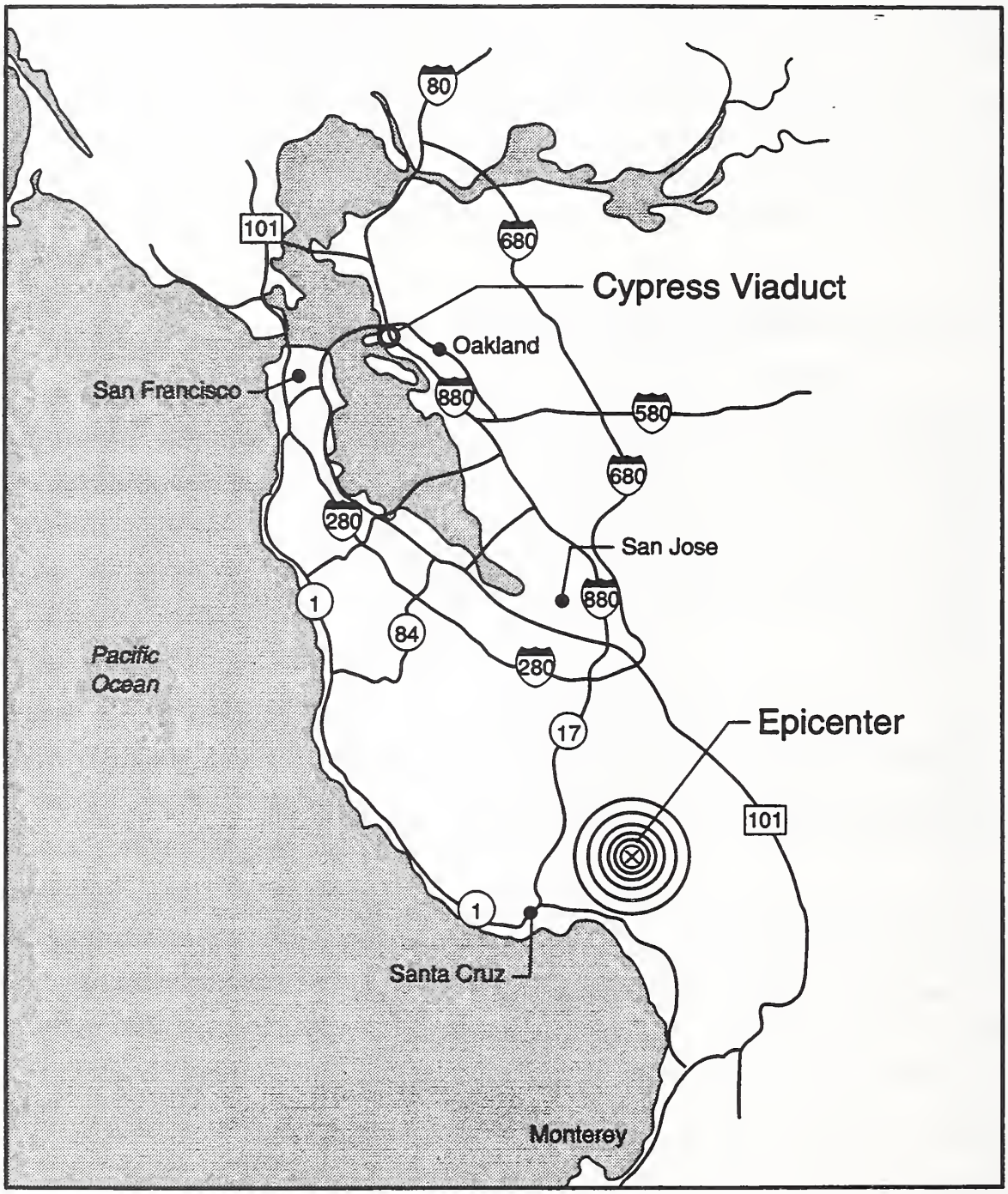

Figure 3-1 Location of Cypress Viaduct

and 14.63 m (48 ft) for the upper deck.

The roadway deck was a reinforced concrete cellular box girder which measured 1.37 m (54 in) deep by 16.56 m (54.33 ft) wide . A typical section is shown in Fig. 3-5. The top flange of the box girder was 165 mm (6.5 in) thick, the bottom flange was 140 mm (5 in) thick and the webs were 203 mm (8 in) thick. For purposes of computing dead weight, the box girder was assumed to be surfaced with 127 mm (5 in) of asphalt.

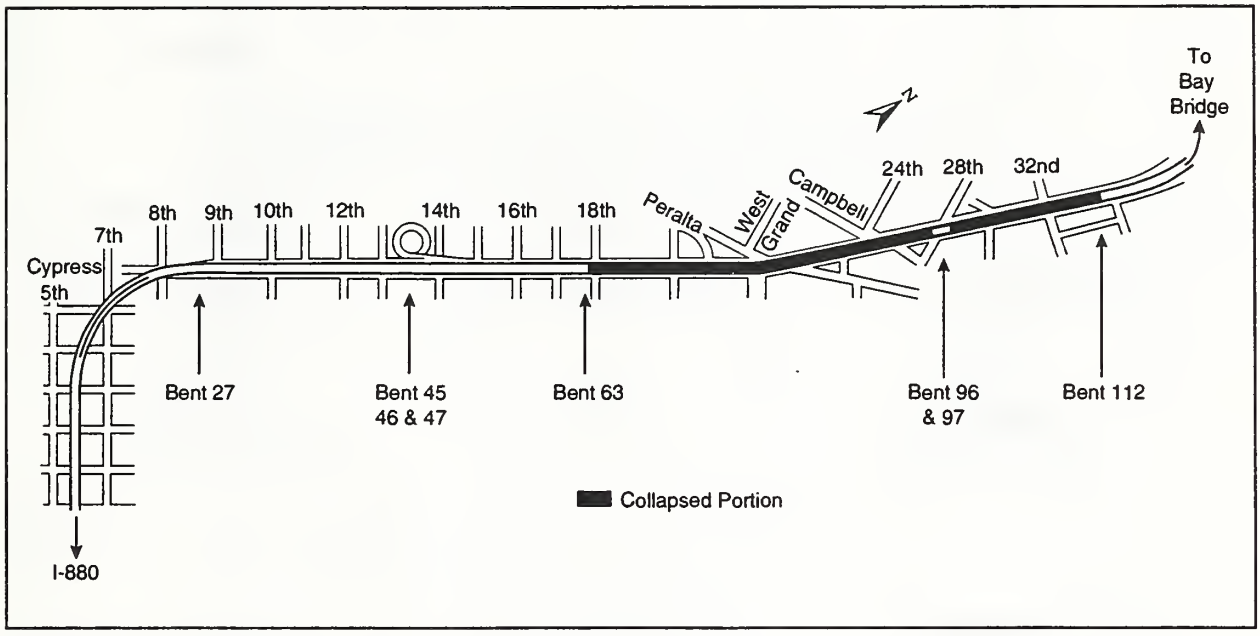

Figure 3-2 Plan of the Cypress Viaduct

The bents were supported on pile caps ranging from 0.91 to 1.52 m (36 to 54 in) thick. The pile caps were in turn supported on 305 mm (1 ft) diameter concrete-filled pipe piles. The number of piles at each column varied, ranging from 18 to 35 piles. The connection between the first level columns and the pile caps was a structural hinge.

The reinforcement layout for the Type B1 bent is shown in Fig. 3-6. The lower level columns are heavily reinforced with 44 #18 (57mm diameter) longitudinal bars. By contrast, the transverse reinforcement was relatively light, consisting of #4 (13 mm diameter) rectangular ties located at 305mm (12 inches) on center. The upper level columns, like the lower level columns, were heavily reinforced with 30 #18 (57mm diameter) bars and #4 (13mm diameter) ties spaced 305mm (12 inches) on center. The positive reinforcement in the lower level beam consisted of 14 #18 (57 mm diameter) bars at center span while the negative reinforcement at the column face consisted of 8 #18 (57 mm diameter) bars. The

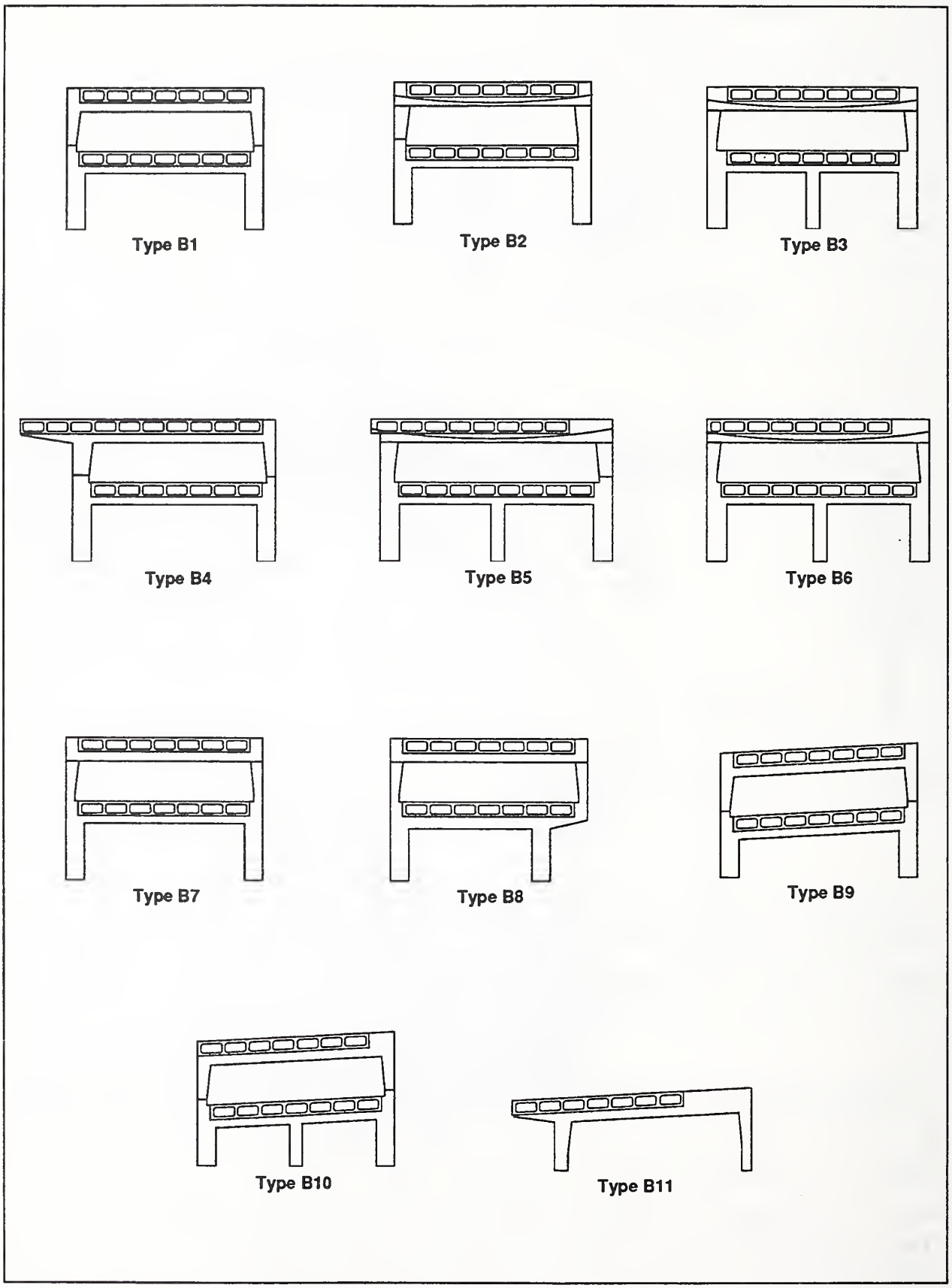

Figure 3-3 Cypress Viaduct Bent Configurations

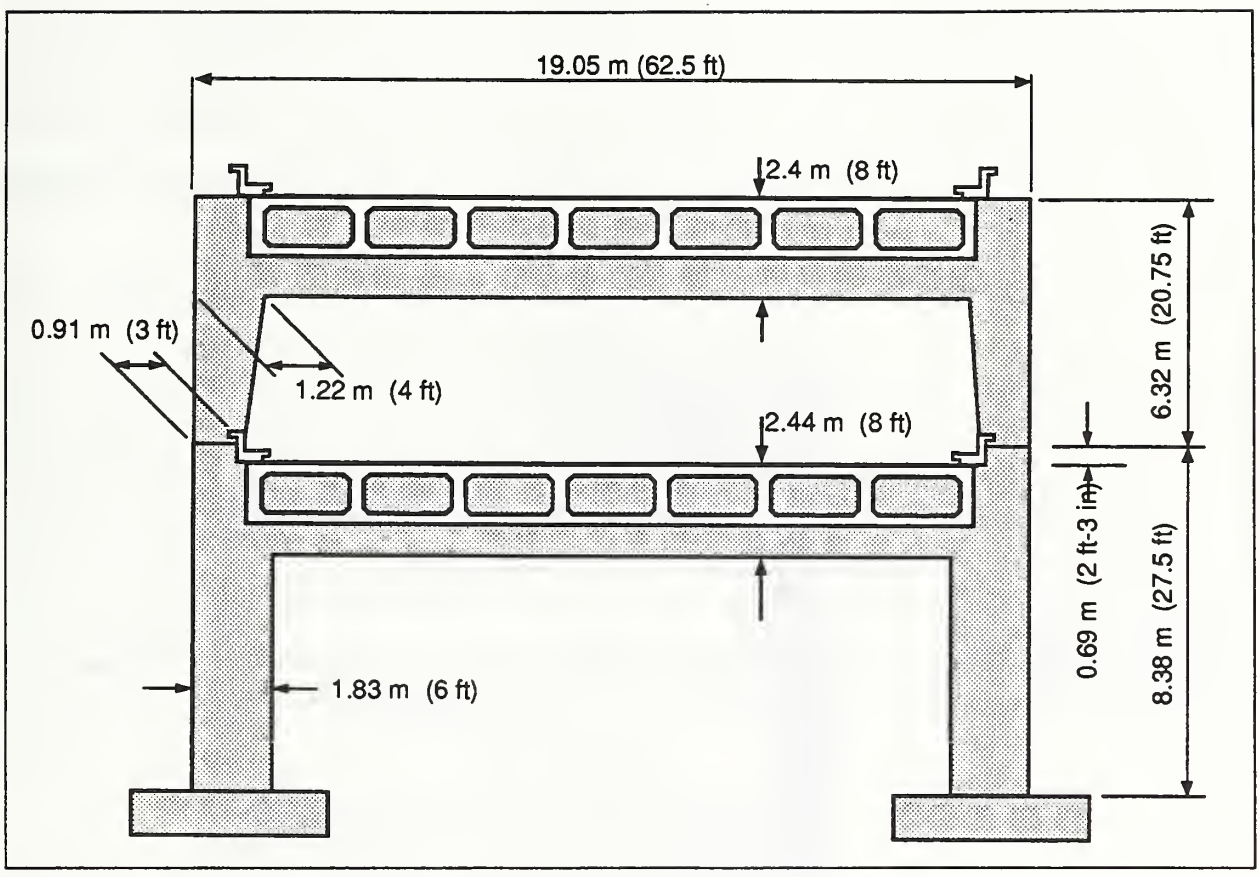

Figure 3-4 Typical Dimensions of the Type B1 Bent

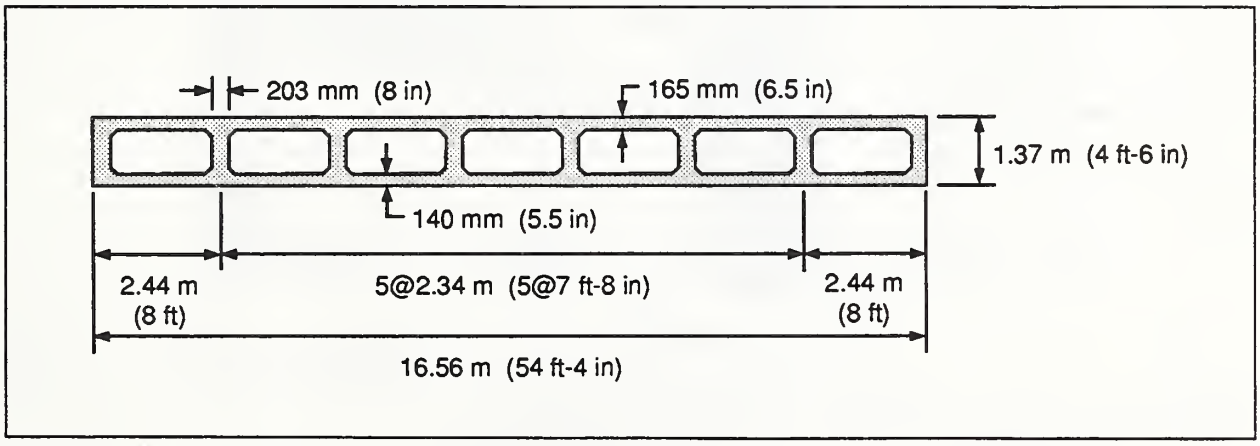

Figure 3-5 Typical Section Through Roadway Deck

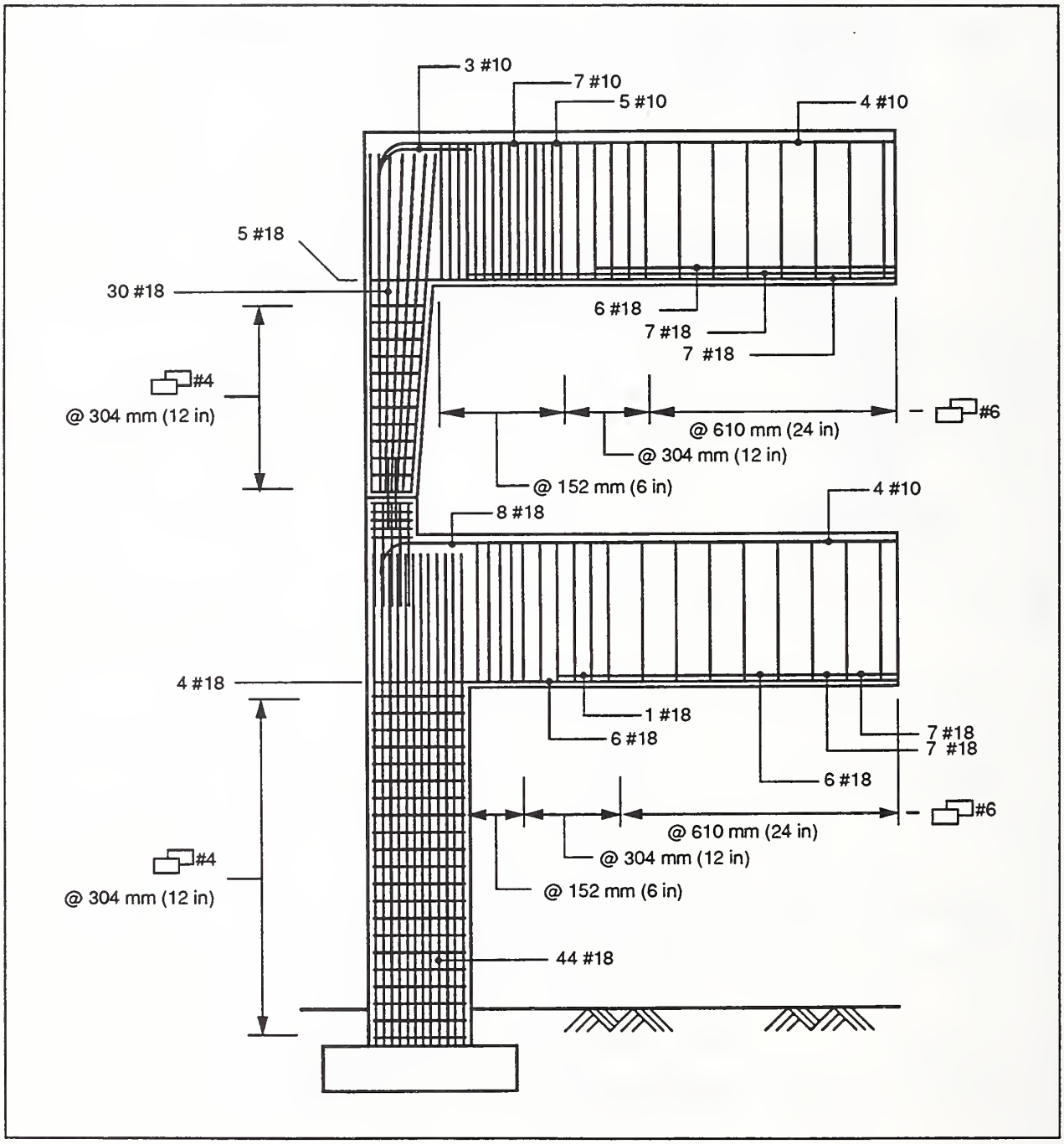

Figure 3-6 Reinforcement Layout for the Type B1 Bent

positive reinforcement in the upper level beam consisted of 20 #18 (57 mm diameter) bars at center span and the negative reinforcement consisted of 10 #10 (32 mm diameter) bars at the column face . #6 (19 mm diameter) rectangular ties, spaced at 152 mm (6 in) to 610 mm (24 in) were used in both the upper and lower level beams.

3.2 Modeling of the Cypress Viaduct

The Cypress Viaduct was modeled as an assemblage of prismatic and tapered members as shown in Fig. 3-7. The dimensions were taken as representative since column lengths, varied along the length of the collapsed portion of the roadway. Centerline dimensions were used with the exception of the columns. Since IDARC permits only vertical column elements, the upper level tapered columns were modeled as vertical elements and the lower level columns were assumed to be collinear with the upper level columns. Rigid links were used to model the joint regions. Hinges were used to model the base fixity condition and the joints between the pedestals and upper level columns while all other joints were assumed to be rigid.

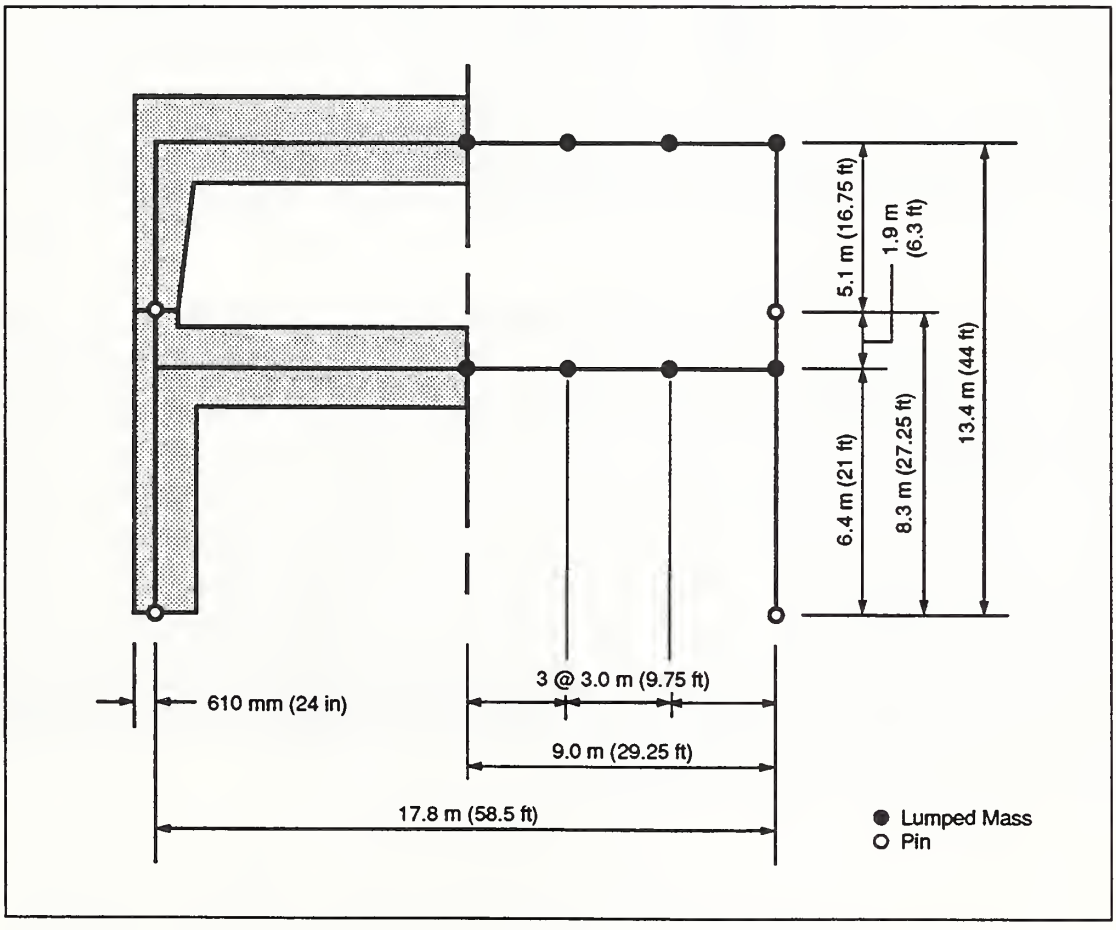

Figure 3-7 IDARC Mode - Geometry

The member (or element) and joint (or node) numbering scheme is shown in Fig. 3-8. Six prismatic members were used to describe the beams. This was done to permit each beam to respond to vertical accelerations in flexure since lumped masses were assigned to each node. The beam elements have transverse and rotational degrees of freedom only (no axial

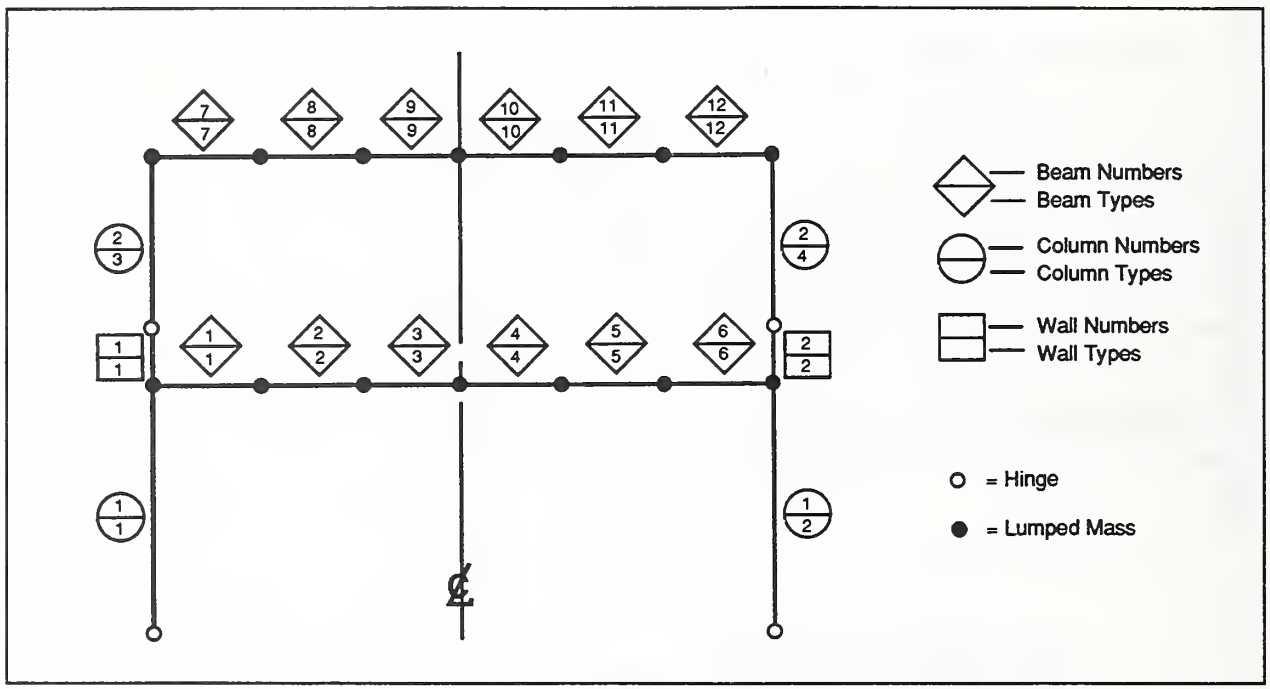

Figure 3-8 IDARC Model - Element Numbers and Material Property Types

deformations). The columns were modeled as single elements, prismatic for the lower level and tapered for the upper level. The columns have axial, transverse and rotational degrees of freedom. The pedestals were modeled with shear wall elements which allow shear as well as flexural behavior.

3.2.1 Member Properties

As described earlier, IDARC requires that the moment-curvature or force-deformation relationships be described for each member end. Determination of these relationships for the beams, columns and shear walls follows.

Beams

A computer program was written to determine the moment-curvature relationship for the beam elements. The program uses a parabolic concrete stress-strain relationship and an linear elastic-perfectly plastic relationship for the longitudinal reinforcement. Compressive strains are incremented and the corresponding stress distribution is computed such that equilibrium is satisfied. The stresses are integrated to produce the moment on the section and the compressive strain and location of neutral axis give the corresponding curvature. The resulting moment-curvature relationship for negative bending at the ends of the upper level beam is shown in Fig. 3-9. This figure illustrates the effect of including strain-hardening of the reinforcing steel. The computer program also computes the moment and corresponding curvature at cracking, first yielding and ultimate (maximum compressive strain).

The IDARC program requires a tri-linear representation of the moment-curvature relationship. The end points of the linear segments generally follow the corresponding cracking, yielding and ultimate points but were adjusted to produce a "best fit" as shown in Fig. 3-10. As noted earlier, each beam was divided into six elements to permit beam flexure produced by vertical acceleration of the beam mass . Due to symmetry of the structure, section properties are required at only four locations (A-D) for each beam. The four sections and the longitudinal reinforcement are shown in Fig. 3-11. The member properties for sections A-D for the lower and upper beams are given in Tables 3-1 and 3-2, respectively.

Columns

The procedure used for determining the moment-curvature relationship for the column elements is similar to that used for the beam elements except that an initial uniform strain resulting from the axial force is included. Fig. 3-12 shows the moment-curvature relationship for the lower-level columns and illustrates the effect of including the dead load axial force. The tri-linear representation of the moment-curvature relationship for the lower level columns, including the gravity load, is shown in Fig. 3-13. The reinforcement layout for the upper and lower level column cross sections are shown in Fig. 3-14. Properties for the lower and upper level columns are given in Tables 3-3 and 3-4, respectively.

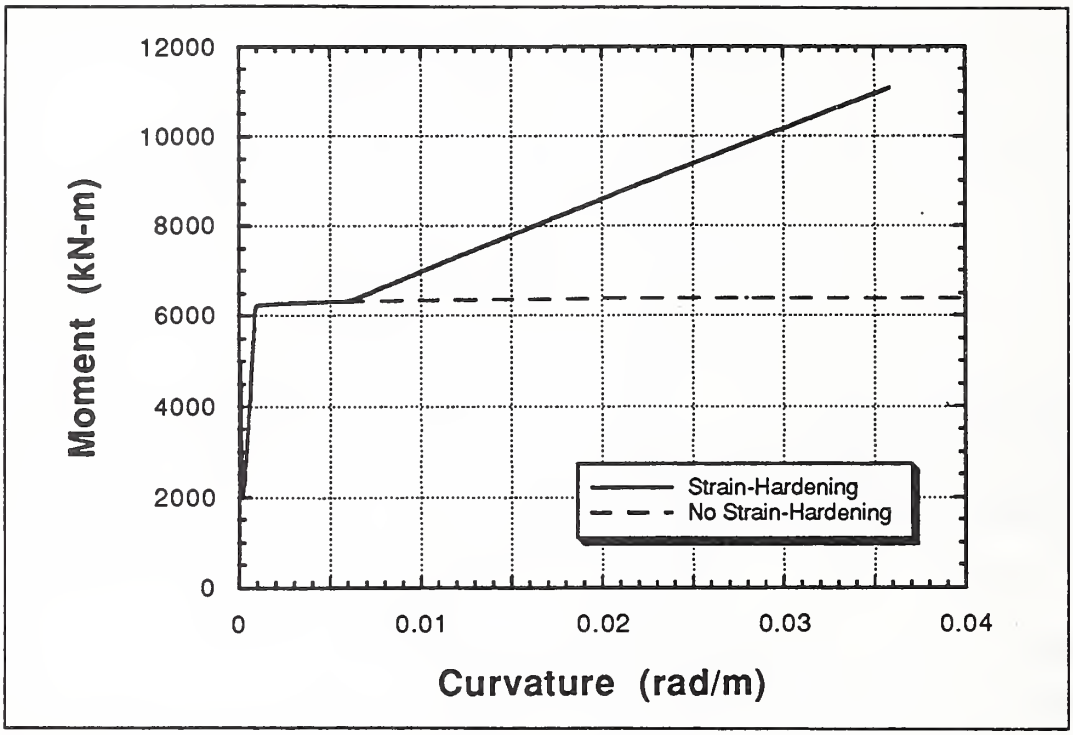

Figure 3-9 Moment-Curvature Relationship for Negative Bending at the Ends of the Upper Level Beam

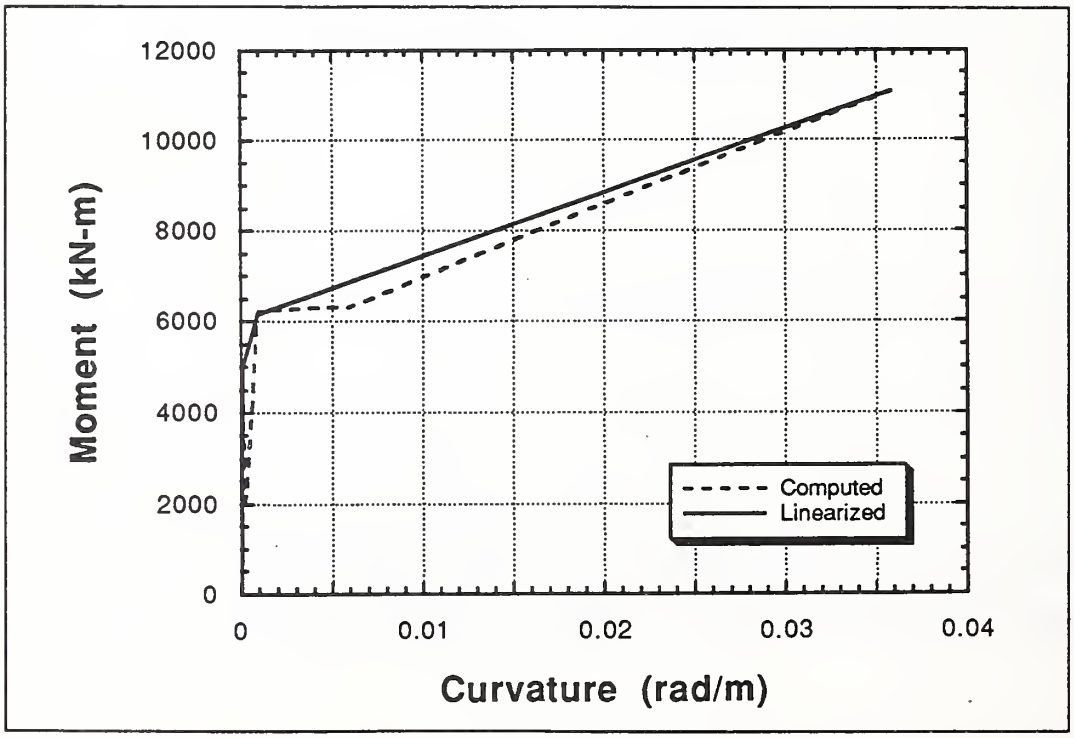

Figure 3-10 Tri-Linear Representation of the Moment-Curvature Relationship for Negative Bending at the Ends of the Upper Level Beam

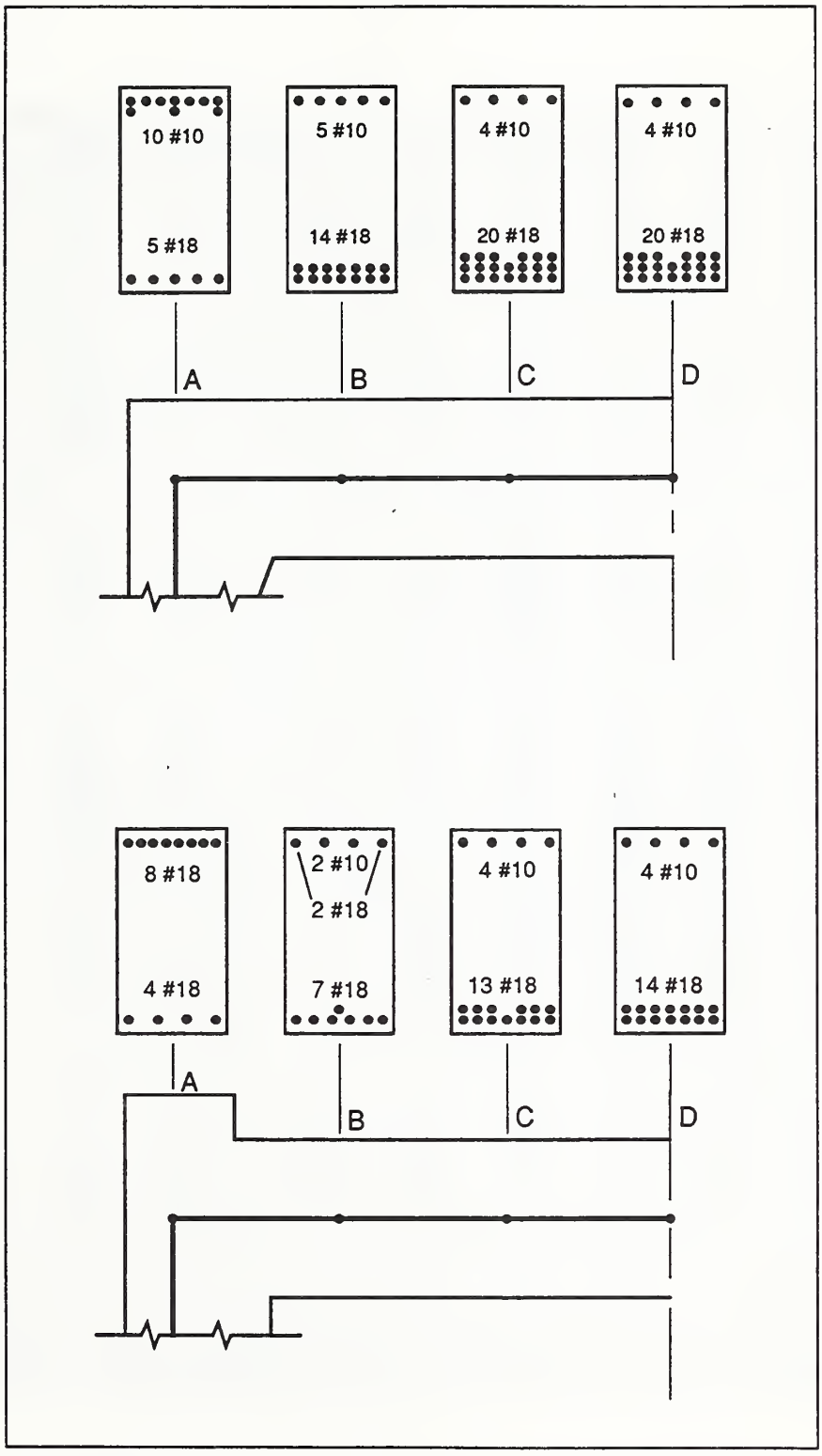

Figure 3-11 Upper and Lower Level Beam Cross Sections

		EI_1 kN-m^2 (kip-in^2)	M_{cr} kN-m (in-kip)	M_y kN-m (in-kip)	ϕ_y rad/mm (rad/in)	ϕ_u rad/mm (rad/in)	EI_3 kN-m^2 (kip-in^2)
A	Pos	4.31E+07 (1.50E+10)	5.16E+03 (4.57E+04)	7.97E+03 (7.05E+04)	9.02E-07 (2.29E-05)	3.46E-05 (8.78E-04)	1.81E+05 (6.29E+07)
A	Neg	4.31E+07 (1.50E+10)	5.32E+03 (4.71E+04)	1.55E+04 (1.37E+05)	9.89E-07 (2.51E-05)	2.24E-05 (5.68E-04)	3.33E+05 (1.16E+08)
B	Pos	4.31E+07 (1.50E+10)	5.19E+03 (4.59E+04)	1.33E+04 (1.18E+05)	9.77E-07 (2.48E-05)	2.24E-05 (5.68E-04)	2.90E+05 (1.01E+08)
B	Neg	4.31E+07 (1.50E+10)	4.62E+03 (4.09E+04)	5.15E+03 (4.56E+04)	8.94E-07 (2.27E-05)	3.63E-05 (9.21E-04)	1.21E+05 (4.23E+07)
C	Pos	4.31E+07 (1.50E+10)	5.48E+03 (4.85E+04)	2.35E+04 (2.08E+05)	1.12E-06 (2.84E-05)	1.21E-05 (3.07E-04)	3.64E+05 (1.27E+08)
C	Neg	4.31E+07 (1.50E+10)	2.09E+03 (1.85E+04)	2.33E+03 (2.06E+04)	8.31E-07 (2.11E-05)	3.24E-05 (8.23E-04)	7.78E+04 (2.71E+07)
D	Pos	4.31E+07 (1.50E+10)	5.54E+03 (4.90E+04)	2.51E+04 (2.22E+05)	1.13E-06 (2.87E-05)	1.14E-05 (2.89E-04)	3.73E+05 (1.30E+08)
D	Neg	4.31E+07 (1.50E+10)	2.09E+03 (1.85E+04)	2.33E+03 (2.06E+04)	8.27E-07 (2.10E-05)	3.08E-05 (7.81E-04)	8.32E+04 (2.90E+07)

Table 3-1 Lower Level Beam Properties

		EI_1 kN-m^2 (kip-in^2)	M_{cr} kN-m (in-kip)	M_y kN-m (in-kip)	ϕ_y rad/mm (rad/in)	ϕ_u rad/mm (rad/in)	EI_3 kN-m^2 (kip-in^2)
A	Pos	4.31E+07 (1.50E+10)	5.06E+03 (4.48E+04)	9.81E+03 (8.68E+04)	9.42E-07 (2.39E-05)	2.51E-05 (6.36E-04)	2.17E+05 (7.57E+07)
A	Neg	4.31E+07 (1.50E+10)	4.98E+03 (4.41E+04)	6.16E+03 (5.45E+04)	9.10E-07 (2.31E-05)	3.59E-05 (9.10E-04)	1.41E+05 (4.90E+07)
B	Pos	4.31E+07 (1.50E+10)	5.56E+03 (4.92E+04)	2.53E+04 (2.24E+05)	1.17E-06 (2.98E-05)	1.17E-05 (2.96E-04)	3.67E+05 (1.28E+08)
B	Neg	4.31E+07 (1.50E+10)	2.88E+03 (2.55E+04)	3.23E+03 (2.86E+04)	8.83E-07 (2.24E-05)	2.96E-05 (7.51E-04)	1.04E+05 (3.62E+07)
C	Pos	4.31E+07 (1.50E+10)	5.79E+03 (5.12E+04)	3.41E+04 (3.02E+05)	1.31E-06 (3.33E-05)	8.51E-06 (2.16E-04)	2.80E+05 (9.77E+07)
C	Neg	4.31E+07 (1.50E+10)	2.44E+03 (2.16E+04)	2.71E+03 (2.40E+04)	8.43E-07 (2.14E-05)	2.21E-05 (5.62E-04)	1.64E+05 (5.70E+07)
D	Pos	4.31E+07 (1.50E+10)	5.79E+03 (5.12E+04)	3.41E+04 (3.02E+05)	1.31E-06 (3.33E-05)	8.51E-06 (2.16E-04)	2.80E+05 (9.77E+07)
D	Neg	4.31E+07 (1.50E+10)	2.44E+03 (2.16E+04)	2.71E+03 (2.40E+04)	8.43E-07 (2.14E-05)	2.21E-05 (5.62E-04)	1.64E+05 (5.70E+07)

Table 3-2 Upper Level Beam Properties

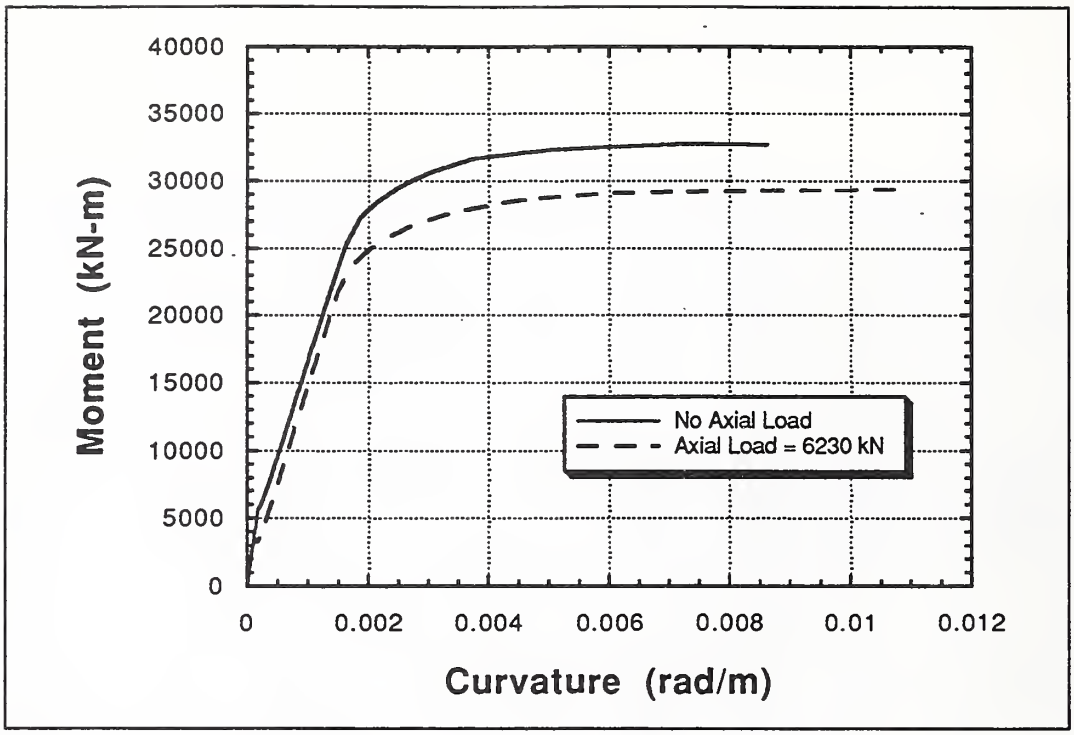

Figure 3-12 Moment-Curvature Relationship for the Lower Level Columns

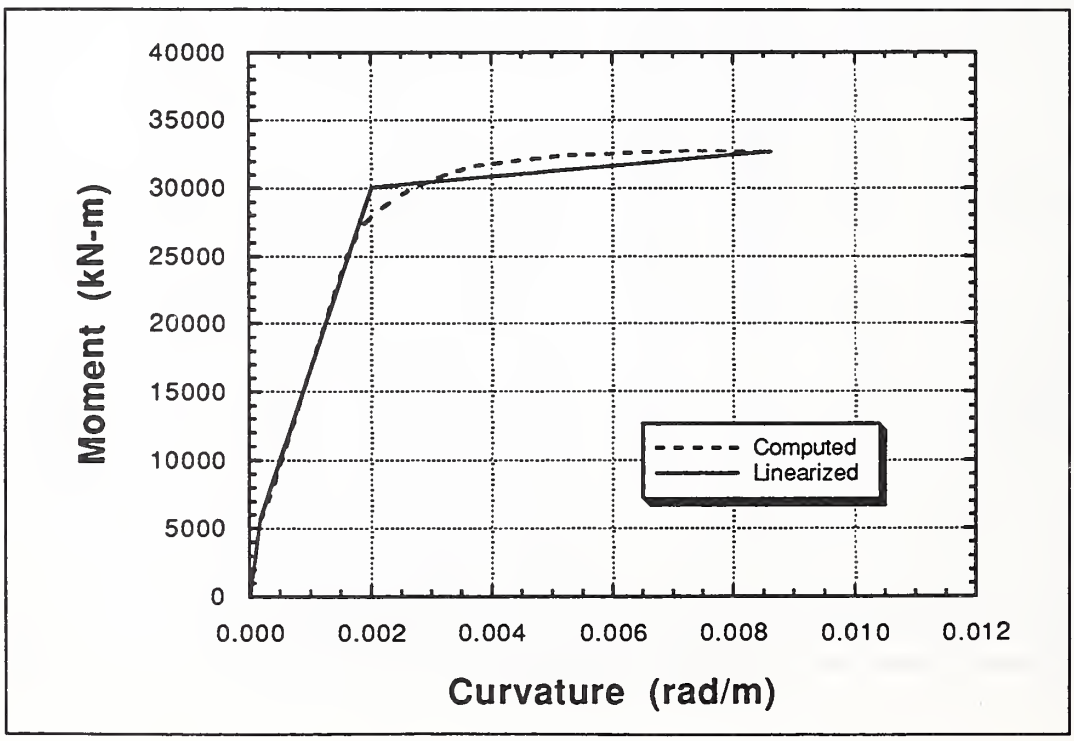

Figure 3-13 Tri-Linear Representation of the Moment-Curvature Relationship for the Lower Level Columns

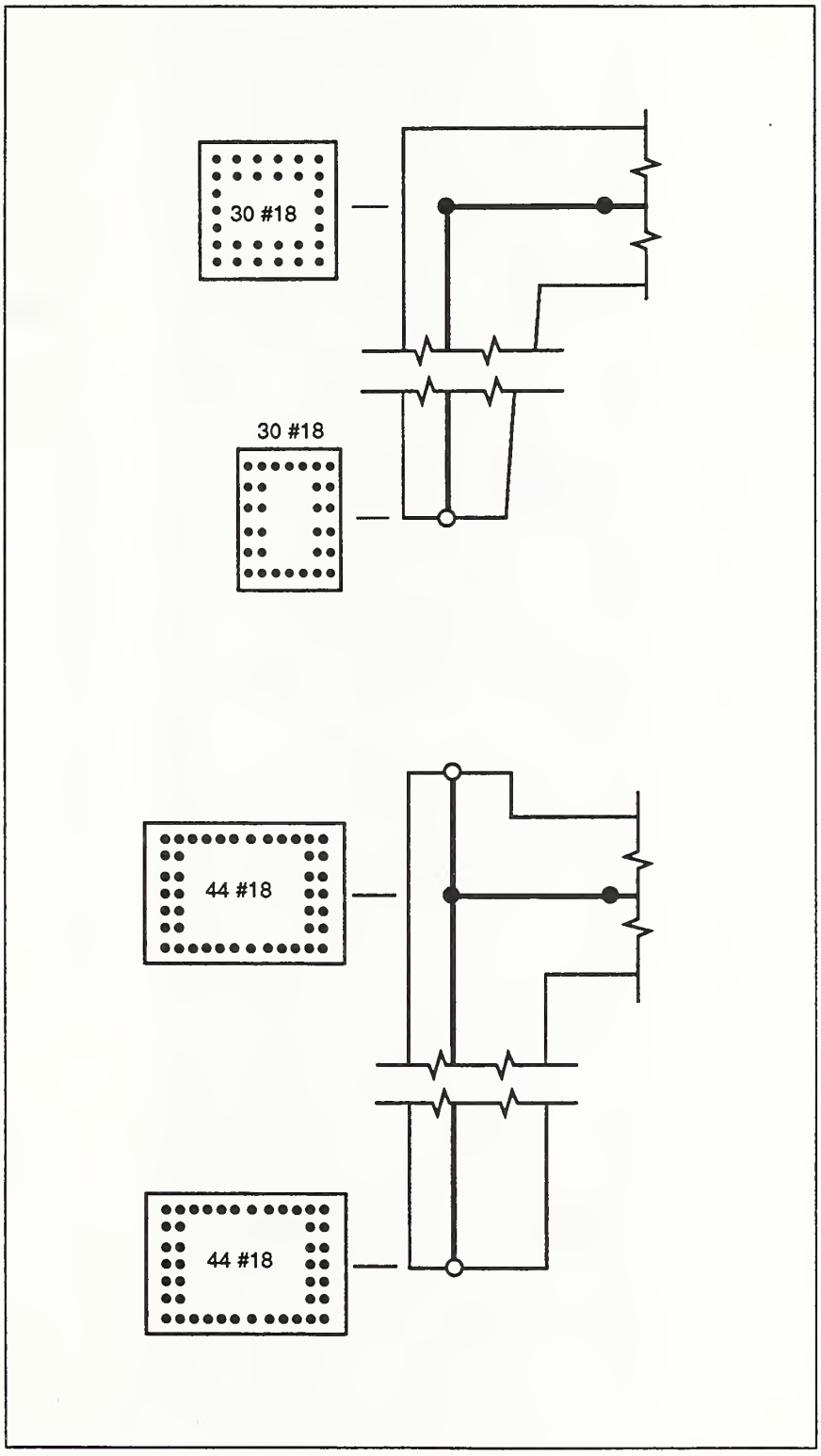

Figure 3-14 Upper and Lower Level Column Cross-Sections

	EA/L kN/m (kip/in)	EI_1 kN-m^2 (kip-in^2)	M_{cr} kN-m (in-kip)	M_y kN-m (in-kip)	ϕ_y rad/mm (rad/in)	ϕ_u rad/mm (rad/in)	EI_3 kN-m^2 (kip-in^2)
Top	1.53E+07 (8.23E+04)	2.40E+07 (8.38E+09)	5.69E+03 (5.04E+04)	3.01E+04 (2.66E+05)	2.02E-06 (5.12E-05)	8.62E-06 (2.19E-04)	3.93E+05 (1.37E+08)
Bot	1.53E+07 (8.23E+04)	2.40E+07 (8.38E+09)	5.69E+03 (5.04E+04)	3.01E+04 (2.66E+05)	2.02E-06 (5.12E-05)	8.62E-06 (2.19E-04)	3.93E+05 (1.37E+08)

Table 3-3 Lower Level Column Properties

	EA/L kN/m (kip/in)	EI_1 kN-m^2 (kip-in^2)	M_{cr} kN-m (in-kip)	M_y kN-m (in-kip)	ϕ_y rad/mm (rad/in)	ϕ_u rad/mm (rad/in)	EI_3 kN-m^2 (kip-in^2)
Top	1.30E+07 (7.41E+04)	6.66E+06 (2.32E+09)	2.17E+03 (1.92E+04)	1.02E+04 (9.03E+04)	2.85E-06 (7.24E-05)	1.46E-05 (3.70E-04)	8.95E+04 (3.12E+07)
Bot	1.02E+07 (5.82E+04)	2.93E+06 (1.02E+09)	1.38E+03 (1.22E+04)	7.28E+03 (6.44E+04)	4.09E-06 (1.04E-04)	1.60E-05 (4.07E-04)	5.31E+04 (1.85E+07)

Table 3-4 Upper Level Column Properties

Pedestals

The pedestals were modeled as shear wall elements in IDARC to capture the shear-type failure that was observed during post-collapse investigations. As noted earlier, the shear wall element in IDARC requires the shear load-deformation relationship. To obtain this relationship, an inelastic finite element analysis of the pedestal region was conducted. The program used was FEM/I [Ewing, 1991]. The features of this finite element program are highlighted, and the finite element model and resulting shear load-deformation relationship are described.

FEM/I is a nonlinear, two-dimensional finite element computer program for the static analysis of concrete or masonry building components. It is based on a 4-node isoparametric quadrilateral element which uses a 2 by 2 Gaussian integration scheme. Concrete and reinforcing steel are modeled separately in an overlaid model in which strain compatibility is enforced at the nodes. The concrete is represented by an orthotropic material model and includes tension stiffening, compression softening, strain softening and a degrading modulus unloading rule. Distributed cracking occurs when the principle tensile strain at a Gauss point exceeds the specified cracking strain. Cracks form perpendicular to the direction of principal tensile strain. Compressive strength reduction after tensile cracking is accounted for as well as compressive strength increase due to lateral confinement. The compression stress-strain relationship used in the present analysis is shown in Fig. 3-15. The reinforcing steel is assumed to be distributed over the entire element. It is represented by an orthotropic material model with a bi-linear stress-strain relationship as shown in Fig. 3-16 and includes unloading. The FEM/I program uses an initial stiffness formulation and incremental solution procedure in which displacements and/or forces are incremented. Iterations are performed with corrections to the load vector to assure equilibrium is obtained within a prescribed convergence tolerance.

A finite element model of the pedestal region is shown in Fig. 3-17. Different material properties were used to describe the pedestal, negative beam reinforcement and beam-column joint region as shown in Fig. 3-18. The pedestal model was restrained as shown in Fig. 3-19 and loaded with fixed gravity load and shear applied at the top of the pedestal in both directions. The resulting shear force-deflection is shown in Fig. 3-20. The shear force-shear strain relationship for the wall element was produced by dividing the displacement by the model height. The ultimate shear strain was determined by calibration with lateral load tests performed on an undamaged portion of the Cypress Viaduct as described in Section 3.2.3. The resulting tri-linear force-strain relationship is shown in Fig. 3-21. The state of the concrete (either cracked or crushed) and steel (yielded) for the lateral load of 2000 kN (450 kips), is shown in Fig. 3-22. A plane of failure extending from the edge of the shear key to

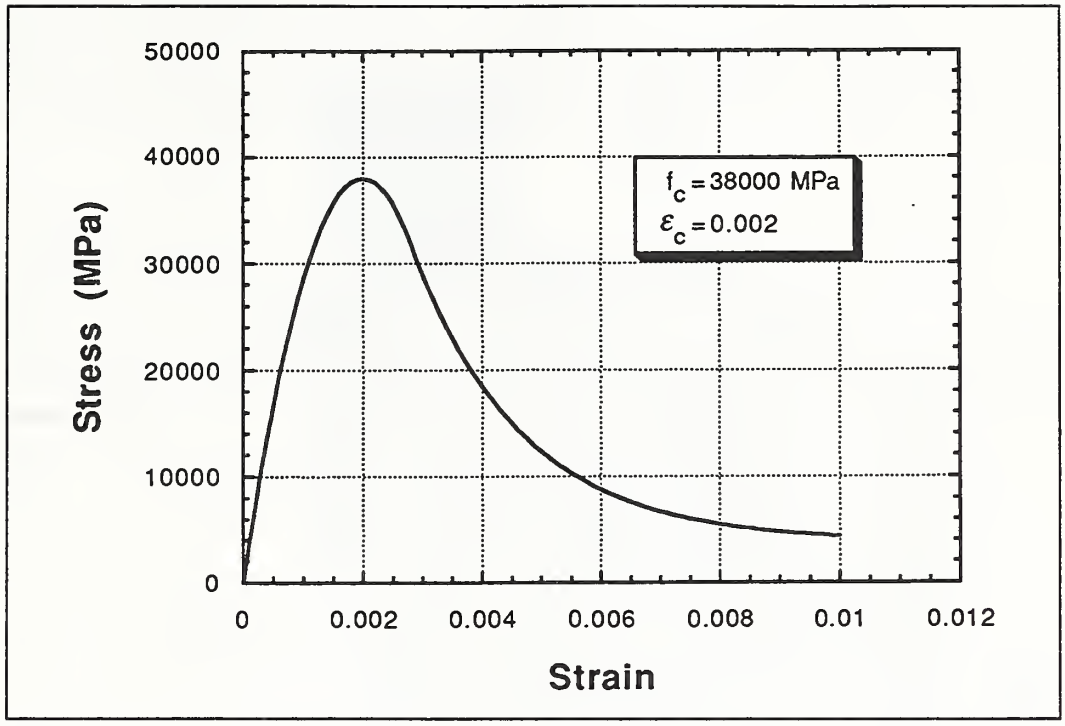

Figure 3-15 Concrete Compression Stress-Strain Relationship Used in the Pedestal Analysis

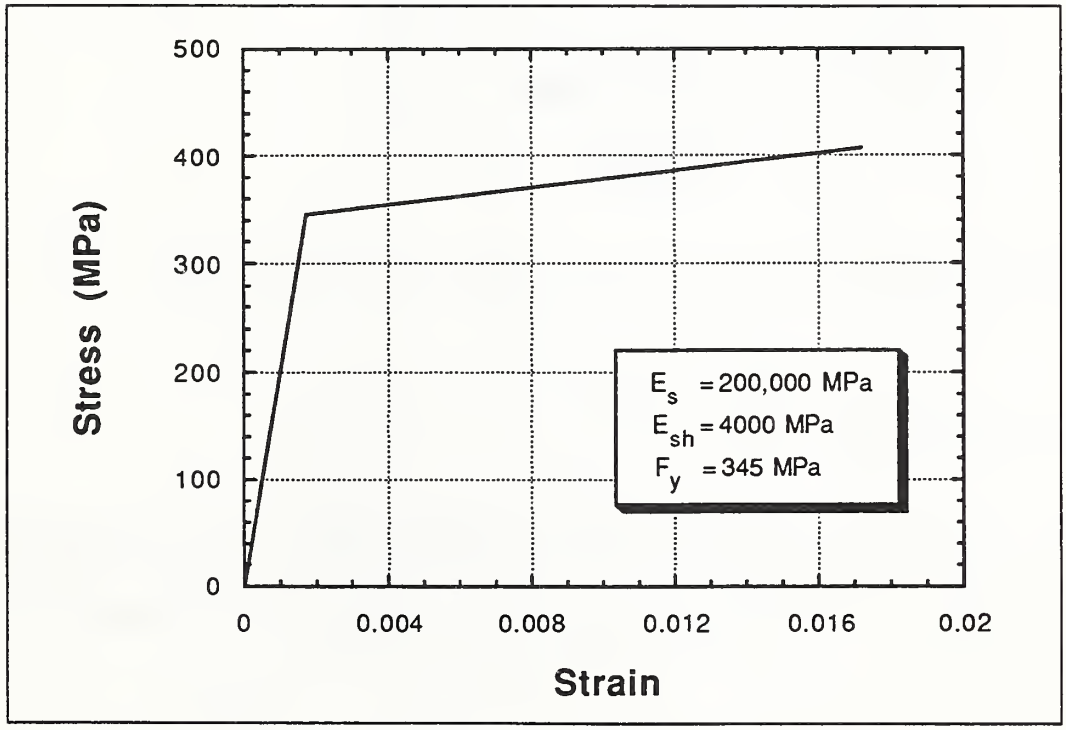

Figure 3-16 Reinforcing Steel Stress-Strain Relationship for the Pedestal Analysis

the negative beam reinforcement can be visualized. Comparison of this analytical prediction of failure of the pedestal region compares favorably with observed failure as evidenced by the photograph of a failed pedestal shown in Fig. 3-23 (Photo courtesy of Nims et al (1989)).

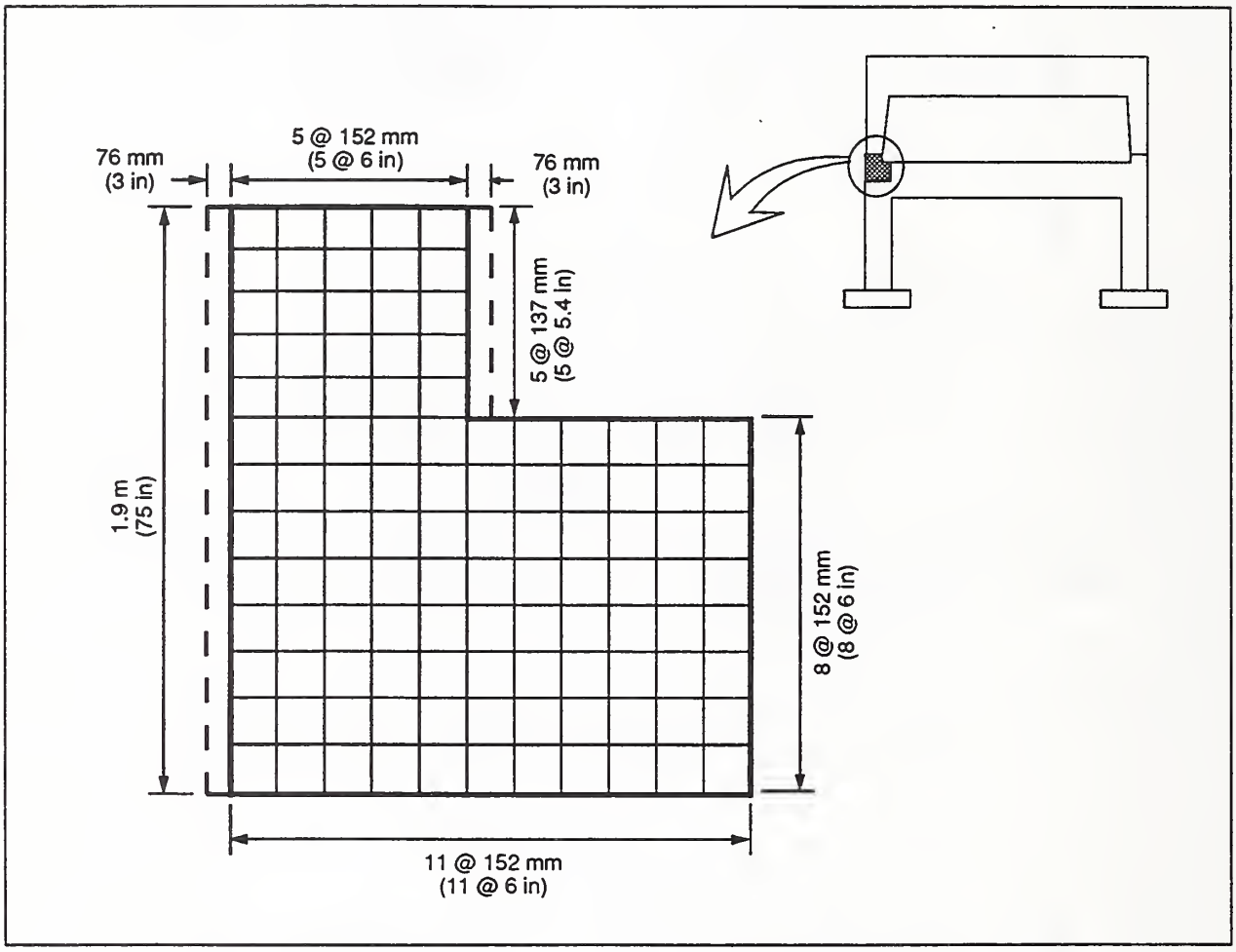

Figure 3-17 Finite Element Model of the Pedestal Region - Geometry

3.2.2 Gravity Loading

IDARC, in its present form, does not permit inelastic action for the static analysis option. Thus, to capture cracking that occurs due to gravity load alone, the gravity load was applied as a dynamic load. The vertical acceleration of 1 g was applied incrementally using the following function:

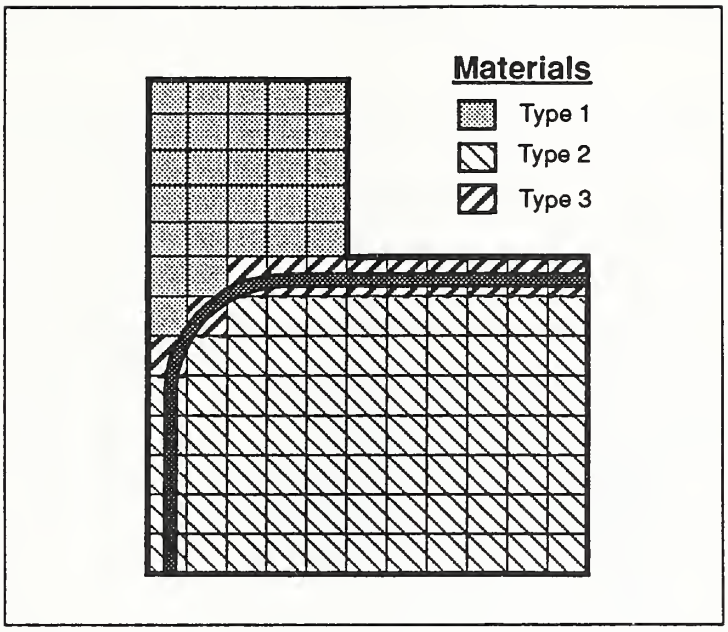

Figure 3-18 Finite Element Model of the Pedestal Region - Material Properties

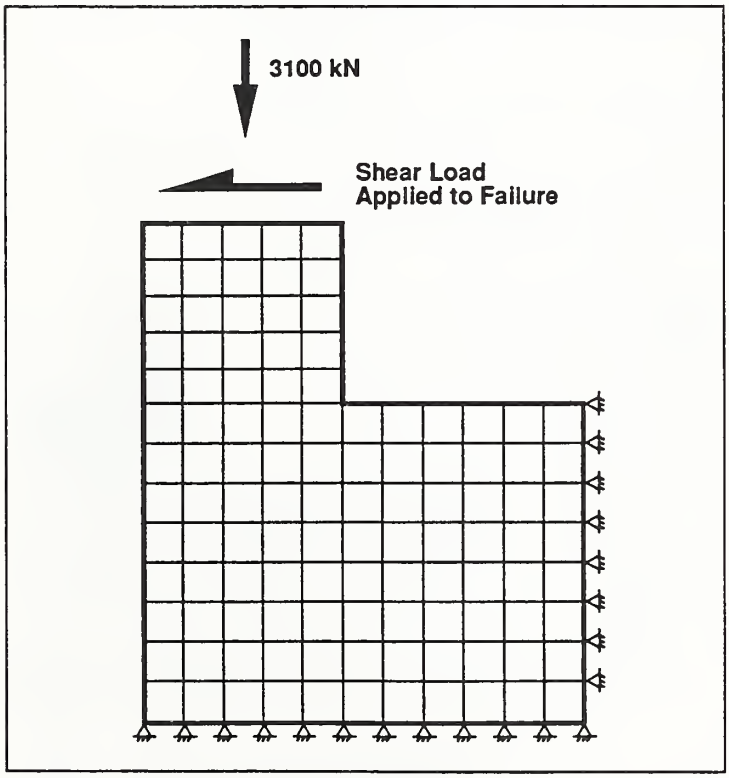

Figure 3-19 Finite Element Model of the Pedestal Region - Loading and Boundary Conditions

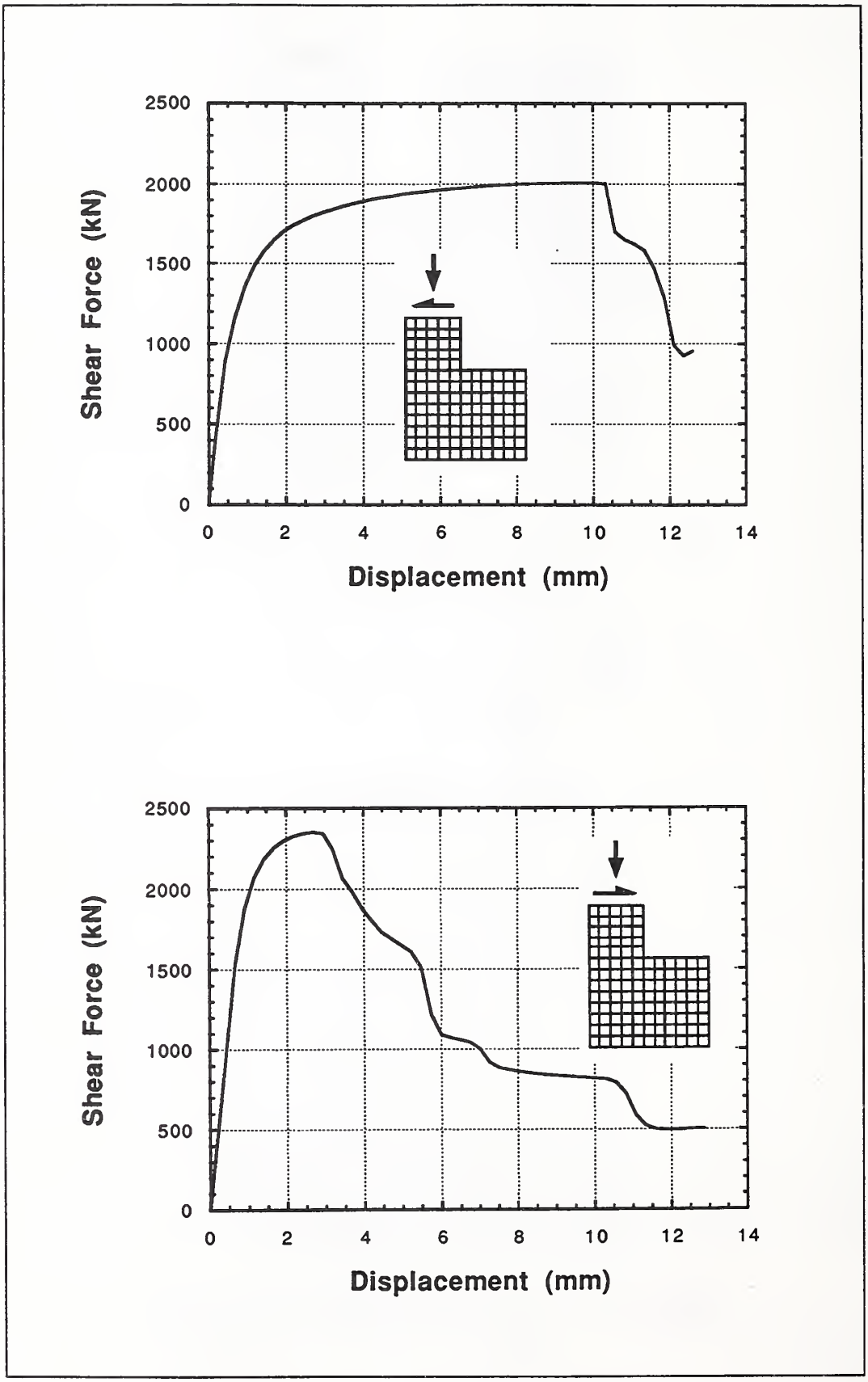

Figure 3-20 Pedestal Shear Force-Displacement Relationships

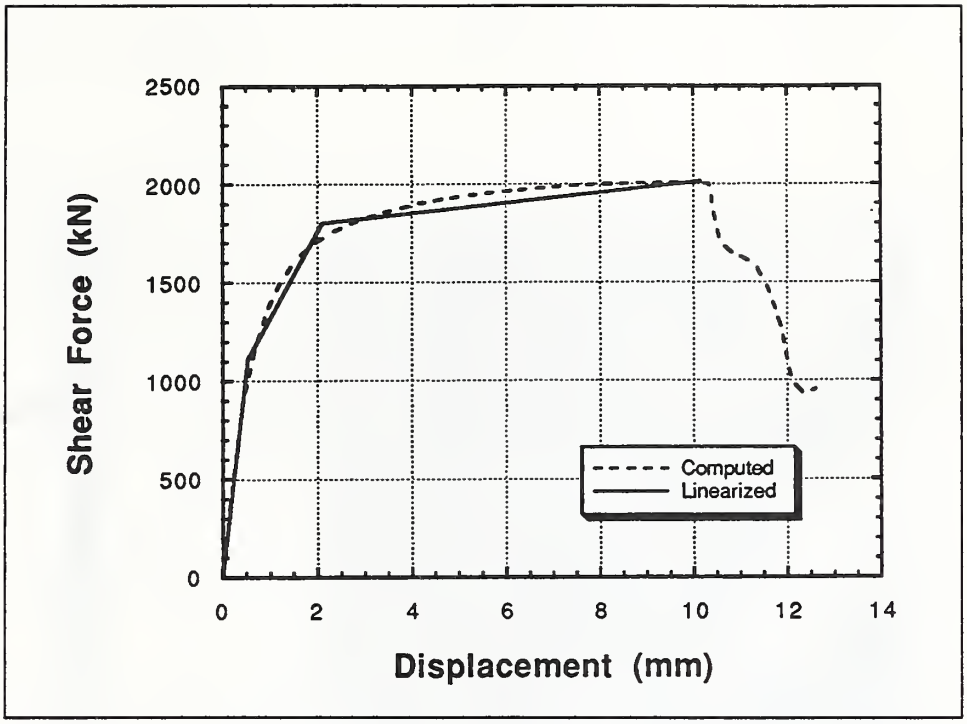

Figure 3-21 Tri-Linear Representation of the Shear Force-Displacement Relationship for the Pedestals

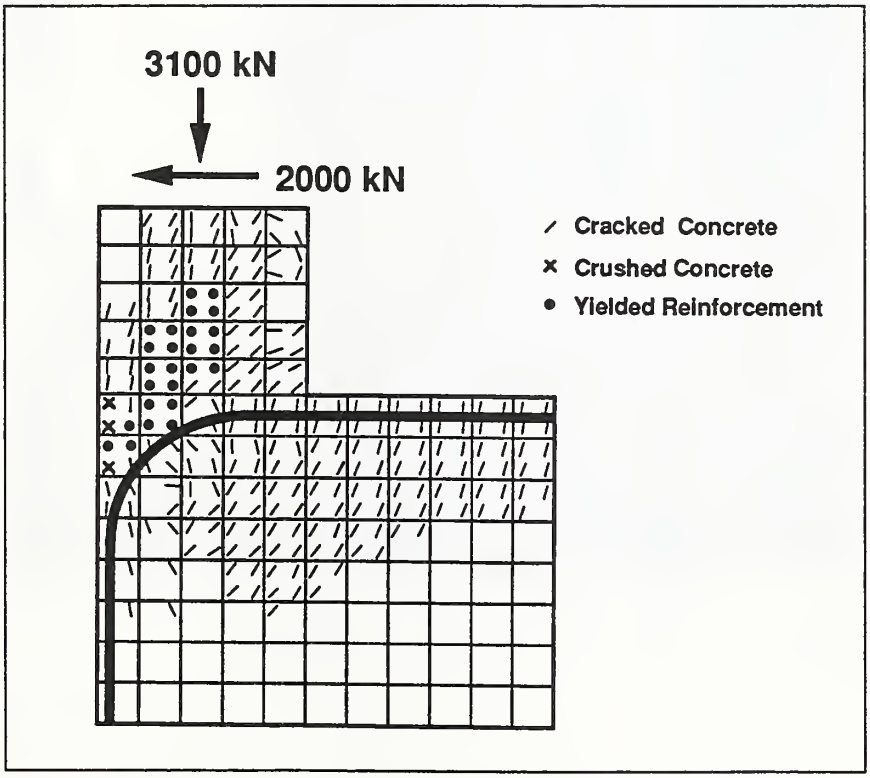

Figure 3-22 Element State at Lateral Failure Load

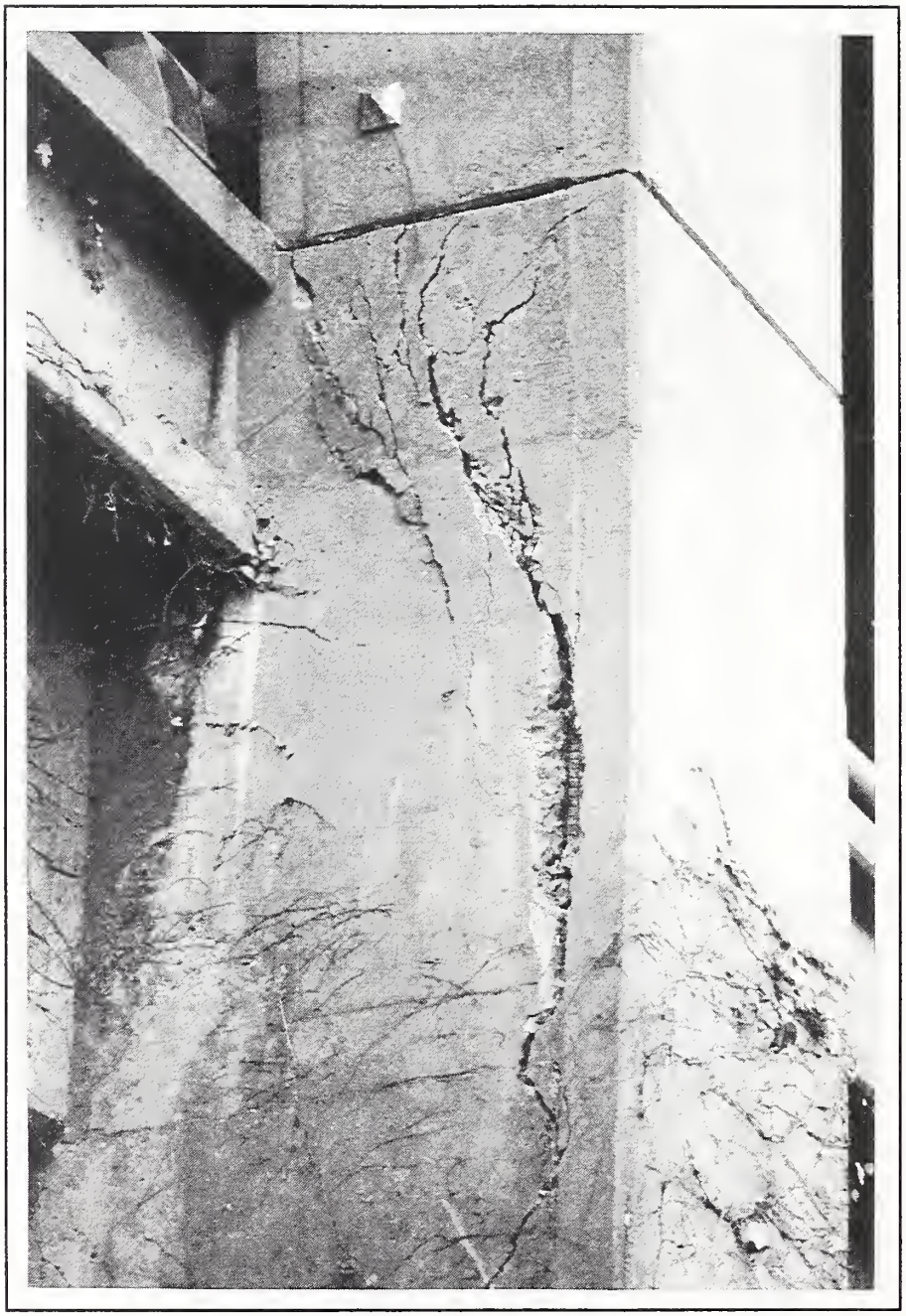

Figure 3-23 Cypress Viaduct Pedestal Failure

$$A_v = 0.5\,(1 - \cos \pi \frac{t}{t_o}) \qquad (3\text{-}1)$$

where A_v is the vertical acceleration expressed in g's, t is the time increment, and t_o is the duration of the ramp. If t_o is selected to be at least two times the fundamental period, dynamic application of the gravity load will not excite the structure and there will be little free vibration. The fundamental period of the Cypress Viaduct bent under study was found to be approximately 0.4 seconds (see Section 3.2.4); therefore, the gravity load was applied over two seconds. Any resulting small vibrations were permitted to damp out for two seconds before the earthquake accelerations were applied.

3.2.3 Validation of model

Several analyses were conducted prior to applying the full duration earthquake in order to better understand the basic behavior of the structure and to validate the IDARC model. First, an elastic gravity load analysis was conducted to determine the appropriate number of beam sections to use to adequately represent beam flexure and to determine if inelastic action resulted from gravity load alone. Next, the fundamental frequency was computed to compare with results from ambient and forced vibration tests conducted on a three-bent portion of the Cypress Viaduct that remained standing. Finally, a lateral load analysis was conducted to compare with test results of the same three-bent structure loaded laterally to failure.

Gravity Load Analysis

An elastic analysis was conducted to obtain the moment and shear diagrams for the type B1 bent of the Cypress Viaduct under gravity load only. The analysis revealed that cracking moment was exceeded in several locations. Thus, the gravity load had to be included in subsequent IDARC analyses as a dynamic load, as described in Section 3.2.2, so that all inelastic action would be included. Additionally, the elastic gravity load analysis was used to check that the IDARC model had the correct boundary conditions assigned, the correct sign conventions for members, etc.

Next, an inelastic gravity load analysis was conducted to insure that, prior to application of earthquake loads, the structure was not significantly damaged (the Cypress Viaduct had been in service for many years without evidence of distress). Inelastic moment and shear diagrams are shown in Fig. 3-24. The analysis indicated that the structure did, indeed, carry

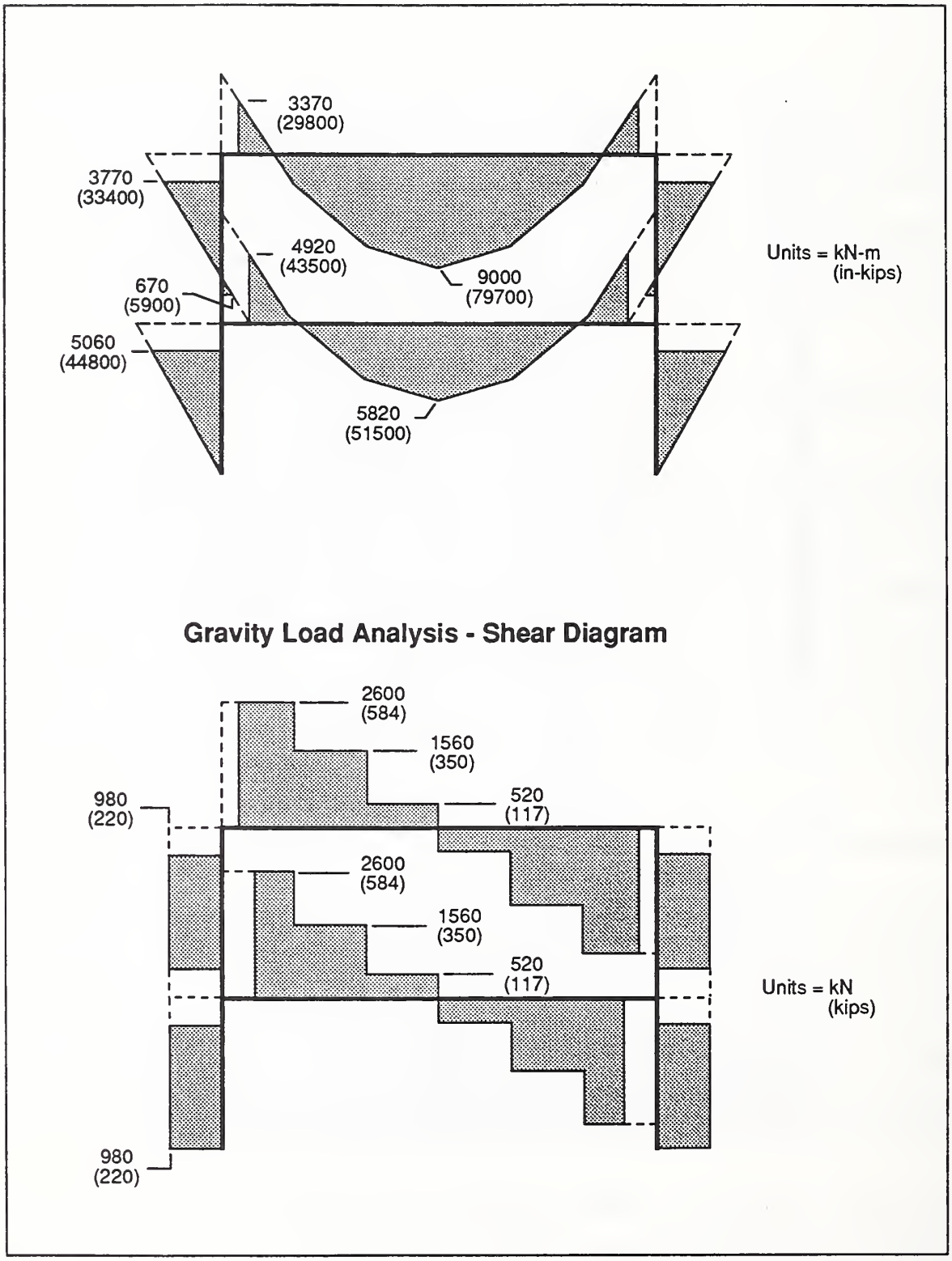

Figure 3-24 Inelastic Moment and Shear Diagrams for Gravity Load Only

the gravity load with only minor cracking. Additionally, the inelastic analysis revealed that the shear in the pedestal region, due to gravity load alone, was approximately 50% of the shear capacity as predicted by finite element analysis of the pedestal. This point will be expanded upon in the discussion of the lateral load test.

Vibration Analysis

Ambient vibration tests were conducted on a three-bent portion of the Cypress Viaduct (Bents 45-47) that remained standing after the Loma Prieta earthquake (see Fig. 3-2) [Housner et al, 1990]. Measurements were made on the span between Bents 45 and 46. The bents were of the Type B1 configuration and were reported to be relatively undamaged. The measured first mode frequency was found to be 2.5 Hz. Also, forced vibration tests were conducted on the three-bent test structure prior to static lateral load tests. Again the first-mode frequency was measured to be 2.5 Hz.

To compare with the measured first-mode frequency, a time-history analysis was conducted on the Type B1 bent with the first level column length adjusted to better approximate the test structure. First, gravity load was applied dynamically and the vibrations allowed to damp out. Next, the Outer Harbor Wharf ground acceleration record, scaled by one half, was applied (see Sections 3.3.1 and 3.3.2). This was done to approximate the minor damage that resulted from the earthquake. Finally, the time-history analysis was conducted for an additional four seconds (no applied accelerations) to allow the structure to vibrate freely. A record of the computed second level accelerations is shown in Fig. 3-25. The last four seconds of free vibration and the results of a Fast Fourier Transform (FFT) on the last four seconds of the computed second-level accelerations are shown in Fig. 3-26. As seen in this figure, the lowest modal frequency was found to be 2.48 Hz which compares favorably with the measured value of 2.5 Hz.

Lateral Load Test

The three-bent test structure mentioned above was tested to failure by loading all three bents laterally with hydraulic jacks [Housner et al, 1990]. A plot of the lateral load per bent vs. the upper level displacement is shown in Fig. 3-27. To simulate this loading condition, the IDARC program was modified to permit application of the lateral load following application of the gravity and earthquake loads dynamically. Results of the IDARC analysis are also shown in Fig. 3-28. Again, the agreement between analysis (heavy line) and test results (light line) is good.

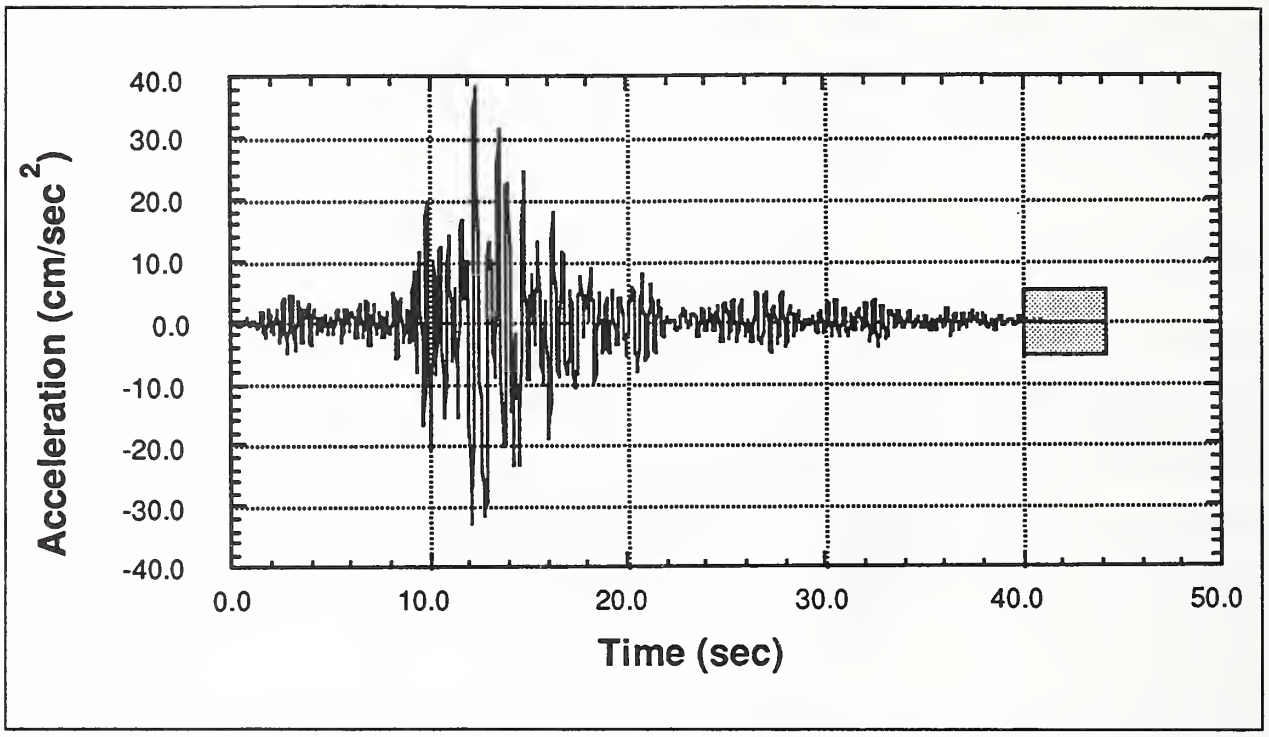

Figure 3-25 Bents 45-47 - Second Level Acceleration Time-History

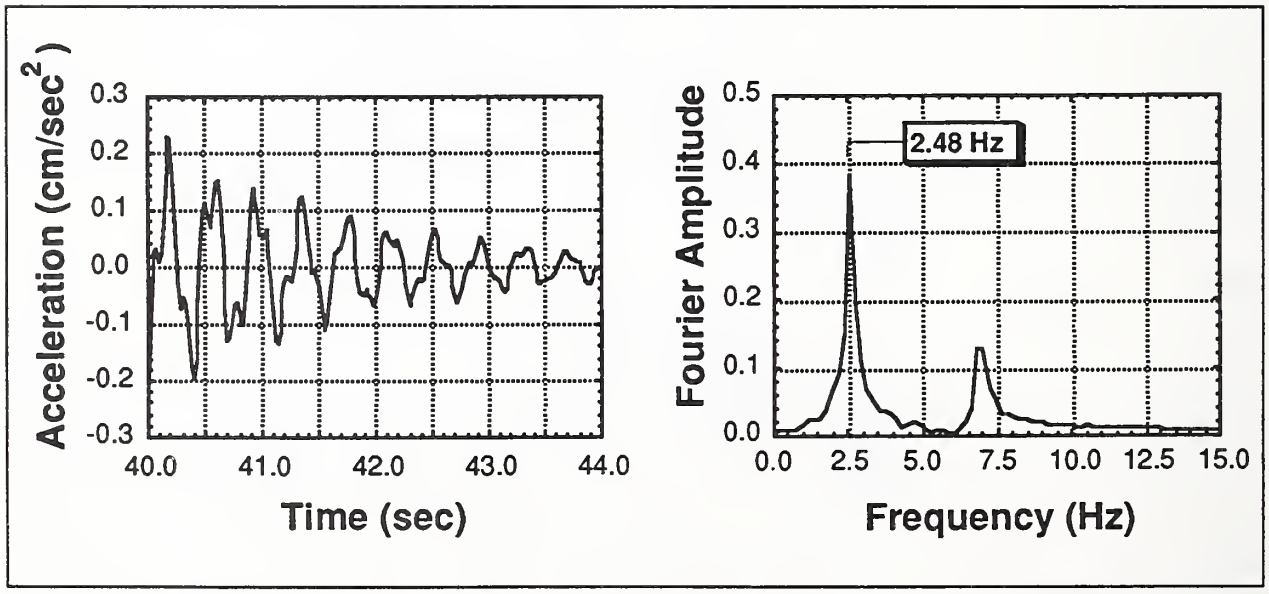

Figure 3-26 Bents 45-47 - Free Vibration Time History and Fourier Amplitude

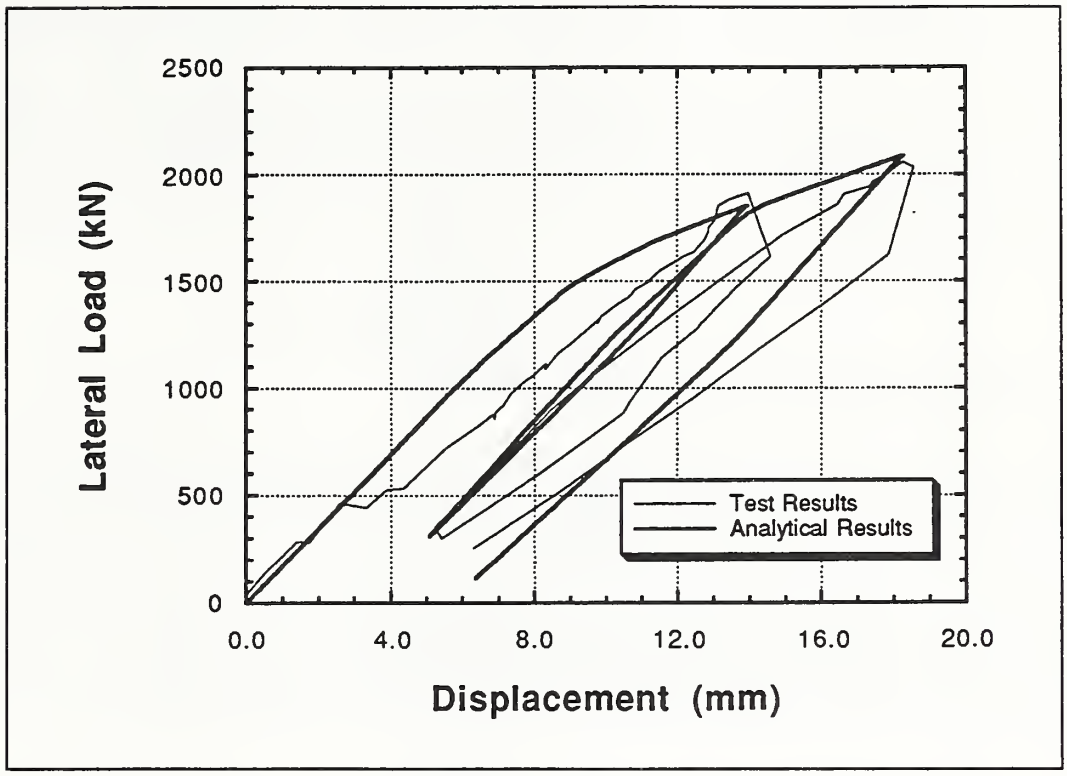

Figure 3-27 Static Lateral Load Test - Lateral Load vs. Deflection

The lateral load test was stopped when cracking in the pedestals was observed. Thus, the capacity of one bent, as determined by failure of the pedestal region, was reported to be 2070 kN (465 kips). Assuming both pedestals share the load equally, this corresponds to a pedestal capacity of 1035 kN (233 kips). The capacity of the pedestal, loaded to produce shear in the same direction as that caused by gravity load, was determined by inelastic finite element analysis to be 2000 kN (450 kips) (see Section 3.2.1 and Fig. 3-20a). The inelastic gravity load analysis predicted a shear of 980 kN (220 kips) in the pedestal (see Section 3.2.3 and Fig. 3-24). The expected lateral failure load of one pedestal is obtained by subtracting the gravity shear from the predicted shear capacity, or 2000-980 = 1020 kN (230 kips). A comparison of this value with the measured capacity of 1035 kN (233 kips) indicates that the pedestal capacity, as determined by inelastic finite element analysis (FEM/I), is quite good.

3.3 The Loma Prieta Earthquake

The Loma Prieta earthquake occurred on October 17, 1989, at 5:04 pm PDT. It was a Magnitude 7.1 earthquake and its epicenter was located near Santa Cruz, California [Lew et al, 1990]. The earthquake, which lasted for 10 to 15 seconds, was felt over an area of about 1,000,000 sq km (400,000 sq mi). The peak horizontal acceleration in the epicentral

region was measured to be 0.64 g. Accelerations recorded in San Francisco and Oakland, 90 to 100 km (55 to 60 mi) from the epicenter, were found to depend greatly on surficial geology. Most notably, accelerations recorded in areas of deep sedimentary deposits were up to three times those recorded on bedrock or more competent soil. The Cypress Viaduct was located in Oakland, and the northernmost portion (that portion that collapsed) was founded on soft Bay Mud.

3.3.1 Acceleration Records Near the Cypress Viaduct

Ground acceleration records were available from three sites near the Cypress Viaduct; Emeryville to the north, Outer Harbor Wharf to the west, and a Two-Story Office Building in Oakland, to the east. Accelerograms of East-West components of motion, produced from strong-motion records from these three sites, are shown in Figs. 3-28 to 3-30. While all three records show strong similarity, the Outer Harbor Wharf Record was selected for the dynamic analyses in this study since it was considered to be the least influenced by nearby structures.

3.3.2 Acceleration Record Used for Dynamic Analysis

The Outer Harbor Wharf horizontal strong-motion records were transformed to 94° which is transverse to the alignment of that portion of the Cypress Viaduct that collapsed. The horizontal and vertical acceleration records used for the dynamic analysis are shown in Fig. 3-31. The peak horizontal acceleration is 323 cm/sec^2, or 0.33 g.

A Husid plot [Idriss, 1979], provides a measure of the energy in an accelerogram and enables an estimate of the duration of strong shaking. The energy in an accelerogram has been shown to be proportional to

$$\int_0^t a^2(t)\,dt \tag{3-2}$$

where $a(t)$ is the acceleration time-history. A Husid plot is a graph of $H(t)$ versus time in which $H(t)$ is the integral in Eq. 3-2, normalized by the integral evaluated for the duration of the accelerogram, or

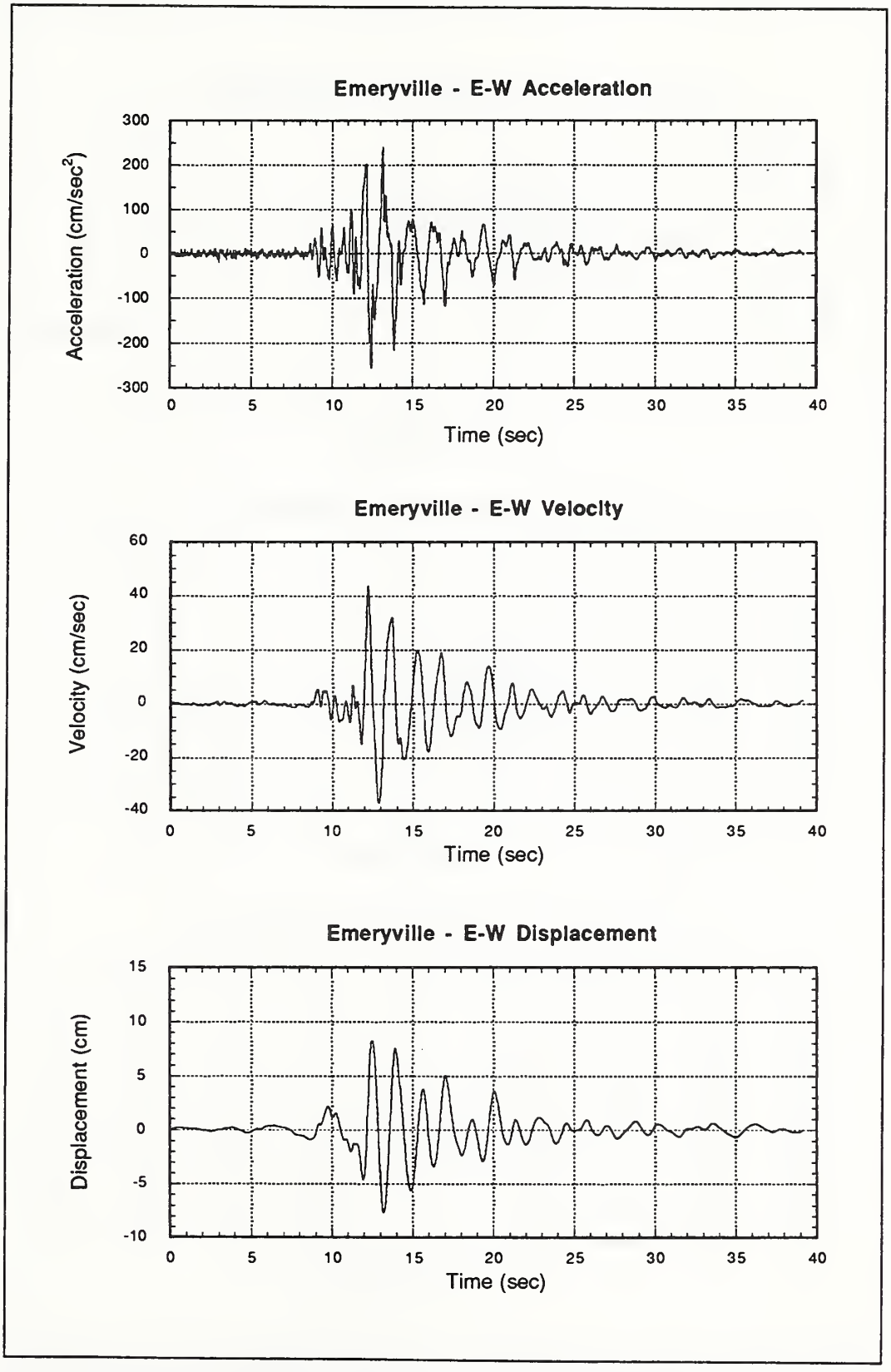

Figure 3-28 Acceleration, Velocity and Displacement for the East-West Component of Motion for the Emeryville Site

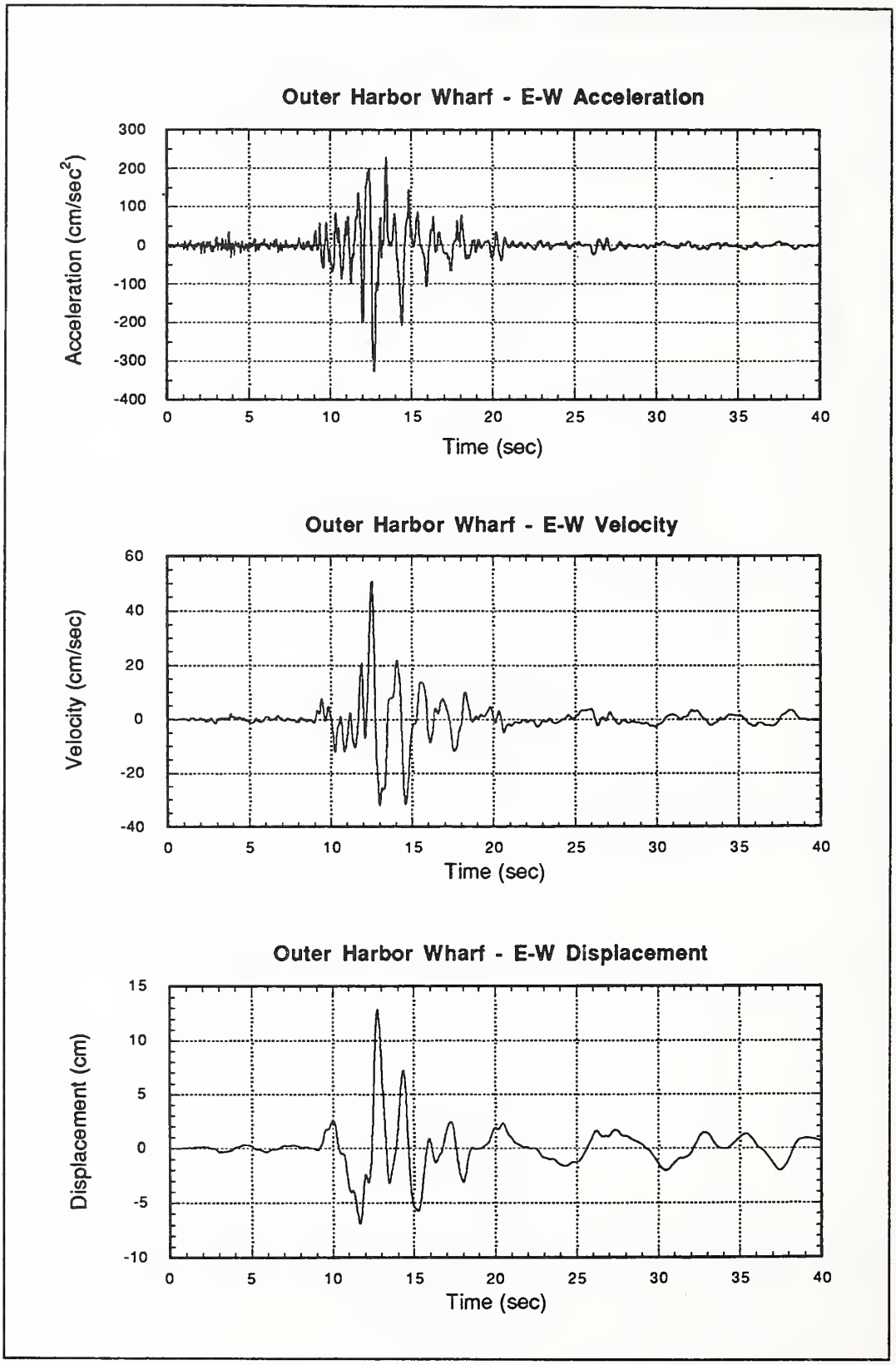

Figure 3-29 Acceleration, Velocity and Displacement for the East-West Component of Motion for the Oakland Two-Story Office Building Site

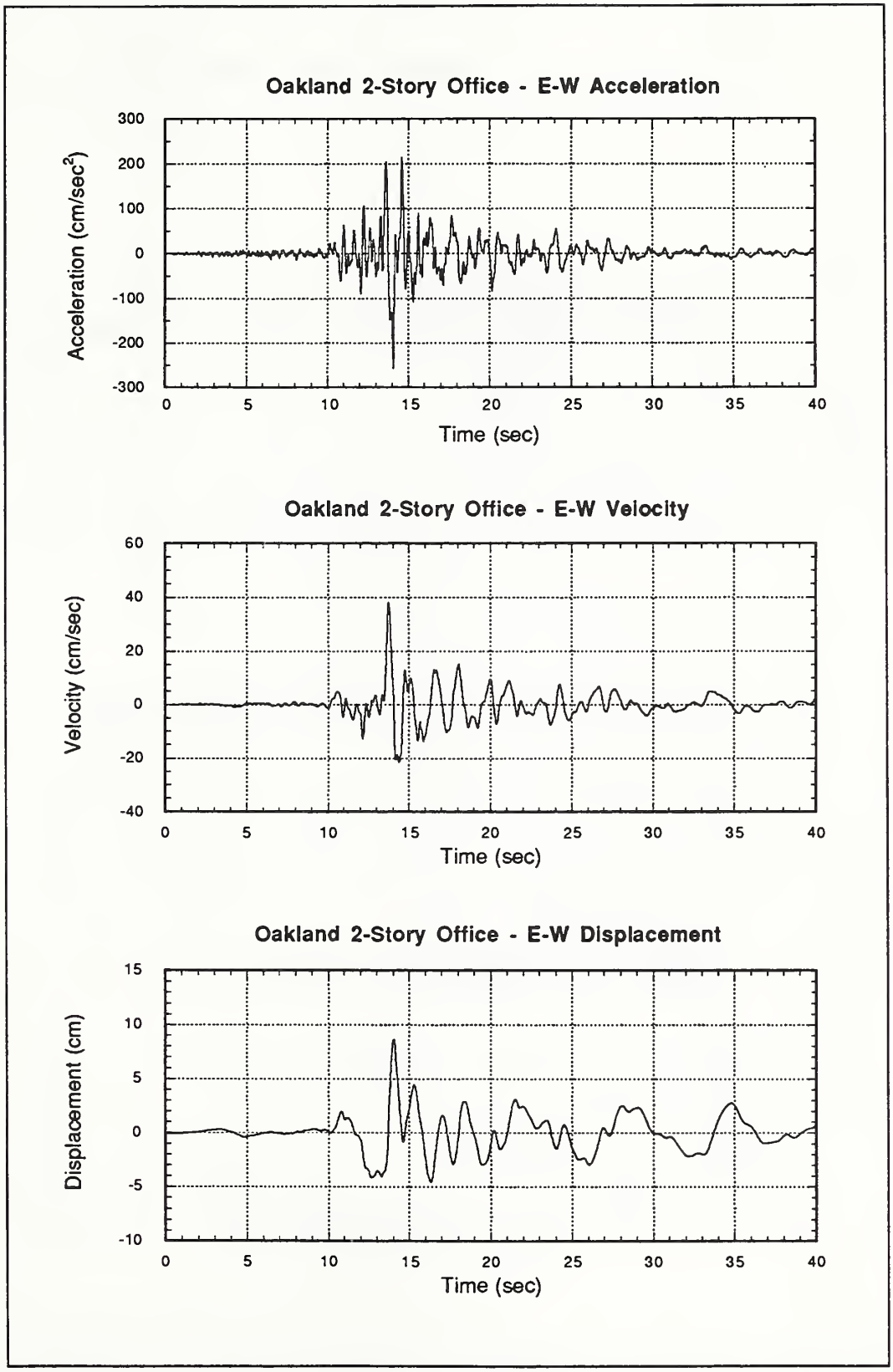

Figure 3-30 Acceleration, Velocity and Displacement for the East-West Component of Motion for the Outer Harbor Wharf Site

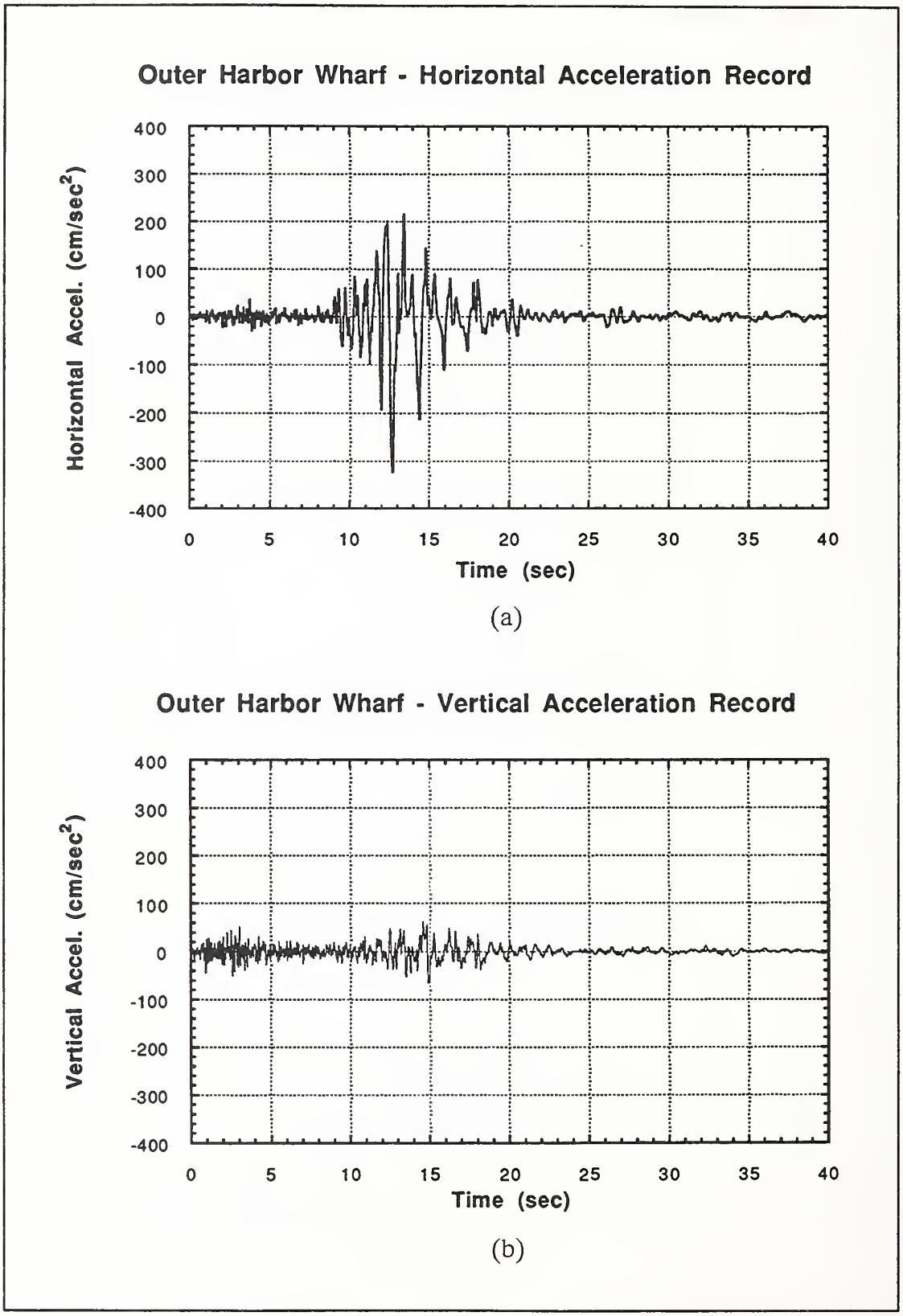

Figure 3-31 Horizontal and Vertical Acceleration Records Used in Dynamic Analyses (Outer Harbor Wharf 94° Component Horizontal Acceleration)

$$H(t) = \frac{\int_0^t a^2(t)\,dt}{\int_0^{t_f} a^2(t)\,dt} \qquad (3\text{-}3)$$

where t_f is the duration of the accelerogram. The Husid plot for the 94° component of horizontal acceleration is shown in Fig. 3-32. It is observed that approximately 80% of the energy is contained in the first 14 seconds of the earthquake. Also, the duration of strong shaking can be estimated as the time interval between 15% and 85% of the calculated energy content, or about 2.7 sec. Thus, it can be concluded that the Cypress Viaduct bents under study experienced ground accelerations as shown in Fig. 3-31, and that failure might be expected to occur within the first 14 seconds. Note that, in the dynamic analyses conducted on the Cypress bents, the full 40 seconds of the acceleration records were used.

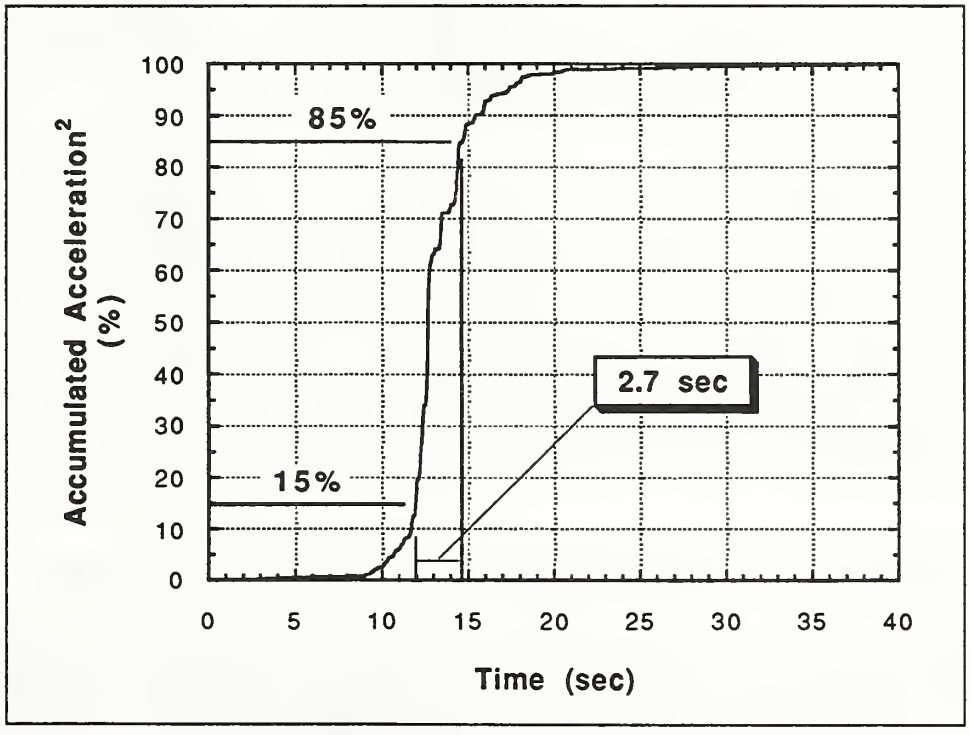

Figure 3-32 Husid Plot of the Outer Harbor Wharf 94° Component Horizontal Acceleration Record

An elastic response spectrum, assuming 2% damping, for the Outer Harbor Wharf 94° horizontal acceleration component is shown in Fig. 3-33. From previous analyses and from results of vibration tests, the first mode frequency of the Cypress Viaduct Type B1 bent was

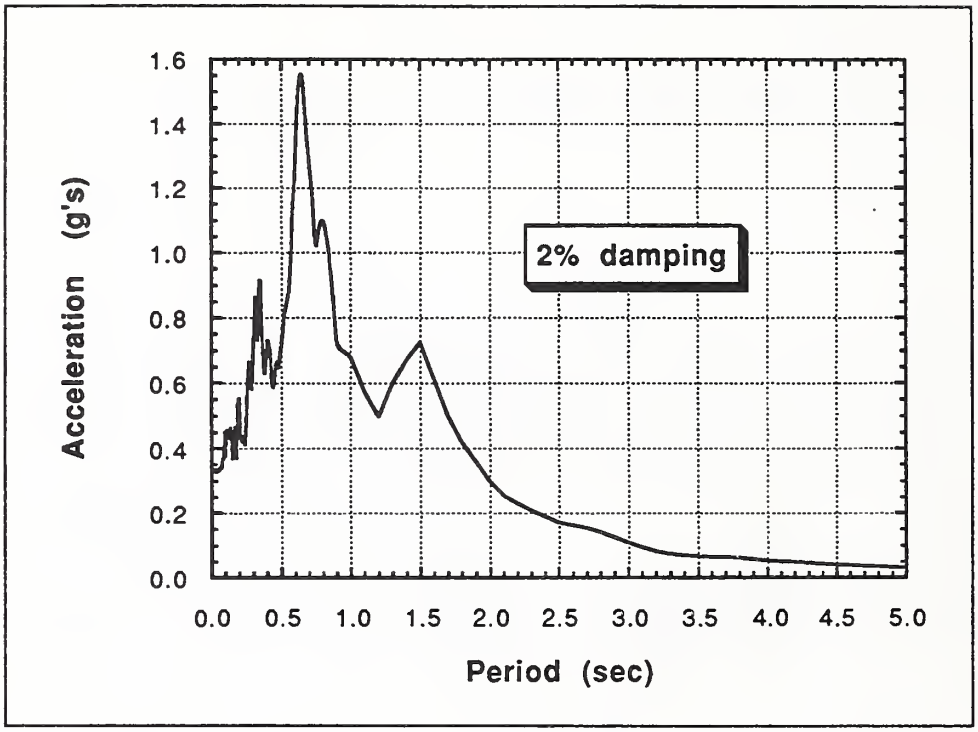

Figure 3-33 Elastic Response Spectrum for the Outer Harbor Wharf 94° Component Horizontal Acceleration

found to be 2.5 Hz which corresponds to a fundamental period of 0.40 sec. The response spectrum indicates an acceleration of approximately 0.7 g at a period of 0.40 sec. which equates to an amplification of 0.7/0.33 or approximately 2.1. It should be further noted that any inelastic action results in a reduced stiffness and corresponding increase in natural period. Such an increase in period would result in a peak acceleration which approaches nearly 1.6 g (dynamic amplification of roughly 4.8) at a period of 0.65 sec.

3.4 Comparison of Analysis Results with Observed Performance

In the following sections, several observations, important to the analytical assessment being conducted, are noted. The results of the dynamic analysis of the Cypress Viaduct (Bent Type B1) are then reported, along with comments relating the analysis results to observed performance.

3.4.1 Description of the Collapse of the Cypress Viaduct

Many investigators surveyed the collapsed Cypress Viaduct and have reported on their findings. The most comprehensive documentation is the Report to Governor George Deukmejian titled "Competing Against Time" [Housner et al, 1990] which draws on the observations and analyses of many investigators.

Failure of the Type B1 Bent

It was noted in Section 3.1 that this analytical investigation was limited to the Type B1 bent. Justification for this is found in [Housner, 1990] where it is noted that,

> "The B1 bents suffered the most damage and failed in a consistent manner throughout the collapsed portion of the Cypress Viaduct. In this portion of the upper roadway, all B1 bents collapsed completely and relatively intact onto the lower roadway. Failure occurred in the lower girder-to-column joints on both sides of the bent, with initial failure of the stub region."

The failure sequence described in [Housner, 1990] is illustrated in Fig. 3-34. Failure of one pedestal was followed quickly by failure of the other pedestal as shown in Fig. 3-34 (a) and (b). The upper level columns, having lost their vertical support, splayed outward as the upper level roadway collapsed onto the lower level as shown in Fig. 3-34 (c) and (d). It is also noted in [Housner, 1990] that,

> "The upper girder-to-column joint sometimes failed completely, but in other cases was just severely cracked. Almost all the damage in this upper joint seems to have been produced as a result of the collapse of the upper deck onto the lower deck."

The significance of this observation is that the upper girder-to-column connections, while likely suffering flexural cracking as a result of inelastic frame action, did not fail prior to shear failure of the pedestals. Had the upper girder-to-column connections failed prior to pedestal failure, by either compressive crushing or bar pullout, the collapse would have likely been in a lateral direction rather than vertical.

Failure of the Pedestals

As determined by finite element analysis of the pedestal region and gravity load analysis, and confirmed by static load tests (see Sections 3.2.1 and 3.2.3), the lateral load capacity of each

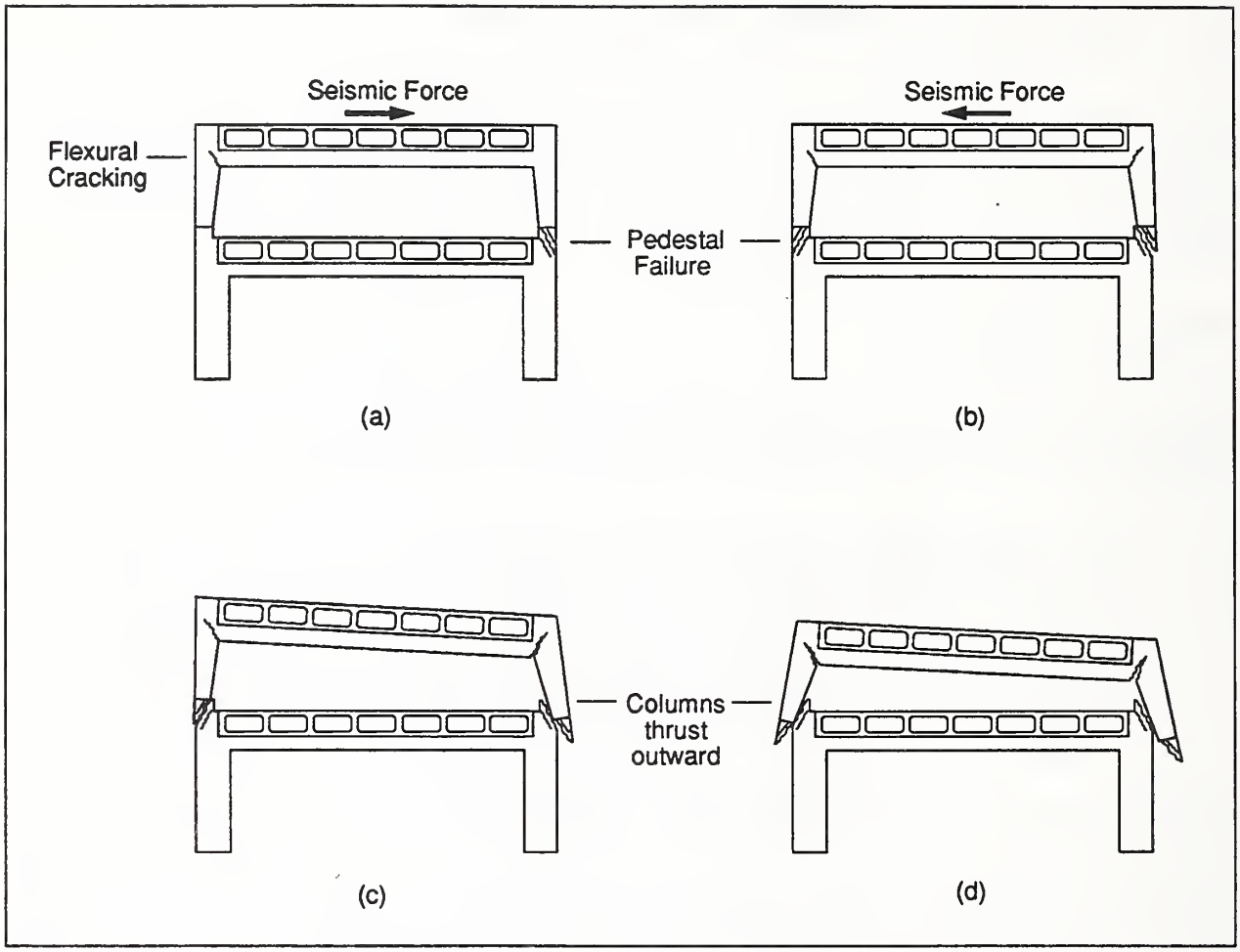

Figure 3-34 Failure Sequence of the Cypress Viaduct Type B1 Bent

pedestal was approximately 1020 kN (230 kips). And, assuming that both pedestals share equally in the lateral load, the calculated lateral resistance of the upper level is 2 x 1020 = 2040 kN (460 kips). The maximum lateral acceleration, as determined from the elastic response spectrum (see Fig. 3-33), was approximately 0.7 g. The upper level bent weighed roughly 635 kg (1400 kips), so the dynamic shear demand is calculated (using g = 9.807 m/sec^2) to be 635 * 0.7 g = 4360 kN (980 kips). It is clear that the demand exceeds the capacity by roughly a factor of two so shear failure of the pedestals would be expected. The horizontal acceleration record (see Fig. 3-31a) indicates that the major acceleration peaks occur between 12 and 15 seconds from the start of the record. Additionally, the Husid plot (see Fig. 3-32) indicates that 85% of the calculated energy is accumulated by roughly 14.5 sec. Thus, it is concluded that one would expect the analysis to indicate shear failure in both pedestals between 12 and 15 seconds from the start of the ground acceleration record.

Failure of the Upper Level Girder-to-Column Joint

The maximum moment in the upper level girder-to-column joint is determined from the shear capacity of the pedestals, assuming that no moment is transmitted by the shear keys. The maximum moment is simply the product of the maximum shear capacity of one pedestal, 2000 kN (450 kips) (see Section 3.2.1), times the upper level column height, 5.1 m (16.75 ft), assuming centerline dimensions, or approximately 10,220 kN-m (90,450 in-kips). This moment is seen to exceed the computed negative yield moment of approximately 6160 kN-m (54,500 in-kip), but is less than the ultimate moment (see Fig. 3-10). On the basis of these calculations, one would expect that the upper level girder-to-column joint would experience moments in excess of member cracking and yielding but the ultimate moment, determined by compressive crushing, would not be reached prior to shear failure of the pedestals.

3.4.2 Inelastic Analysis of the Cypress Viaduct

An inelastic analysis of the Cypress Viaduct Type B1 bent was carried out using the IDARC computer program using the model described previously. The model was subjected to both horizontal and vertical ground motions in addition to gravity loading as described in Section 3.2.2. Results are reported here.

Failure of the Pedestals

As reported earlier, the IDARC program computes member and story damage (see Sections 2.2.4 and 2.4.1). For purposes of ascertaining failure in the pedestal regions, the component damage index was used. Review of component damage indices for all components revealed that the first element to fail was the left side pedestal (modeled as a shear wall). Fig. 3-35 shows a three-part plot of the horizontal acceleration record, left side pedestal shear force versus time, and pedestal damage index versus time. It can be seen that the analysis predicts a component damage index of 1.0, which corresponds to failure, at approximately 12.5 seconds from the beginning of the earthquake. This is consistent with the prediction of pedestal failure between 12 and 15 seconds as described in Section 3.4.1. Analysis results beyond failure of an element are meaningless since the IDARC program is not capable of accounting for the drastic changes in structural configuration that result from a brittle shear failure or from compressive crushing.

Failure of the Upper Level Girder-to-Column Joint

The upper level girder-to-column joint was expected to sustain flexural cracking and yielding of the reinforcement, but not fail prior to failure of the pedestals (see Section 3.4.1). This was observed in the analysis results. Component damage indices for the upper level girder at the left girder-to-column joint is shown in Fig. 3-36. As can be seen, the damage index increased noticeably about the time the first large ground acceleration occurred (around 12.5 seconds) but was still well below a value that would suggest failure at the girder-to-column joint. The analysis, of course, was not able to simulate the subsequent failure that, according to Housner [1990], was a result of the upper level columns being thrust outward as the upper level deck collapsed onto the lower level deck.

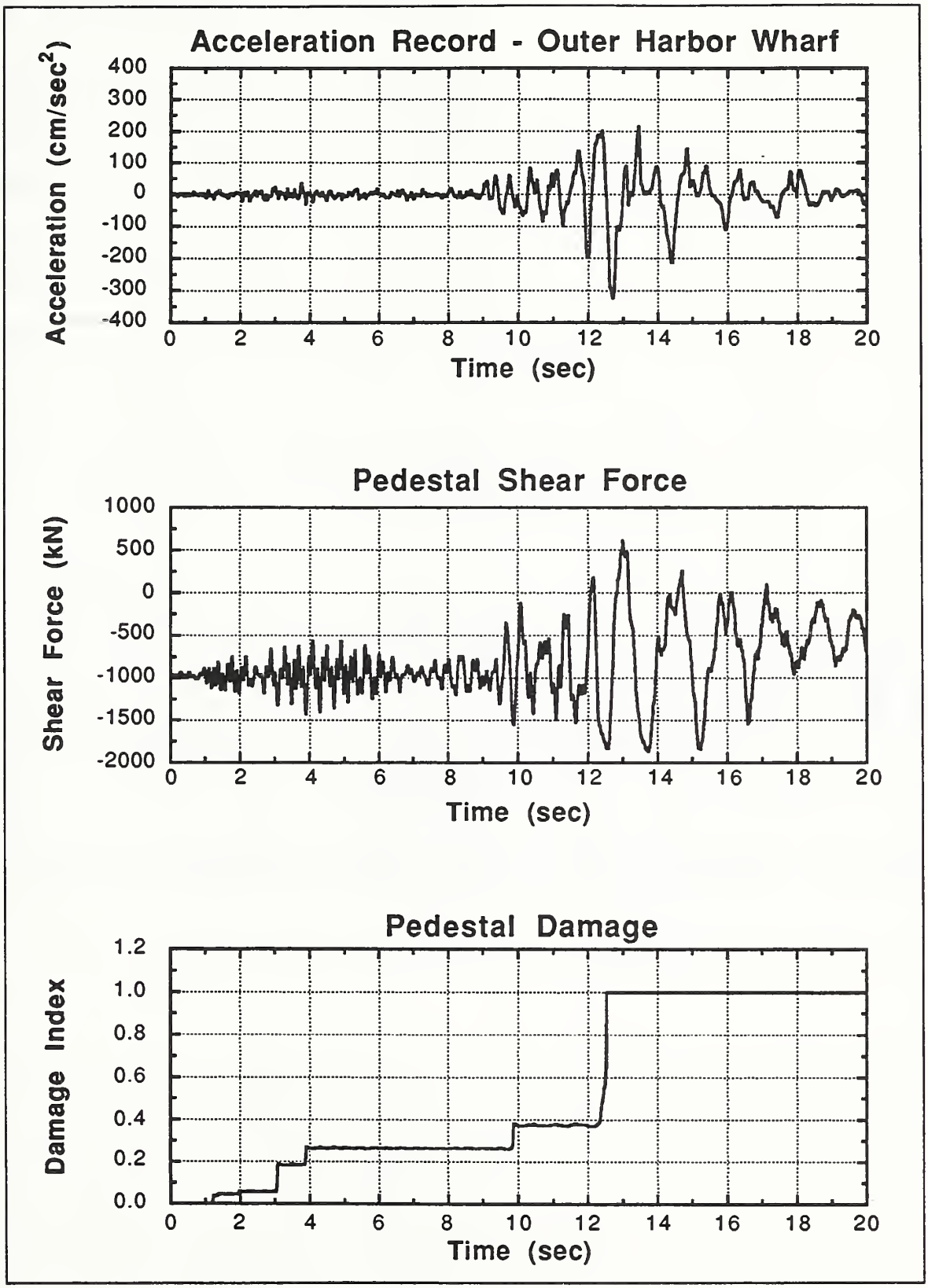

Figure 3-35 Analytical Results for Left Pedestal

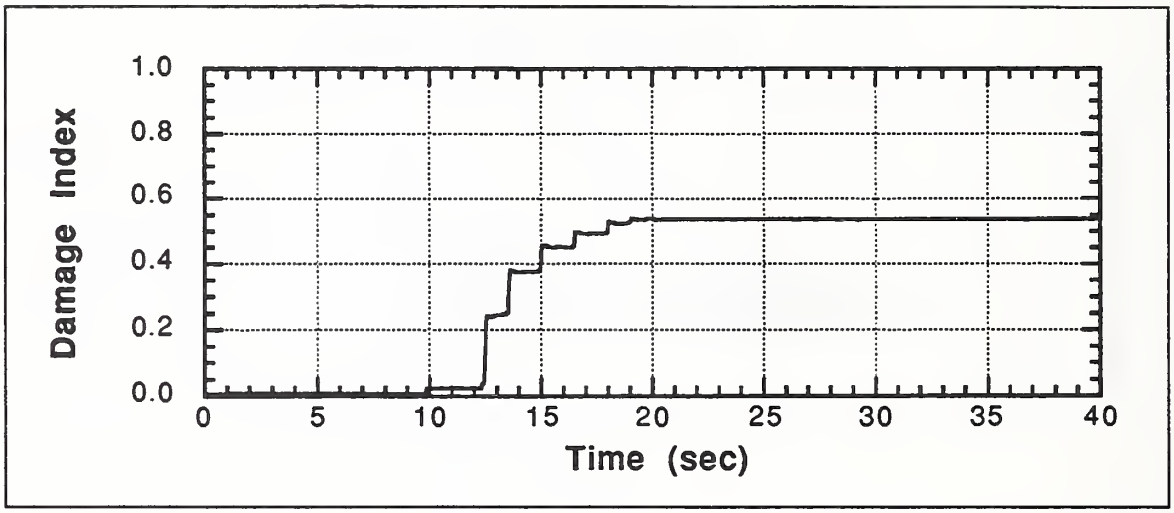

Figure 3-36 Component Damage Index for Upper Level Girder-to-Column Joint

4.0 Summary and Conclusions

The purpose of this project was to develop, by applying existing technology, the capability to evaluate accurately the ability of elevated highway structures to survive a major earthquake. The Loma Prieta earthquake of October 15, 1989, provided the engineering profession with data on the performance of structures against which analytical simulations can be compared. Accounts of the failure of the Cypress Viaduct, along with subsequent vibration tests and static tests to failure of a portion of the structure that remained standing and relatively undamaged, provided the opportunity to evaluate the effectiveness of both inelastic dynamic computer analysis as well as modeling techniques. In this section, the inelastic damage analysis that was developed, refined and tested is summarized along with comparisons made with the performance of the Cypress Viaduct. Conclusions are drawn from the study which, it is hoped, will enable engineers to use the techniques described herein to evaluate the capacity of elevated highway structures to survive a major earthquake.

4.1 Summary

A review of existing analysis capabilities indicated that IDARC, a computer program for the seismic damage analysis of reinforced concrete structures, came closest to meeting the needs of the project. Among the features that set IDARC apart were (i) a distributed flexibility model to represent implicitly the spread of plasticity, (ii) a versatile force-deformation hysteretic model which is able to capture stiffness degradation, strength decay and pinching behavior, and (iii) a shear wall element which is able to model shear and flexure independently, thereby enabling shear-type failures to be detected. Modifications were made to the IDARC computer program to accommodate internal hinges (releases), hinged base conditions, circular columns, and nonuniform members. Also, the program was thoroughly checked to determine the causes of perceived drift and an equilibrium correction was added to the shear wall element.

Typical transverse bents which supported the elevated roadway decks of the Cypress Viaduct were modeled using discrete components consisting of beam, column and shear wall elements. An inelastic finite element analysis was performed on the pedestal regions of the bents to provide the shear load vs. displacement behavior for use in modeling this region with the IDARC shear wall element. The newly developed tapered elements with distributed flexibility were used to model the upper level columns and the discrete hinge feature, also newly implemented, was used to model the shear key detail between the upper level columns and pedestals. Gravity load was simulated by applying gradually 1 g in the

vertical direction before applying the horizontal and vertical ground accelerations to the base of the structure.

Ambient vibration as well as forced vibration tests were conduced on a three-bent portion of the Cypress Viaduct that remained standing after the Loma Prieta earthquake. The measured first mode frequency was found to be 2.5 Hz. To compare with the measured first-mode frequency, a time-history analysis was conducted on the test bent configuration by first applying the Emeryville record (scaled by one half) and then allowing the structure to vibrate freely. A Fast Fourier Transform (FFT) was conducted on the free vibration response from which the lowest frequency was found to be 2.48 Hz thus comparing well with the measured value of 2.5 Hz.

The three-bent test structure was tested to failure by loading all three bents laterally with hydraulic jacks and the lateral load per bent vs. the upper level displacement was recorded. Results of the IDARC analysis show good agreement between analysis and test results. The shear capacity of the pedestals, as determined by test, was found to be 1035 kN (233 kips) which compares favorably with the analytically determined failure load of 1020 kN (230 kips).

It is emphasized that the model of the Cypress Viaduct Type B1 bent developed in this study was not changed or modified to produce better agreement with the experimantal results. The agreement of the computed and measured first mode frequency indicated accurate modeling of the structural stiffness and mass distribution as well as approximated stiffness reduction due to cracking. Agreement of the computed and measured lateral load capacity and displacement indicated accurate modeling of structural stiffness and load-deformation relationships of the pedestal regions as determined by a smeared-crack approach finite element analysis.

A time-history analysis of the typical Cypress Viaduct bent indicated that failure of one or both pedestals, which would precipitate total collapse of the structure, occurred at approximately 12.5 seconds -- following the first large (greater than 200 cm/sec^2) ground acceleration. The component damage indices, computed by IDARC, were used to ascertain that failure (in the case of the pedestals brittle failure) was obtained. The analysis predicted that failure of the pedestals was reached before any other component failed which is consistent with observed performance.

4.2 Conclusions

This study has led to a number conclusions regarding the application of state-of-the-art inelastic dynamic analysis of reinforced concrete structures to elevated highway structures.

(i) Performance of elevated highway structures subjected to strong ground motions associated with major earthquakes can be predicted analytically using component model inelastic dynamic finite element analysis.

(ii) Great care must be taken in defining the component properties, both elastic and inelastic including hysteretic behavior. It may be necessary to depend on either component test results or, as was the case in this study, additional analyses to arrive at suitable behavioral models for the components used to represent the prototype structure.

(iii) It is important to understand all viable failure modes and be able to quantify the failure modes in a structural component. Likewise, the analysis capability must be able to capture all anticipated failure modes and handle them in a consistent manner.

(iv) A carefully developed analytical model can be used to evaluate the performance of a given structure under a variety of earthquake loadings or the effectiveness of structural repair and/or retrofit strategies.

(v) Component damage modeling appears to be an effective way of assessing the dynamic response of a structure. The global damage index, since it is an average of component indices, did not, in the case of the Cypress Viaduct analysis, identify collapse of the structure. This may not be true for structures that exhibit more ductility than was evident in the Cypress Viaduct.

(vi) Determination of state or condition of the structure under study, prior to application of horizontal and vertical components of ground motion, may be achieved by applying self weight and service loads dynamically as described in this report. The motivation to do this is that all features that are a part of the dynamic analysis, cracking yielding, damage computation, etc. are included with no additional effort.

5.0 References

Bathe, K.-J. and Wilson, E.L. (1976), *Numerical Methods in Finite Element Analysis*, Prentice-Hall, Inc, New Jersey.

Clough, R. W. and Penzien, J. (1975), *Dynamics of Structures*, McGraw-Hill, New York.

Ewing, R. D., El-Mustapha, A. M. and Kariotis, J. C. (1991), "FEM/I: A Finite Element Computer Program for the Nonlinear Static Analysis of Reinforced Masonry Buildings," Report No. 2.2-1, EKEH, California.

Kaanan, A. E. and Powell, G. H. (1973), "DRAIN-2D, A General Purpose Computer Program for Dynamic Analysis of Planar Structures," UCB/EERC Report 73-6, Earthquake Engineering Research Center, University of California, Berkeley.

Housner, G. W. et al (1990), "Competing Against Time -- Report to Governor George Deukmejian from The Governor's Board of Inquiry on the 1989 Loma Prieta Earthquake," State of California, Office of Planning and Research.

Idriss, I. M. (1979), "Characteristics of Earthquake Ground Motions," Earthquake Engineering and Soil Mechanics, Proc. ASCE Geotechnical Division Specialty Conference, Pasadena, California., June, 1978.

Kunnath, S.K., Reinhorn, A.M. and Park, Y.J. (1990), "Analytical Modeling of Inelastic Seismic Response of RC Structures", J. Struct. Eng., ASCE, 116, 4, pp. 996-1017.

Lew, H. S. et al (1990), "Performance of Structures During the Loma Prieta Earthquake of October 17, 1989," NIST Special Publication 778, National Institute of Standards and Technology, Gaithersburg.

Nims, D. K. et al (1989), "Collapse of the Cypress Street Viaduct as a Result of the Loma Prieta Earthquake," Report No. UBC/EERC-89/16, University of California at Berkeley.

Otani, S. (1974), "SAKE, A Computer Program for Inelastic Response of R/C Frames Subject to Earthquakes," Civil Engineering Studies, SRS No. 413, University of Illinois, Urbana.

Park, R. and Paulay, T. (1975), *Reinforced Concrete Structures*, John Wiley & Sons, New York,

Park, Y.J., Ang, A.H-S and Wen, Y.K. (1984), "Seismic Damage Analysis and Damage Limiting Design of R/C Buildings", Civil Engineering Studies, SRS No.516, University of Illinois, Urbana.

Park, Y.J., Reinhorn, A.M. and Kunnath, S.K. (1987), "IDARC - Inelastic Damage Analysis of Reinforced Concrete Frame - Shear-Wall Structures," Technical Report NCEER-87-0008, State University of New York at Buffalo.

Rodriguez-Gomez, S., Chung, Y. S. and Meyer, C. (1990), "SARCF-II User's Guide - Seismic Analysis of Reinforced Concrete Frames," Technical Report No. NCEER-90-0027, State University of New York at Buffalo.

Appendix A: Flexibility Coefficients

The flexibility coefficients required to develop the element stiffness matrices are derived from integration of the ***(M/EI)*** diagram. The contraflexure point for an element varies as a function of the end moments of the element. Two expressions can be dervied for the general cases of the contraflexure point lying either within or outside the element.

For the case in which the contraflexure point does not lie within the element (i.e., single curvature), the following expressions are obtained:

$$f_{11} = \frac{1}{4(EI)_a} + \frac{1}{12(EI)_b} \tag{A-1}$$

$$f_{12} = f_{21} = \frac{1}{12(EI)_a} - \frac{1}{12(EI)_b} \tag{A-2}$$

$$f_{22} = \frac{1}{12(EI)_a} + \frac{1}{4(EI)_b} \tag{A-3}$$

where ***EI*** is the member flexural stiffness and ***a,b*** refer to the member ends.

For the case in which the contraflexure point lies within the element (i.e., reverse curvature), the following expressions are obtained:

$$f_{11} = \frac{1}{12(EI)_a}(6\alpha - 4\alpha^2 + \alpha^3) + \frac{1}{12(EI)_b}(1 - 3\alpha + 3\alpha^2 - \alpha^3) + \frac{1}{12(EI)_0}(3 - 3\alpha + \alpha^2) \tag{A-4}$$

$$f_{12} = f_{21} = \frac{1}{12(EI)_a}(-2\alpha^2 + \alpha^3) + \frac{1}{12(EI)_b}(-1 + \alpha + \alpha^2 - \alpha^3) + \frac{1}{12(EI)_0}(-1 - \alpha + \alpha^2) \tag{A-5}$$

$$f_{22} = \frac{1}{12(EI)_a}(\alpha^3) + \frac{1}{12(EI)_b}(3 - \alpha - \alpha^2 - \alpha^3) + \frac{1}{12(EI)_0}(1 + \alpha + \alpha^2) \tag{A-6}$$

where:

$$\alpha = \frac{\Delta M_A}{\Delta M_A + \Delta M_B} \tag{A-7}$$

NIST-114A
(REV. 3-90)

U.S. DEPARTMENT OF COMMERCE
NATIONAL INSTITUTE OF STANDARDS AND TECHNOLOGY

BIBLIOGRAPHIC DATA SHEET

1. PUBLICATION OR REPORT NUMBER
NISTIR 4857

2. PERFORMING ORGANIZATION REPORT NUMBER

3. PUBLICATION DATE
AUGUST 1992

4. TITLE AND SUBTITLE

Application of Inelastic Damage Analysis to Double-Deck Highway Structures

5. AUTHOR(S)

John L. Gross and Sashi K. Kunnath

6. PERFORMING ORGANIZATION (IF JOINT OR OTHER THAN NIST, SEE INSTRUCTIONS)

U.S. DEPARTMENT OF COMMERCE
NATIONAL INSTITUTE OF STANDARDS AND TECHNOLOGY
GAITHERSBURG, MD 20899

7. CONTRACT/GRANT NUMBER

8. TYPE OF REPORT AND PERIOD COVERED

9. SPONSORING ORGANIZATION NAME AND COMPLETE ADDRESS (STREET, CITY, STATE, ZIP)

United States Geological Survey

10. SUPPLEMENTARY NOTES

11. ABSTRACT (A 200-WORD OR LESS FACTUAL SUMMARY OF MOST SIGNIFICANT INFORMATION. IF DOCUMENT INCLUDES A SIGNIFICANT BIBLIOGRAPHY OR LITERATURE SURVEY, MENTION IT HERE.)

The Loma Prieta earthquake of October 17, 1989, caused extensive damage to many highway structures and particularly to double-deck structures. The most notable was the collapse of the Cypress Viaduct (Interstate 880). A study was undertaken by NIST to identify, using computer-based analysis methods, causes of structural failure of elevated highway structures resulting from the Loma Prieta earthquake and thereby reveal the potential for damage or collapse of similar strutures nationwide. The IDARC analysis program, developed at the University of Buffalo, was used in the inelastic seismic analysis. Features of the program and enhancements incorporated to model the Cypress Viaduct structure are described. To accurately determine beam and column moment-curvature relationships, separate computer analyses were conducted. In addition, a smeared-crack approach finite element analysis was employed to determine the lateral load-deformation relationship of the pedestal regions. The model of the Cypress Viaduct was subjected to the Oakland Outer Harbor Wharf ground acceleration record in the plane of the bent. The analytical model was calibrated using static lateral load tests, ambient and forced vibration tests, and observed performance. Results of time-history analyses, which include a prediction of member damage, indicate that collapse was initiated by a shear failure of the pedestal regions as concluded by the Governor's Board of Inquiry. The analytical and modeling procedures reported herein may be used to facilitate comparison and selection of effective approaches to seismic strengthening.

12. KEY WORDS (6 TO 12 ENTRIES; ALPHABETICAL ORDER; CAPITALIZE ONLY PROPER NAMES; AND SEPARATE KEY WORDS BY SEMICOLONS)

Computer analysis; computer modeling; damage; earthquake; finite element analysis; highway structures; inelastic analysis; reinforced concrete; seismic analysis; structural analysis.

13. AVAILABILITY

X	UNLIMITED
	FOR OFFICIAL DISTRIBUTION. DO NOT RELEASE TO NATIONAL TECHNICAL INFORMATION SERVICE (NTIS).
	ORDER FROM SUPERINTENDENT OF DOCUMENTS, U.S. GOVERNMENT PRINTING OFFICE, WASHINGTON, DC 20402.
X	ORDER FROM NATIONAL TECHNICAL INFORMATION SERVICE (NTIS), SPRINGFIELD, VA 22161.

14. NUMBER OF PRINTED PAGES
83

15. PRICE
A05

ELECTRONIC FORM